INTEGRATED RESERVOIR MODELLING WORKFLOW AND OPTIMIZATION FRAMEWORK FOR CO2 SEQUESTRATION USING WATER ALTERNATING GAS PROCESS UNDER GEOLOGICAL UNCERTAINTIES

ヴォ, タン, フン

九州大学
KYUSHU UNIVERSITY

INTEGRATED RESERVOIR MODELLING WORKFLOW AND OPTIMIZATION FRAMEWORK FOR CO_2 SEQUESTRATION USING WATER ALTERNATING GAS PROCESS UNDER GEOLOGICAL UNCERTAINTIES

by

Vo Thanh Hung

A dissertation submitted to Kyushu University

for the degree of Doctor of Engineering

Supervised by

Assoc.Prof. Yuichi Sugai

Department of Earth Resources Engineering

Graduate School of Engineering

Kyushu University

Fukuoka, Japan

July 2020

Abstract

Carbon Capture and Storage (CCS) is an attractive emerging method to mitigate and slow down greenhouse gases emission. In this vein, carbon storage in deep saline aquifers is touted as the most suitable site because it is identified as the largest storage capacity. However, the construction of realistic 3D geological models for this storage formation is a significant issue. The lack of subsurface datasets in these storage sites is an obstacle to build a realistic model. Also, injection strategies are strongly influenced by CO_2 sequestration efficiency. The water alternating gas (WAG) process is a common technique to improve sweep efficiency in EOR projects. This process could be a promising technique in the CCS aspect. Besides, the modelling and numerical simulation are useful tools to evaluate the reasonable 3D models and effective injection technique. However, geological uncertainties (e.g., porosity and permeability distributions) are crucial factors for modelling and reservoir simulation results.

Therefore, this study was proposed a systematic workflow to integrate 3D modelling, reservoir simulation, and geological uncertainties. The new modelling framework was developed with available subsurface data. This framework could enhance the accuracy of 3D porosity and permeability models. Also, the robust optimization approach was implemented to improve CO_2 trapping using the WAG process under geological uncertainties. Ultimately, the systematic workflow could increase the 90% amount of CO_2 injection stored in the storage site.

This dissertation composes of six chapters as follows:

Chapter 1 presents the research motivation, background, and objectives, as well as the outline of the dissertation. Furthermore, this chapter introduces previous studies on Artificial Neural Networks, Geostatistical modelling, Water Alternating Gas process.

Chapter 2 describes the literature review of CO_2 sequestration modelling, geological uncertainties, optimization under geological uncertainty, and study area. Detail information on geological modelling and reservoir simulation of CO_2 sequestration was provided in this chapter. The critical role of geological risk was highlighted, focusing on geological CO_2 sequestration. Also, robust optimization under geological uncertainties was introduced based on previous studies. Furthermore, the study area was presented for a better understanding of the characteristic of fluvial sandstone reservoirs in Cuu Long Basin, Vietnam. Ultimately, the available data is introduced for a better understanding of subsurface pieces of information to conduct the modelling and simulation studies.

Chapter 3 describes the development of an integrated geological modelling workflow. Adopting the object-based modelling, Sequential Gaussian Simulation, and Artificial Neural Network (ANN), a new modelling workflow named "encapsulated framework" was developed to construct the reasonable 3D porosity and permeability models in Nam Vang field. The advantages, methodology of the encapsulated framework build the models, as well as the comparison with traditional framework, were presented in this chapter. Petrel package was employed as the object-based method to construct the lithofacies models. Also, Sequential Gaussian Simulation was adapted to rank the lithofacies distribution. Then, Artificial Neural Networks was predicted the petrophysical models using seismic attributes and well log measurement. To integrating the ranking lithofacies and ANN models, the co-kriging was used to distribute the final porosity and permeability models. Also, conventional models were constructed for comparison purposes. Finally, the ECLIPSE simulator was performed the Drill Stem Test matching to evaluate the accuracy between the new and traditional models. The results of history matching indicated that the developed porosity and permeability

models are better for future field development plan as well as the CO_2 sequestration assessment.

Chapter 4 discusses the simulation workflow and results of CO_2 sequestration in a fluvial sandstone reservoir. The defining problems are the first step of reservoir simulation work. Then, the dynamic datasets were collected to import in the simulator. Besides, this chapter was conducted several simulation scenarios to evaluate the impact of geological factors and injection strategies for CO_2 sequestration. The sensitivity analysis was performed to determine the suitable injection rate for the project. This injection rate used throughout the work for consistent simulation results. The channel distribution and anisotropy were changed to investigate the CO_2 plume migration in a fluvial sandstone reservoir. Also, the injection strategies comprise continuously, and WAG injection was compared to determine the effective injection methods for further studies. The simulation results indicated that WAG technology was enhanced the solubility and residual trapping when comparing with continuous CO_2 injection. This increase was due to the migration of CO_2 after injection caused by drainage and imbibition processes in porous media. Therefore, the WAG technique was suggested for optimization studies.

Chapter 5 describes the optimization framework of CO_2 sequestration using the Water Alternating Gas process under geological uncertainties. A robust optimization workflow was used to determine the optimal cycle length of water and gas injection under geological uncertainties. A total of 200 geological realizations of the 3D porosity, horizontal and vertical permeability distributions were generated to consider the geological constraints. The first step of this workflow is to rank all realizations by quantifying CO_2 cumulative injection to select P10, P50, and P90 that represent the overall uncertainty of a reservoir. The WAG process was evaluated using CMG-GEM

compositional reservoir simulation software. The experimental design created 250 simulation jobs, including the cycle length and geological uncertainty parameters. Then, the generated jobs were assessed using the compositional reservoir simulator to calculate the CO_2 storage amounts by the end of 20 years-injection followings by 40 post-injection years. Subsequently, the robust optimization procedure was applied to determine the true optimal solution of the high CO_2 trapping by considering the geological uncertainties in porosity, permeability, and anisotropy models. The nominal optimization based on a single realization was conducted for comparison. The proposed robust optimization workflow under geological uncertainties resulted in higher CO_2 trapping than the nominal realization optimization. This study suggested a fast and reliable robust optimization workflow that can represent the uncertainties of the main parameters, including petrophysical properties, geology, and economic factor, for CO_2 sequestration

Chapter 6 summarizes the conclusions of the findings of this research, including the recommendations and the possibility of a future project.

Acknowledgment

Three years have been passed for my research and life at Kyushu University, Fukuoka, Japan. I earned a lot of valuable lessons here. Thanks to **JESUS CHRIST** for your patient to listen to me.

This dissertation has been done by help and support from many individuals.

First and foremost, I would like to express my most profound appreciation to my advisor, **Associate Professor Yuichi Sugai**, for supporting me during my study, guiding me with his patience to complete my research.

My sincere gratitude also goes to **Professor Kyuro Sasaki** for the discussion as well as his encouragement in my research.

I would like to appreciate to **Assistant Professor Ronald Nguele**, for all the comments, suggestions, and advice for improving this work.

Deep gratitude and acknowledge goes to following thesis examiners **Associate Professor Akira Sato** and **Associate Professor Kiyonobu Kasama** for their constructive comments to improve this dissertation.

Sincere appreciation and acknowledgment to the Japan International Cooperation Agency (**JICA**) for the financial support during three years in Japan through a program of Asean University Network, the Southeast Asia Engineering Education Development Network (**AUN/SEED-Net**).

Special thanks go to entire members of the Resource Production and Safety Engineering Laboratory (**Kaihatsu**) for their kind supports.

Last but not least, my deepest gratitude to **my beloved family** for their love, advice, encouragement, and endorsement to me all the time.

Table of Contents

List of Figures

List of Tables

CHAPTER 1

INTRODUCTION

1. 1. Research Motivation

Reduction in global climate change is an emergency issue for our society. Due to industrial activities, the concentration of CO_2 is rising in the atmosphere every year. Thus, Carbon dioxide (CO_2) capture and storage (CCS) is a potential solution to reduce the amount of CO_2 emission in the earth's atmosphere. CO_2 could store in different storage candidates, including deep saline aquifers, unminable coal seams, depleted petroleum reservoirs, and depleted unconventional reservoirs (**Figure 1.1**) (Bachu, 2002; Jin et al., 2017). Among these candidates, the deep saline aquifers have the largest storage capacity (Lackner, 2003). However, the economic and environmental aspects related to CO_2 storage in saline aquifers need to consider before industrial-scale CO_2 storage can occur (Bruant et al., 2002; IPCC, 2005). Thus, this study will emphasize the fundamental assessment of saline aquifers.

In deep saline aquifers, the diversity of physicochemical processes is affected by CO_2 trapping and storage. There is four trapping mechanism (Juanes et al., 2006). The first trapping mechanism is structural or stratigraphic trapping to prevent CO_2 from escaping to the surface (Hesse and Woods, 2010). The second mechanism is residual trapping, where the CO_2 trapped in the rock pores by capillary forces (Juanes et al., 2006). The third mechanism is the dissolution of CO_2 in storage formations (Spycher and Pruess, 2005).

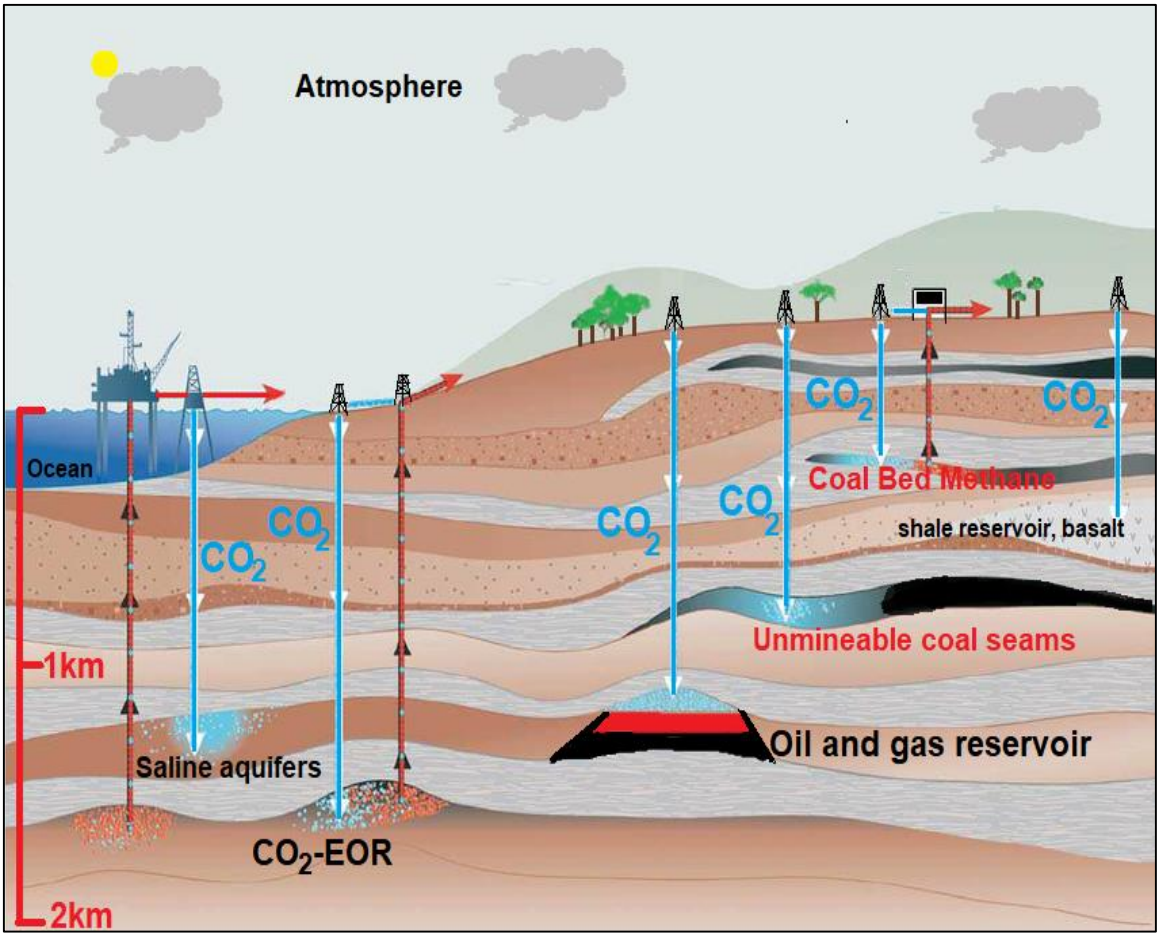

Figure 1.1 Potential options for storing CO_2 in geological formations modified from (IPCC, 2005)

This trapping can enhance CO_2 storage safety since the amount of CO_2 leakage is minimal. The last is mineral trapping, whereby the CO_2 can store safest in storage media as a result of geochemistry; however, mineralization is a prolonged thermodynamic process and can take hundreds to thousands of years or more to complete (Bachu et al., 1994). Thus, this work will focus on residual and solubility trapping rather than mineral trapping. Since we cannot perform the pilots directly, at Vietnam and many potential sites, to investigate the CO_2 storage because of the high cost, modelling and simulation are the main streams of this work.

Moreover, numerous studies have shown that CO_2 storage efficiency depends on reservoir heterogeneity (Al-Khdheeawi et al., 2018b; Ambrose et al., 2008; Dai et al., 2018; Flett et al., 2007). Also, permeability heterogeneity is essential to control CO_2 migration (Flett et al., 2007; Obi and Blunt, 2006), while these authors suggested that the geological models with high-resolution heterogeneity are necessary for the different storage mechanism.

However, in CO_2 simulation is required high computational cost. It needs to incorporate heterogeneity and geological realism. In order to build a realistic model, the subsurface data is necessary for reservoir characterization. For conventional modelling workflow, enough data requires for building the petrophysical accuracy model. However, the cost center of the geo-storage project is the constraint to obtain all data measurements to construct the geological model. Thus, the efficient geological modelling workflow needs to develop for storage sites. Therefore, this study will propose an integrated modelling framework using Artificial Neural Network and Geostatistic modelling to enhance the modelling process.

Furthermore, injection strategies could improve efficiency and security storage. Recently, the WAG process has been proposed to enhance security and maximize the amount of CO_2 trapping because of the capability to enhance macroscopic and microscopic sweep efficiencies in storage reservoirs (Al-Khdheeawi et al., 2018a; Rogers and Grigg, 2001).

Many studies have demonstrated the better performance of WAG than CO_2 continuous in terms of residual and solubility trapping (Juanes et al., 2006; Rasmusson et al., 2016). However, few studies proposed the optimization framework for the WAG process. Also, heterogeneity uncertainties such as facies, porosity, and permeability exhibit notable

effects on the performance of the WAG process. These uncertainties are significant for monitoring and optimization of CO_2 storage.

To address the issues about geological modelling and optimization CO_2 storage, the interesting question raised here: Could we optimize the CO_2-WAG process under geological uncertainties? To answer this question, the integrated framework between geological modelling and robust optimization WAG process is required. Thus, the unique geological modelling workflow needs to create to achieve optimal reservoir modelling, storage optimization, as well as uncertainty assessment.

1. 2. Background

1. 2. 1. Artificial Neural network

Artificial Neural Network (ANN) is a power tool, which helps automatically identify the relationship between multiple known parameters and a single unknown parameter. The way defines the behavior of a neural network that their individually computed elements are connected and by the strength of those connections, or weights (Vo Thanh et al., 2019a). Weights are automatically adjusted by training the network following a specified learning rule until it properly performs the desired task (Ahmadi, 2015).

ANN applications have two stages: the training stage, where the ANN learns the hidden relationship of data while the predicting stage of ANN used to predict new outputs from input data not used during the training stage (Ruiz- Serna et al., 2019). Also, ANN could be roughly categorized into two types in terms of their learning features: supervised and unsupervised (Anderson and McNeill, 1992). This research used a supervised ANN model that takes multiple inputs and returns one or several outputs from trial and error algorithm (Petrel, 2017). These inputs included seismic attributes and well log values. Each input

multiplied by weight; the result then summed and passed through a nonlinear function to produce the output (Nikravesh, 1998; Du et al., 2003; Mahdavi and Kharrat, 2009; Darabi et al., 2010; Iturrarn-Viveros and Parra, 2014). **Figure 1.2** depicts the architecture of the ANN model.

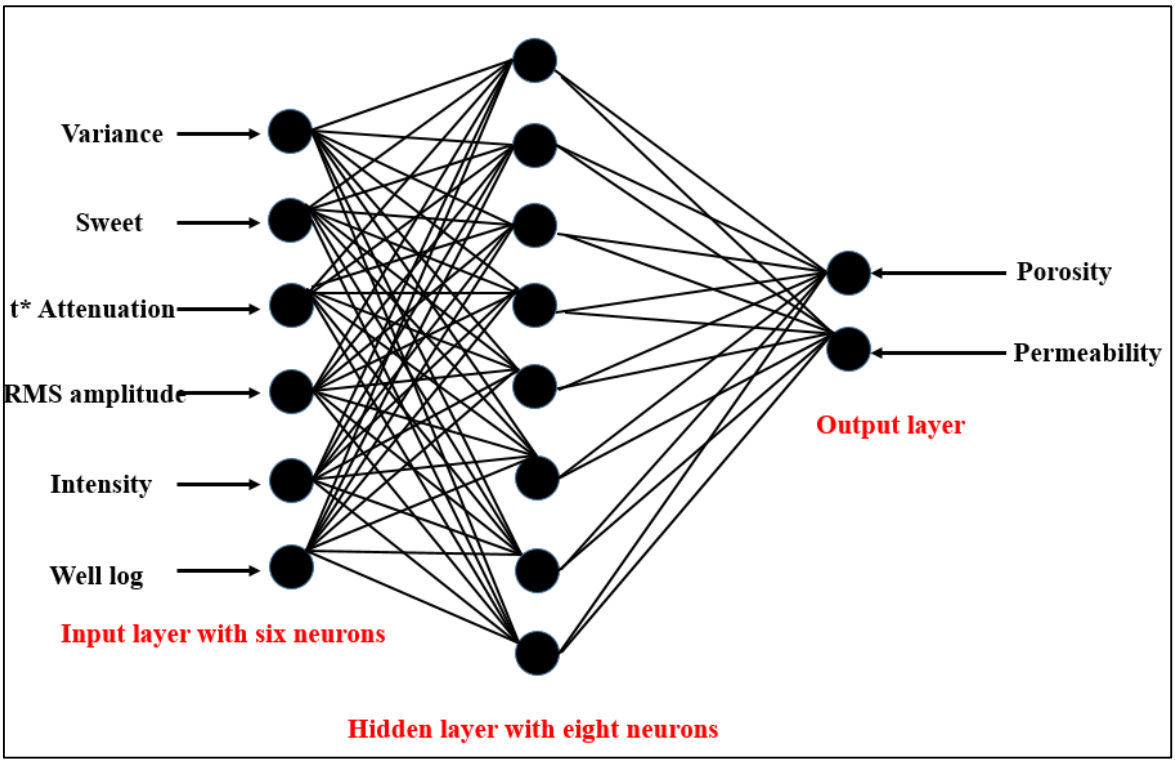

Figure 1.2 The schematic of ANN model for prediction porosity and permeability

The quality of ANN model would be validated using the following formulas:

$$R^2 = 1 - \frac{\sum_{i=1}^{n} (y_{i,sam} - y_{i,pred})^2}{\sum_{i=1}^{n} (y_{i,sam} - \bar{x}_{i,sam})^2} \qquad (1\text{-}1)$$

$$RMSE = \sqrt{\frac{1}{n} \sum_{i=1}^{n} (y_{i,sam} - y_{i,pred})^2} \qquad (1\text{-}2)$$

Where $y_{i,sam}$, $y_{i,pred}$, $\bar{y}_{i,sam}$ are data points from actual numerical values, the prediction values by the neural network, and the average of actual data, respectively.

1. 2. 2. Geostatistical modelling

1. 2. 2. 1. Object-based modelling

Object-based modeling is the algorithm to represent each facies unit. More specifically, the object is a template of cells that contain two main facies types: background floodplain and channel sand. The impermeable background floodplain (usually shale), which defined as the matrix within which the *sand* objects embedded. The channel sand considered to be the best reservoir quality due to the relatively high energy of deposition and consequent coarse grain size (Shmaryan and Deutsch, 1999).

The facies type is clearly at well location. The challenge of object-based modeling schemes is honoring an abundance of local well data. Thus, the iterative procedure adopted in the fluvial object modeling process is very efficient (Deutsch and Tran, 2002). The significant parameters of channel objects are Width, thickness, orientation, amplitude, and wavelength (**Figure 1.3**).

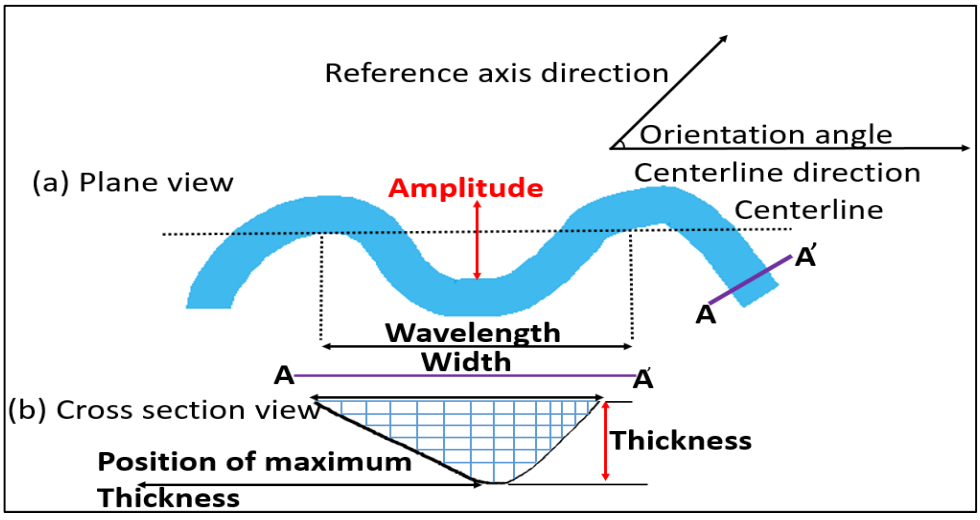

Figure 1.3 The major parameter for channel object (Deutsch and Tran, 2002)

1. 2. 2. 2. Sequential Gaussian Simulation (SGS) and Co-kriging

Petrophysical property modeling is a crucial step in reservoir characterization. It directly influenced by fluid flow simulation (Vo Thanh et al., 2019b). The sequential Gaussian simulation (SGSIM), is the popular geostatistical algorithm for creating stochastic random fields of continuous variables such as porosity and permeability. The SGSIM is more effective than the Truncated Gaussian Simulation because it considers only values within a search neighborhood through the cumulative probability function computation (Al-mudhafar, 2018). The process of conditional simulation combines transforming data into a normal distribution, computing and modeling variograms, and creating properties. This process is used sequentially sampling from conditional distributions. It is defined as the variable at each grid as a random variable following Gaussian distribution (Manchuk and Deutsch, 2012). For the first data points, the SGSIM selects the simple kriging algorithm procedure after the generation of the variogram.

However, the SGSIM then randomly determines the location of estimation is based on the seed number to generate multiple realizations. Moreover, the estimated values are used for the evaluation of the following missing values. Finally, the step by step for the Conditional Sequential Gaussian Simulation can summarize by the following steps (Pyrcz and Deutsch, 2014; Vo Thanh et al., 2019b):

- Change all the original selected data into Gaussian distribution with mean $\mu = 0$ and variance $\sigma^2 = 1$ via the normal score transformation (Z-distribution).
- Generate the variogram for the selected data.

- Select the location of the evaluation randomly through the seed numbers. Calculate the variable value and the related error variance at that location using the simple kriging approach.
- Generate the local conditional cumulative distribution function for the variable at that location for a random selection of the values using that function.
- Repeat the process for all locations of evaluation.
- Repeat all steps for different realizations.

1. 2. 3. Geological Modelling guide to decision

The geological modelling approach developed year by year. The current trend has changed from the comprehensive full-field models to models where a specific goal is to address the decision models (Hellman and T. Hultgreen, 2017). The decision models are necessary for all phases, from appraisal to production optimization. These models need advance modelling techniques and integrated workflows. However, they usually adapted the standard workflow and including all data available. In the development phase, the decision model helps us to place the production and injection wells to maximize the oil production forecast.

In the appraisal phase, the decision model support for well-testing well for production test simulation. Regarding the CO_2 storage feasibility project, the decision models support to address the critical question such as storage capacity, plume migration, and CO_2 leakage (Hellman and T. Hultgreen, 2017). Also, the porosity and permeability models play an essential role in the investigation of the CO_2 storage project. However, the uncertainty of these models is always presented in the geological modelling workflow. Thus, our study

proposed an integrated modelling workflow to reduce project risk and to enhance the optimization process. Figure 1.4 shows the modelling workflow proposed in our research.

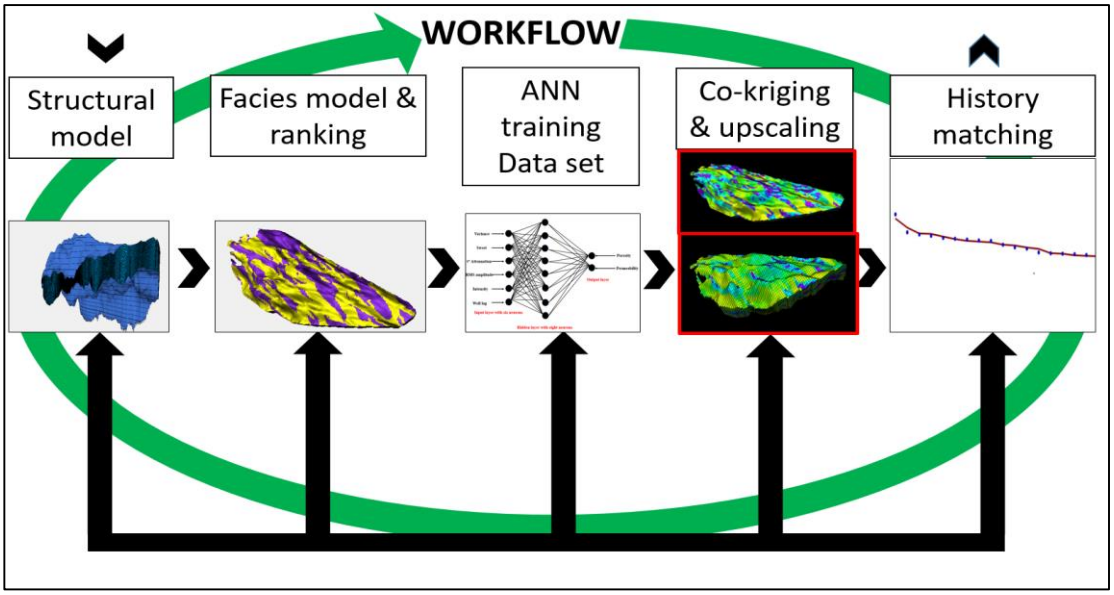

Figure 1.4 The integrated modelling workflow (Vo Thanh et al., 2019b)

1. 2. 4. CO_2-Water-Alternating-Gas (WAG) sequestration process

WAG injection is a popular Enhanced Oil Recovery (EOR) technique. This method entailed injecting a slug of gas into the reservoir alternated by water. The gas-injected dissolution in oil could reduce hydrocarbon viscosity and increase recovery. In contrast, water flooding is used to control the stability of CO_2 front, improve sweep efficiency throughout gas flooding, decrease gas mobility ratio, and prevent CO_2 channeling (Christensen et al., 2001). The WAG process optimization for EOR minimizes the total amount of gas injection is required to dissolve hydrocarbon (Song et al., 2014). Recently, the WAG technique has employed to enhance oil recovery and carbon storage because of its capability to strengthen macroscopic and microscopic sweep efficiencies in petroleum reservoirs (Zhong et al., 2019). Also, geochemistry occurs during WAG injection into reservoir formations, and thus CO_2 can be sequestered. Even though numerous chemical

reactions are associated with WAG injection into reservoir formations, we ignored the geochemistry consideration, which means the mineral trapping did not consider during the simulation. Mineralization is a prolonged thermodynamic process. It can take hundreds to thousands of years or more to complete (Bachu et al., 1994).

Moreover, we had run hundreds of simulations to find optimal solutions. If we include the geochemistry, the simulation time would be computationally prohibitive. Thus, we investigated the effective enhancement of solubility, and residual trapping observed during WAG optimization for CO_2 sequestration. This enhancement could potentially offset the costs of water injection by optimizing the alternating cycles of injection. One WAG cycle is defined as a complete cycle of CO_2–water injection (Zhang and Agarwal, 2013).

Figure 1.5 illustrates the schematic of WAG operations. The red and dark blue blocks represent CO_2 and water injections, respectively, and the width of blocks indicates the injection period (Vo Thanh et al., 2020).

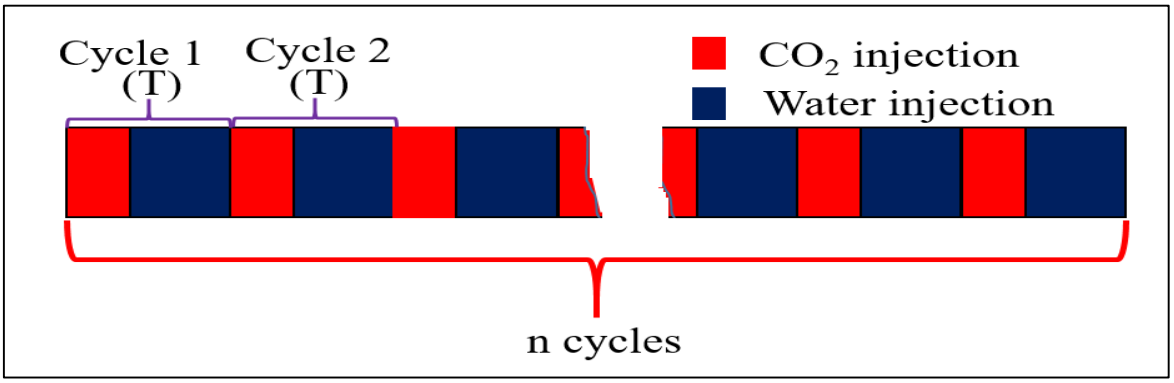

Figure 1.5 Illustration of the WAG process (Vo Thanh et al., 2020)

1. 3. Research objectives

The objective of this dissertation to develop an efficiency multi-task for optimization CO_2 trapping of fluvial sandstone in the Nam Vang field, Cuu Long Basin. These general objectives aim to follow specific goals:

1. To generate the reasonable geological model with limited data
2. To propose an efficient method for prediction porosity and permeability model
3. To evaluate the role of rock types (facies model) for improving the accuracy porosity and permeability model
4. To demonstrate the vital role of geological uncertainty in CO_2 sequestration project
5. To develop the optimization framework from static modelling to dynamic simulation for CO_2 geo-sequestration using the WAG process.

1. 4. Dissertation outline

This study focuses on the connection between integrated geological modelling and reservoir simulation for CO_2 sequestration. This dissertation composes of six chapters which highlighted as follows:

Chapter 1 introduced the motivation and background of research and showed the main goals of this dissertation.

Chapter 2 includes the literature review of CO_2 sequestration modelling, geological uncertainties, robust optimization workflow, and the geological characteristic of the Nam Vang field. An overview of target formation introduced here. The available subsurface characterization data sets presented.

Chapter 3 explains the procedure of the integrated geological modelling workflow of fluvial sandstone at the Nam Vang field, Vietnam. The modelling framework used in this

research comprises: (1) building a structural model to display zones, and layering of reservoirs; object-based modelling for facies distribution; (2) predicting porosity and permeability models using ANN, (3) constructing a 3D petrophysical model through SGS and co-kriging to integrate the prediction porosity, permeability, and facies models; (4) history matching to validate the accuracy of the porosity and permeability models. Finally, the conventional and integrated workflow compared to a demonstration of the useful new modelling workflow. This chapter was published from **Energy Resources, Part A: Recovery, Utilization, and environmental effects and International Journal of Greenhouse Gas Control** (Vo Thanh et al., 2019d, 2019a).

Chapter 4 introduces the field scale simulation of CO_2 sequestration. This chapter explains the importance of WAG injection for CO_2 sequestration. The simulation scenarios will conduct to demonstrate the effectiveness of WAG techniques. The simulation result of base case WAG injection will use for the innovative optimization workflow in **Chapter 5**.

Chapter 5 presents the robust optimization for the WAG process under geological uncertainties. Multiple geological realizations were created for the optimization process. This chapter introduces the full ranking geological realizations by integrating geological modelling and reservoir simulation in a single workflow. Then, these ranking realizations adapted for nominal and robust optimization. The comparison of two optimization workflow demonstrated the role of geological uncertainties in CO_2 sequestration assessment. The robust optimization led to 90% enhanced total CO_2 trapping. This chapter was published from **Journal Natural Gas Science and Engineering** (Vo Thanh et al., 2020)

Chapter 6 summarizes the main finding of this study and the direction of future work.

CHAPTER 2

LITERATURE REVIEW

2. 1. Geological Modelling of CO_2 sequestration

Geological modelling is an essential tool to include the geometry of geological bodies and their reservoir properties (Johnson, 2009). This tool supports dynamic simulation of CO_2 sequestration in the subsurface (Eigestad et al., 2009). In order to perform the reservoir simulation, reasonable models need to consider. Also, the CO_2 storage sites are limited subsurface datasets due to the cost projects. This challenge could solve by integrating the available subsurface pieces of information to construct the model representing the geometry and properties in a consistent system (Kaufmann and Martin, 2008; Wu et al., 2005).

On the other hand, the geological models play an essential role in coupling fluid-flow simulation and seismic inversion modelling. Also, the results of static models could employ for predicting the CO_2 migration and trapping capacity in subsurface formations (Shogenov et al., 2017). Moreover, the geological modelling could reproduce the petrophysical distributions, faults, fractured in storage sites.

Francu et al., (2017) utilized the geological modelling to assess the potential CO_2 sequestration in Abandoned Oil and Gas Field LBr-1 in the Vienna Basin. These authors have drawn clear pictures about subsurface models in depleted reservoirs to determine the maximum possibility of CO_2 storage. Recently, Alcalde et al. (2014) integrated seismic, well log, and regional data to generate the 3D models of Hontomín CO_2 storage site, Spain. These authors could estimate the maximum theoretical CO_2 storage capacity of 5.85 Mt.

They expected that the high-quality geological model could use in the development of future CO_2 storage projects.

Furthermore, geological heterogeneities are a substantial impact on CO_2 storage sites. Issautier et al. (2013) conducted the modelling of CO_2 injection in fluvial reservoirs by emphasizing the effect of heterogeneities on CO_2 storage capacity and performance.

They changed the distribution of facies distribution in the reservoir model. However, these authors did not mention the effect of geostatistical modelling in their studies. In the most recently, Nguyen et al.,(2017b) applied the geostatistical modelling to support for CO_2 storage evaluation in Deep saline aquifers, Ordos basin, China.

They used the two-point and object-based to produce the facies model in meandering depositional environment. Lately, (Nguyen et al., 2017a) performed the sensitivity analysis of CO_2 storage using object-based modelling. They found that the geometry channel had a strong influence on CO_2 plume migration. Therefore, the geostatistical modelling is necessary for CO_2 storage assessment. Besides, the geologic model could improve by basin-scale modelling. Mehnert et al.,(2014) adapted the basin-scale modelling to estimate the CO_2 trapping in the basal sandstone of the Illinois Basin. They can found the pressure drop during CO_2 injection on a large scale. In this storage site, 56% of the injected CO_2 is trapped via residual trapping. 15% of injected CO_2 is trapped via dissolution trapping, while 29% remain as mobile trapping. Recently, Hsieh et al. (2017) proposed a multi-sequestration shale-sandstone-basalt system. They used TOUGHREACT to perform reactive geochemical transport. The simulation results are indicated that the mineral sequestration in the multi-system is quicker than in the shale-sandstone system.

These findings suggested that the long-term trapping could be improved by rapidly fix carbonate minerals in the shale-sandstone-basalt system. Furthermore, March et al. (2018) conducted the CO_2 storage assessment in naturally fractured reservoirs. These authors utilized the dual porous system to evaluate the CO_2 storage performance in the fracture-matrix grid cell. The results illustrated that the CO_2 trapped mostly in the fracture grid.

This study proved that naturally fractured reservoirs are potential CO_2 storage sites in the future. However, these fractured zones are easy to allow CO_2 to leak back to the surface. Therefore, modelling CO_2 leakage is vital in any storage site. Vialle et al. (2016) used TOUGH2 to conduct the multi-phase flow simulation of CO_2 leakage in a fractured cap-rock. These authors found that the effective permeability controlled the hydrodynamic of the leakage and considering as the mitigation strategies.

Also, the sensitivity of relative permeability and capillary pressure could be enhanced the evaluation mitigation strategies in a fractured cap-rock. However, these authors conducted the simulation in a short time. The leakage assessment is needed to investigate in a longer time.

Miocic et al. (2019) conducted the 420000 years assessment of fault leakage rates in geological Carbon storage sites. In the CCS project, CO_2 must be retained for 10000 years to be useful as mitigation tools. In order to reduce CO_2 leakage, we must consider the best candidates to inject CO_2 in the subsurface. Geological modelling is a suitable tool to solve this issue. Geological models support for measurement, monitoring, and verification. Therefore, geological modelling workflow needs to develop to enhance the realistic models in CO_2 storage sites. Lawton et al. (2019) developed the geostatic model for CO_2 injection at the Field Research Station, Southern Alberta, Canada. They investigated the static and

dynamic CO_2 storage capacity in the field. Also, these authors used the seismic method to observe the CO_2 plume shape in storage formation.

In most recently, geostatistic methods are standard in constructing the 3D models for CO_2 Storage capacity in depleted reservoirs (Zhong and Carr, 2019). This study built the 3D static model to evaluate the CO_2 storage potential in the Jacksonburg-Stringtown oil field, West Virginia, USA. The estimated theoretical CO_2 storage capacity for this field varies from 24 to 383 million metric tons. The evaluated results of CO_2 sequestration indicated that the Jacksonburg-Stringtown oil field has potential for CO_2-EOR and storage projects. Furthermore, Artificial Neural Networks (ANN) is a useful approach to support for geological modelling aspect. Integrating Artificial Neural network methods and geostatistical techniques could improve 3D geological modelling in the subsurface. Esmaeilzadeh et al. (2013) used ANN and geostatic to enhance the 3D porosity model in one of Iran's oil field. They applied the ANN to create the transformation between the well log and core measurement. Then, these results will be employed to distribute 3D porosity models using geostatistical approaches. Also, ANN was used to build the porosity and permeability models in the fractured granite reservoir. Nguyen et al. (2014) employed ANN to predict the petrophysical accuracy models in granite reservoirs.

Later, Vo Thanh et al., (2019c) developed the integrated workflow to construct the 3D geological models to evaluate the CO_2 storage potential in fractured granite reservoirs, Cuu Long Basin, Vietnam. Thus, this study was adapted the ANN and geostatistic methods to develop the effective modelling workflow in fluvial sandstone reservoirs.

2. 2. Geological uncertainty

Geological uncertainty is necessary for modelling and simulation in CO_2 sequestration sites. Notably, the limitation of subsurface datasets is the increasing geological uncertainties of geological models. Therefore, geological uncertainties will create a barrier to precisely the future reservoir performance and negatively impacts the economic aspect (Al-Mudhafar, 2016). Thus, geological uncertainty plays an important role in CO_2 sequestration studies. Uncertainty analysis is a useful tool to investigate the geological uncertainty in the subsurface. Li and Zhang (2014) proposed the experiment design and response surface analysis to evaluate the long-term leakage risk for the Nugget Sandstone in Moxa Arch, Wyoming. Also, the Latin Hypercube and ANN was used for surrogate modelling to optimize the geological CO_2 storage (Pan et al., 2014).

This study generated multiple realizations of porosity and permeability to represent the uncertainty in geological models. Dai et al. (2014a) proposed the integrated framework for CO_2 sequestration and Enhance Oil Recovery. The uncertainty parameters were used to determine the objective functions using Monte Carlo Simulation. Sarkarfarshi et al. (2014) conducted a sensitivity analysis for CO_2 geo-sequestration.

They found that reservoir porosity, residual brine saturation, and capillary pressure are the most influential factors in the uncertainty of CO_2 plume migration. Jia et al., (2018) utilized the Polynomial Chaos Expansion for uncertainty qualification of CO_2-EOR and storage project. The uncertainty of porosity and permeability was considered for forecasting CO_2 storage capacity. Furthermore, Temitope et al. (2016) used the experimental design for uncertainty analysis and optimization of CO_2 trapping in saline aquifers. They determined the residual and solubility trapping index in the PUNQ-S3 models. These authors provide

the most influential factor in CO_2 trapping capacity to decide with less risk and more confidence. Besides, Heath et al. (2012) considered the geologic heterogeneity and economic uncertainty for subsurface Carbon Dioxide Storage. They proposed the novel average scheme of CO_2 injection using geological realizations of porosity and permeability properties. Also, this study included the costs of operation of injection wells in the Mount Simon formation in the Illinois basin, USA. This result is indicated the costs of CCS projects could be sensitive to geological heterogeneity.

Moreover, Si Le et al. (2017) considered geological uncertainty for their evaluation CO_2-EOR and storage performance using the Water Alternating Gas process. These authors found that geological uncertainty is also affecting CO_2-EOR performance and the Net Present Value of CCS projects. Also, Demsey et al. (2015) reduced the uncertainty of geological CO_2 storage using a large number of permeability realizations. They simulated CO_2 injection/brine production for many realizations of permeability models and collecting ensemble results as an uncertainty bracket log for the correct outputs. These authors confirmed that dynamic uncertainty reduction by new data assimilation using the Bayesian approach.

For enhancing residual and solubility trapping, geological uncertainty strongly affects the performance of controlled injection schemes in aquifer property distribution (Shamshiri and Jafarpour, 2012).

Lately, Ma et al. (2019) used Ensemble Kalman Filter considering the uncertainty hydraulic aquifer properties for predicting CO_2 plume migration from monitoring data. Recently, Chen et al. (2020) applied the data assimilation method to reduce geological uncertainty in predicting CO_2 plume migration, CO_2 leakage through a wellbore. These

authors demonstrated the crucial role of geological uncertainty in storage sites. For optimization project, many authors considered geological uncertainties for their studies such as SAGD operation (Yang et al., 2011); optimal well positioning (Jin et al., 2015); CO_2 plume characteristic (Jeong and Srinivasan, 2016); CO_2 low salinity water alternating Gas (Dang et al., 2016); CO_2-EOR and storage (William Ampomah et al., 2017); Water flooding and risk management (Siraj et al., 2016); Microbial Enhanced Oil Recovery (Ansah and Vo Thanh, 2020),

Besides, the surface characterization of a deep saline aquifer is poorly defined, finding the optimal solutions under geological uncertainties are strongly recommended for CO_2 sequestration (Petvipusit et al., 2014).

2. 3. Optimization of CO_2 sequestration

For enhancing the CO_2 storage performance, it is necessary to define the optimal design factor that impacts the CO_2 injection process in the subsurface. For the CCUS project, two goals must achieve: CO_2 flooding performance to improve the feasibility of the Enhanced Oil Recovery project and CO_2 storage performance to optimize the reduction of greenhouse gas emission (William Ampomah et al., 2017; Balch and McPherson, 2016).

Many researchers investigated the co-optimization of CO_2-EOR and storage (Ettehadtavakkol et al., 2014; Forooghi et al., 2009; Van't Veld et al., 2013; Wang et al., 2018a). However, some of these works used limited data or sector models.

There are many approaches to the optimization process. Recently, several studies in petroleum engineering to focus on using neural network for their optimization studies (Amini and Mohaghegh, 2019; Dai et al., 2014b, 2014a; Dang et al., 2020; Ertekin and Sun,

2019; Kim et al., 2017; Sina Hosseini Boosari, 2019). Also, reservoir simulation simulators are useful tools for evaluating the CO_2-EOR and storage performance in the subsurface. However, petrophysical parameter and rock-fluid measurement uncertainties are strongly affected by reservoir simulation results (William Ampomah et al., 2017).

The geological uncertainties could be reduced using a history matching process and considering the operational parameters in reservoir performance simulation (W. Ampomah et al., 2017).

Therefore, the optimization approaches under geological uncertainties are necessary for CO_2-EOR and storage projects. Recently, optimization under geological uncertainties was adopted in many studies. To decreasing the uncertainties and improving the possibility of a successful project, robust optimization has used to solve the challenge of geological uncertainties in subsurface studies.

For unconventional reservoirs, robust optimization workflow used to enhance the NPV value and oil production performance (Nguyen et al., 2016; Yang et al., 2011). In the low salinity waterflooding project, Dang et al. (2017) proposed the workflow for history matching and robust optimization under geological uncertainties. This study was demonstrated that robust optimization could be employed to decrease uncertainties in low salinity water injection optimization based on well placement. Later, Dang et al. (2018) adapted the robust optimization workflow for alkaline-surfactant-polymer flooding in the EOR process. These authors found that the robust optimization workflow could increase the NPV project and reducing the geological uncertainties. In CO_2- Gas-Assisted Gravity Drainage process, Al-Mudhafar et al. (2018) proposed the robust optimization of CO_2 flooding under geological uncertainties in a fluvial reservoir. This study was stated the

robust optimization workflow resulted in higher oil production and net present value than nominal single realization optimization. Regarding the robust optimization of CO_2 sequestration, Shamshiri (2012) considered 100 geological realizations during controlled CO_2 injection for improving residual and solubility trapping in heterogeneous reservoirs. Also, Petvipusit et al. (2014) proposed a robust objective function for CO_2 sequestration. They suggested the new formulation of economic criteria for optimizing the CO_2 injection rates. The simulation study of the proposed method was indicated the effectiveness of robust optimization of CO_2 sequestration under geological uncertainties.

Regarding the injection strategies for optimization CO_2-EOR and storage, Ghaderi et al. (2012) applied the WAG process for CO_2-EOR storage in a tight oil reservoir using an experimental design approach. They considered the WAG ratio and CO_2 slug for their optimization process. The optimization of WAG parameters was provided the highest oil recovery, storage, and net present value. Also, Wang et al. (2018b) proposed the economic study for co-optimization of CO_2-EOR and storage using the WAG process. For enhancing CO_2 trapping, Herring et al. (2016) found that the cyclic CO_2 injection is a potential solution to increase residual trapping for geo-sequestration projects.

On the other hand, Al-Khdheeawi et al. (2018a) investigated the enhancement of CO_2 trapping using injection strategies. This study was demonstrated the efficiency of the WAG process. The CO_2 plume migration reduced by WAG injection. Also, this technique could improve the residual and solubility trapping efficiency. Thus, they preferred the WAG process for CCS projects rather than continuous CO_2 injection.

Also, the WAG process was useful for the optimization of CO_2 storage in saline aquifers. Zhang and Agarwal (2013) used TOUGH2 and GA optimizer for numerical simulation and

optimization of CO_2 storage in saline aquifers. They found that optimization of the WAG process could be accelerated the capillary trapping, dissolution trapping, and immobilizing the CO_2 plume in reservoirs. The synergy of robust optimization workflow and WAG process will investigate in detail in this dissertation.

2. 4. General information of study area

Cuu Long Basin (Mekong Basin) is the largest basin, and the most central hydrocarbon producing basin in Vietnam (Bojesen-Koefoed et al., 2009). The Cuu Long Basin constitutes an Early Tertiary rift basin located on the southern shelf of Vietnam, covering an area of approximately 25,000 km² (Hung and Le, 2004). This basin was generated as the result of Indochina's extrusion along Three Pagodas Fault and Red River Fault because of the collision of India to Eurasia during Paleocene (Morley, 2002). The Cuu Long Basin comprises of four main structures (Hung and Le, 2004):

- The Southwest sub-basin discovered at the west-central horst, depression to the east area.
- The Southeast sub-basin: depression with the main structures at the of Central horst
- The Central horst: separated between the Southwest Cuu Long depression and the Southeast Cuu Long depression.
- The Northern sub-basin: contained the trending faults and minor faults in Cuu Long Basin.

Generally, the tectonic evolution history of Cuu Long Basin can divide into several main stages (Schmidt et al., 2019):

- The pre-rift uplift/initial rifting phase found on Late Cretaceous–Eocene

- The main rifting phase/initial ocean floor spreading phase filled with Late Eocene-Oligocene. This phase led to the development of the main structural features within the basins, following extensional and transtensional deformations.
- The regional subsidence/renewed rifting found on Early-Middle Miocene. A change marked this from typically fault-controlled subsidence to thermally controlled, high-rate subsidence.
- The partial inversion/regional subsidence filled with Late Miocene. During this stage, the whole area became dominated by compression, which, in combination with the dextral strike-slip fault system east offshore Vietnam, probably generated basin uplift/partial inversion.
- The regional subsidence/renewed rifting found on Pliocene-Pleistocene. Diverse tectonic activity, from low to moderate-amplitude differential uplift, acted across the basins in the area.

Nam Vang field, the study area, is located in the northwestern margin in the Cuu Long Basin, offshore southern Vietnam, approximately 160 km east of Vung Tau City (Hung Vo Thanh et al., 2019c)

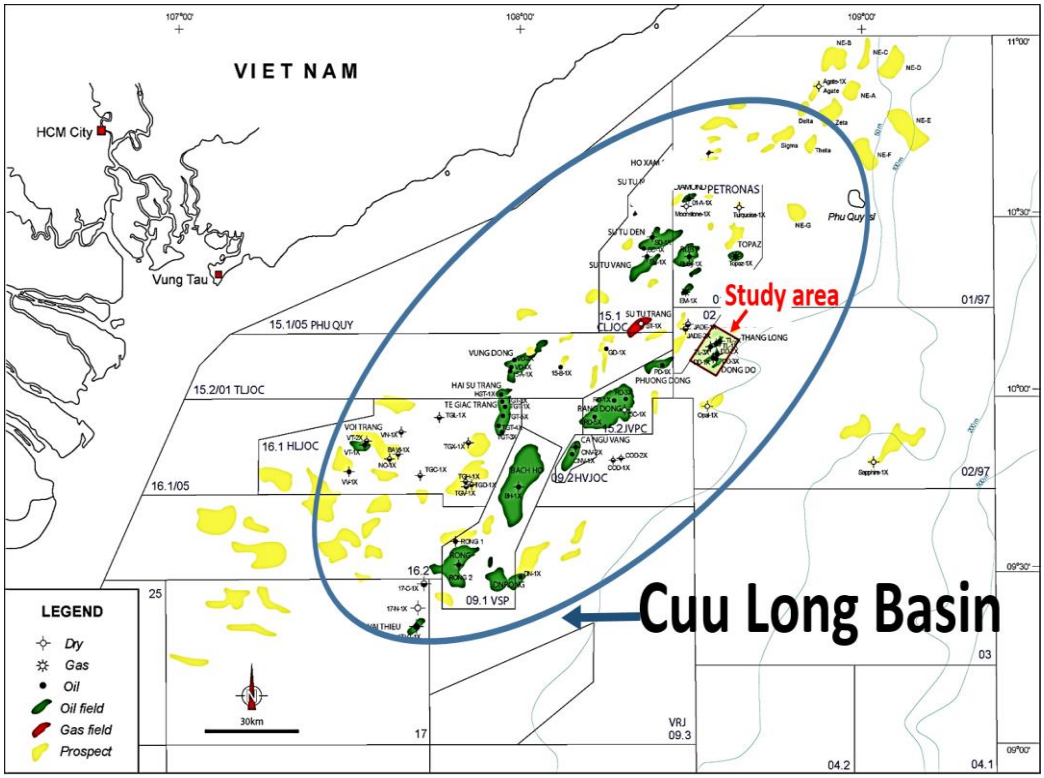

Figure 2.1 The location of Cuu Long Basin and study area (Vo Thanh et al., 2020)

2. 4. 1. Geological overview of Nam Vang field

Generally, the subsurface interpretation of the Nam Vang field is consistent with the regional stratigraphic framework of the Cuu Long Basin. Formation tops have been picked based on the integration of the mud log, wireline log, seismic data, biostratigraphic and petrography analyses from cuttings, sidewall core samples, core samples, and the correlation with the offset wells in the surround Cuu Long Basin. These formations classified as following (Hung Vo Thanh et al., 2019c):

- Pre-tertiary basement
- Lower Oligocene–Lower Tra Tan formation (E sequence)
- Upper Oligocene–Middle Tra Tan formation (D sequence)
- Upper Oligocene–Upper Tra Tan formation (C sequence)

- Lower Miocene–Lower Bach Ho formation (BI.1 sequence)
- Lower Miocene–Upper Bach Ho formation (BI.2 sequence)
- Middle Miocene‑Lower Con Son formation (BII.1 sequence)
- Middle Miocene‑Upper Con Son formation (BII.2 sequence)

However, the basement fractured reservoir and Oligocene sandstone reservoir are the major reservoirs in the Nam Vang field. The fractured basement reservoir is comprised of granite and granodiorite, which are contained metamorphic and volcanic and can divide into two zones. The first zone consists of weathered granitoid with thickness varying from a few meters to tens of meters. The second zone is freshly fractured granite, and these fractures are partly filled mainly by secondary calcite and zeolite.

Some of the dyke rocks are also cut granitoid (Cuong and Warren, 2009). The source rock of the Nam Vang field is lacustrine shale of D and E sequences with a large amount of total organic carbon (TOC) and hydrocarbon index values. These formations also generated the seal for Oligocene sandstone and fractured granitoid basement reservoirs. The general stratigraphic of Nam Vang depict in **Figure 2.2**.

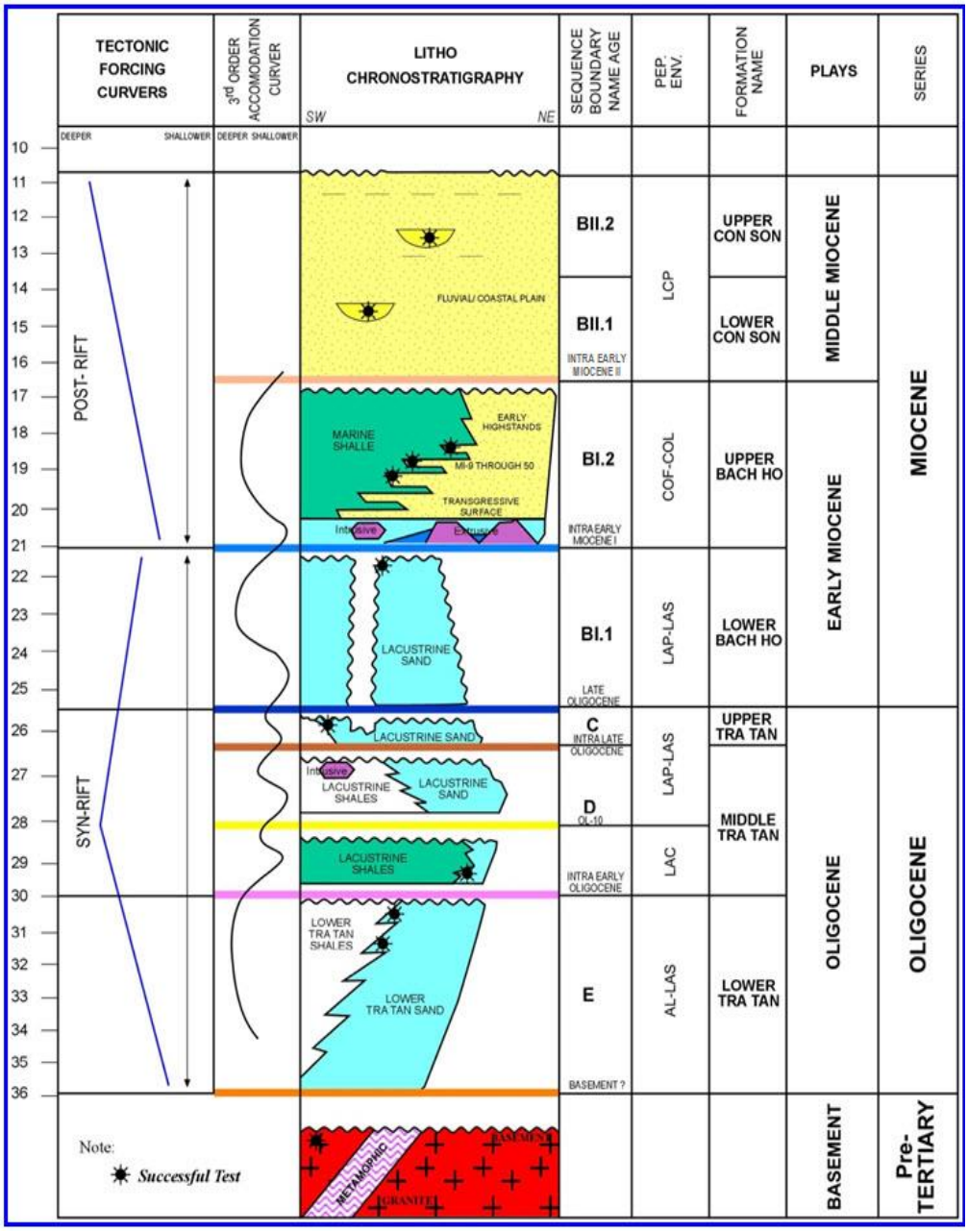

Figure 2.2 The general stratigraphy of Nam Vang field (Vo Thanh et al., 2019c)

This study focuses on the Oligocene sandstone of Tra Tan formation (E sequences). The Late Oligocene sediment source is predominant mudstones with interbedding of sandstones. Depositional environments include fluvial in the southwestern basin to lacustrine in the northeastern basin. **Figure 2.3** shows the general stratigraphic sequences of the study area.

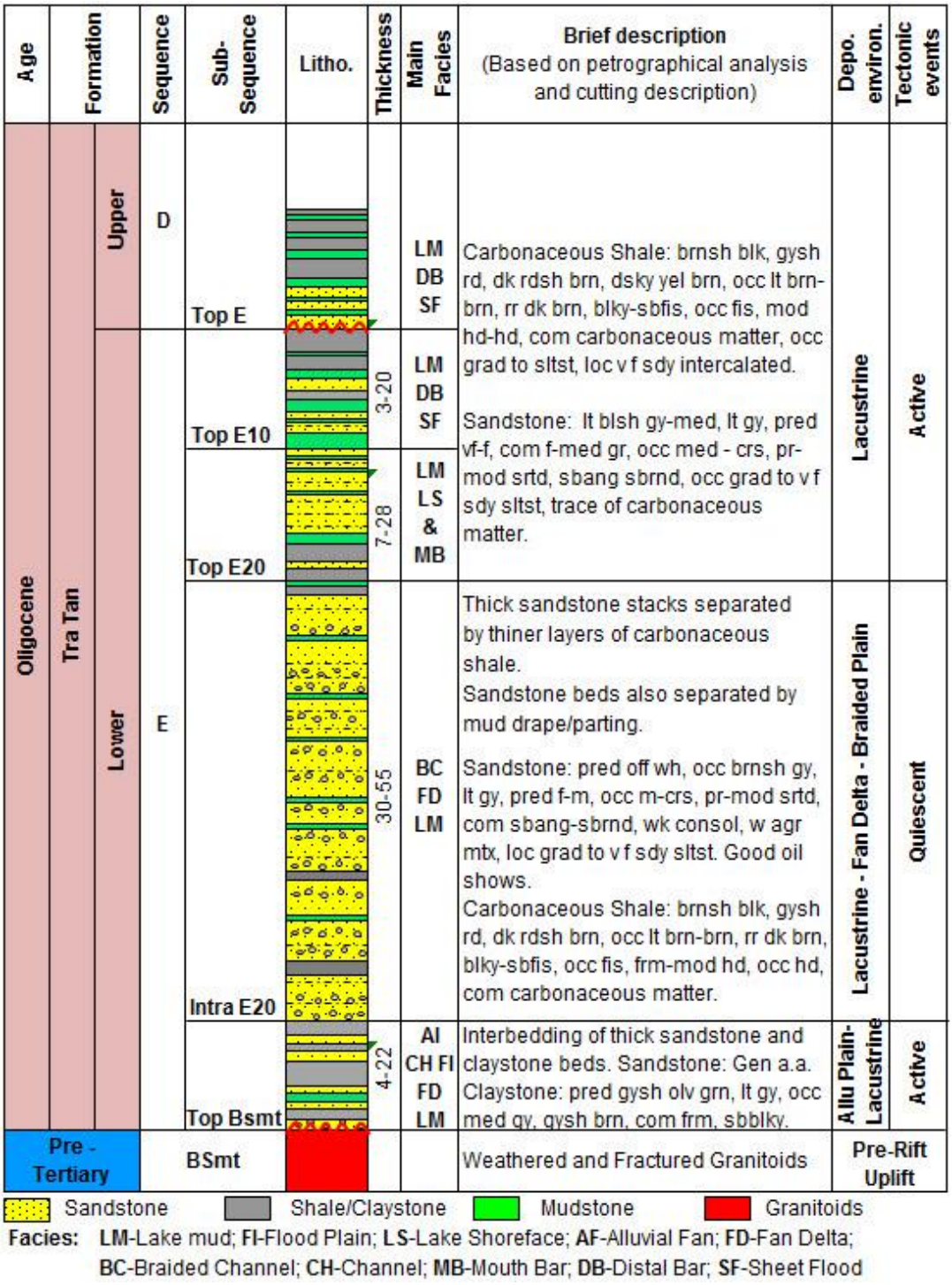

Figure 2.3 The general stratigraphy of study area

2. 4. 2. Data available

This research was used the seismic and well log data to build the reservoir model for CO_2 storage assessment (Vo Thanh et al., 2020). **Figure 2.4** is illustrated some type of data for this study. The list of detail data outline below:

1. Thickness and depth map for main pay reservoirs
2. The three well log data included lithology information and reservoir properties. Three pieces of well log data (NV-1X, NV-2X, and NV-3X) applied in the modeling process.
3. The well-testing measure the bottom pressure from NV-2X well.
4. The production history from three producer wells used to perform history matching through cumulative production and bottom hole pressure data.

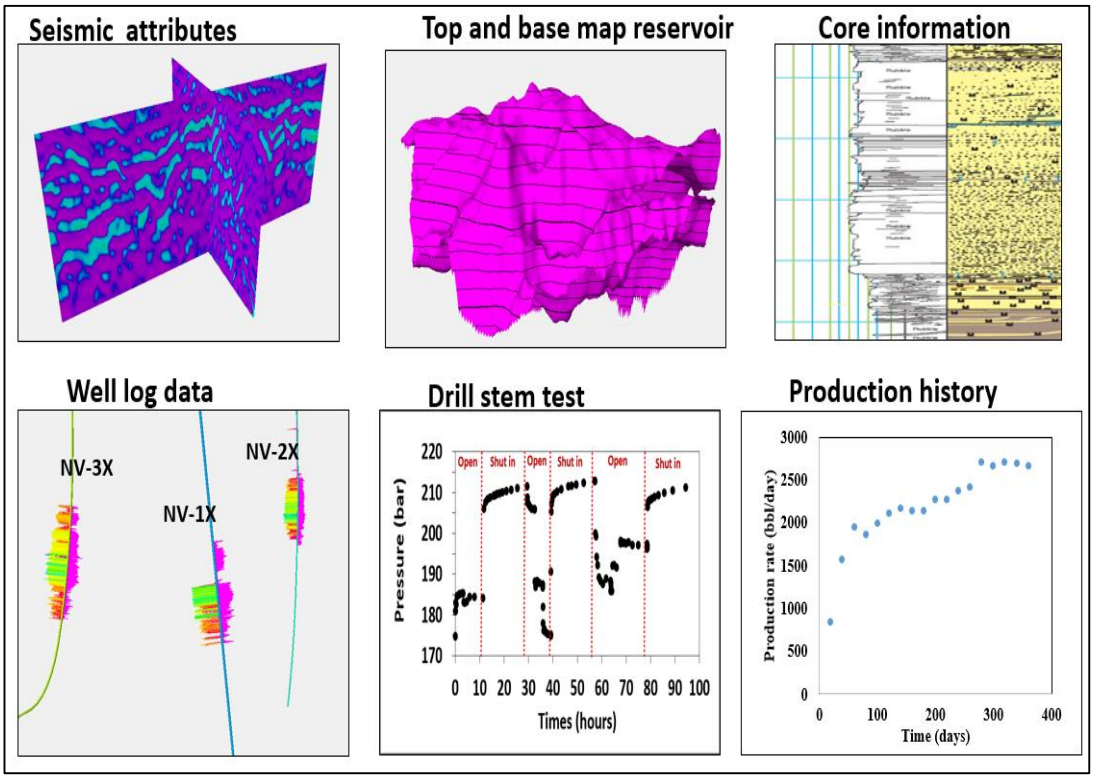

Figure 2.4 Data available for geological construction model

CHAPTER 3

INTEGRATED GEOLOGICAL MODELLING OF FLUVIAL SANDSTONE RESERVOIR FOR CO_2 SEQUESTRATION

3. 1. Introduction

Geological modelling plays a vital role in production hydrocarbon and CO_2 sequestration. The purpose of modelling is to represent the characterization of the subsurface reservoir. Therefore, it is useful for selecting the potential storage sites where could not quickly to obtain from direct observation. Recently, 3D geological modelling has considered an effective tool for investigating CO_2 storage capacity (Nguyen et al., 2017a; Zhong and Carr, 2019). However, these studies proposed the conventional modelling framework for their assessment.

The traditional workflow has focused on a geostatistical method to distribute the 3D porosity and permeability model. The limitation of core data and well data are the main challenge facing the conventional modelling process. Thus, it is necessary to develop the integrated modelling workflow to address the disadvantage of the traditional modelling framework. For this reason, this work proposed the integrated modelling procedure for enhancing more accuracy than the conventional method. This new modelling workflow used an artificial neural network (ANN), geostatistic, and object-based modelling to construct the 3D rock types (facies), porosity, and permeability models. Also, the development of technology has resulted in the deployment of Artificial Neural Network (ANN) effectively forecast porosity and permeability with data limitation (Adibifard et al., 2014; Aminian and Ameri, 2005; Zargari et al., 2013).

Furthermore, the ANN was integrated geostatistical modelling for enhancing modelling process in the granite fracture reservoir (Vo Thanh et al., 2019a). The most common approaches of geostatistical modelling are Sequential Indicator Simulation (SIS) and Sequential Gaussian Simulation (SGS). Generally, SIS applies a variogram or two-point statistical model for facies modelling the different types of reservoirs (Deutsch, 2006; Seifert and Jensen, 2000). Even though it is a flexible method, with requires little parameters. SIS has several limitations to capture the realistic depositional environment. For example, channel forms, length, thickness, and sinuosity (Vo Thanh et al., 2019b). In this aspect, Multi-point statistic (MPS) has proposed as a more efficient approach to representing the geological formation (Guardiano and Srivastava, 1993; Strebelle, 2006; Strebelle and Journel, 2001).

Despite the merits of MPS over SIS, both have two disadvantages: (i) stationarity and (ii) ergodicity (Nguyen et al., 2017b). These demerits are addressed by the object-based method (OBM). Moreover, the OBM can create efficient facies modelling in fluvial channel reservoirs (Georgsen et al., 2009; Holden et al., 1998; Shishmanidi et al., 2014; Vo Thanh et al., 2018). Therefore, OBM was adopted in this study to assign the background facies to model the conceptual model jointly. This method is the first connector between static and dynamic simulation to enhance the accuracy dynamic simulation model (Alpak et al., 2017; Hu and Jenni, 2006; Suzuki and Caers, 2006).

Moreover, for the porosity and permeability modelling, Sequential Gaussian Simulation (SGS) is the most common approach to capture the reservoir heterogeneity (Gringarten and Deutsch, 1999; Pyrcz and Deutsch, 2014). In this study, SGS used for ranking the suitable

rock type (lithofacies) model through the relationship between well log and continuous properties value.

Although the individual merits and lacks the methodologies mentioned above, not much work has considered integration of co-kriging, SGS, ANN, and OBM to capture reservoir heterogeneity during geological modelling. Since geological modelling is still a challenging problem for the CO_2 storage project. Thus, this chapter introduces an integrated workflow to improve the geological modelling process in a fluvial sandstone reservoir in offshore Vietnam. We developed an e – framework (where "e" stands for encapsulated) that employs Artificial Intelligence Neural Network coupled to object-based modelling and geostatistical method (precisely, SGS and co-kriging) to build the realistic 3D geological model for CO_2 sequestration assessment.

3. 2. Research Methodology

We proposed the integrated workflow for enhancement accuracy of geological modelling in storage formations. The procedure of this framework elaborated as follows:

The first step was to construct a structural model from seismic interpretation in the modelling workflow. A high-resolution model with suitable grid cells, zones, and layers considered for the modelling process.

The second step was to create the facies model by using the object-based method. The object-based facies model was represented the fluvial depositional environment in the reservoir. The facies model was construed as a conditional petrophysical model through the SGS technique to select the most suitable fluvial channel distribution. Then, the next step was to generate the seismic attributes based on their correlated coefficients and well log values.

These seismic attributes were further ranked through many trials and testing iterations through ANN training. The number of seismic attributes considered was: Chaos, Dip deviation, Envelope, Ant-tracking, Flatness, Polarity, Genetic Inversion, RMS amplitude, Intensity, Sweet, Variance, Outcrop attributes, t* Attenuation.

The fourth step was to rank the group of seismic attributes for porosity and permeability prediction. In this step, the training data was separated into two parts; 70% used for the training data and the remainder to calculate the error.

The maximum number of iterations and percent error was carefully considered to avoid overtraining during the ANN process. The suitable group was selected through the highest correlation coefficient between predicted and well log values. The predicted and well log values were also visually checked to observe the consistency between them.

If the coefficient values were not high enough, then the seismic attributes were reselected to regenerate new training data. The fifth step was the seismic resampling process to generate the prediction model cube, which illustrates the distribution of predicted porosity and permeability. This step converted the seismic cube into a 3D model. After this, a co-kriging process was adapted to integrate the ranking facies model and predicted ANN values in the 3D petrophysical model.

Then, we can use this model for history matching to compare with conventional modelling workflow. The traditional modelling workflow is shown in **Figure 3.1(a)**. The summary of the integrated modelling workflow is depicted in **Figure 3.1(b)**.

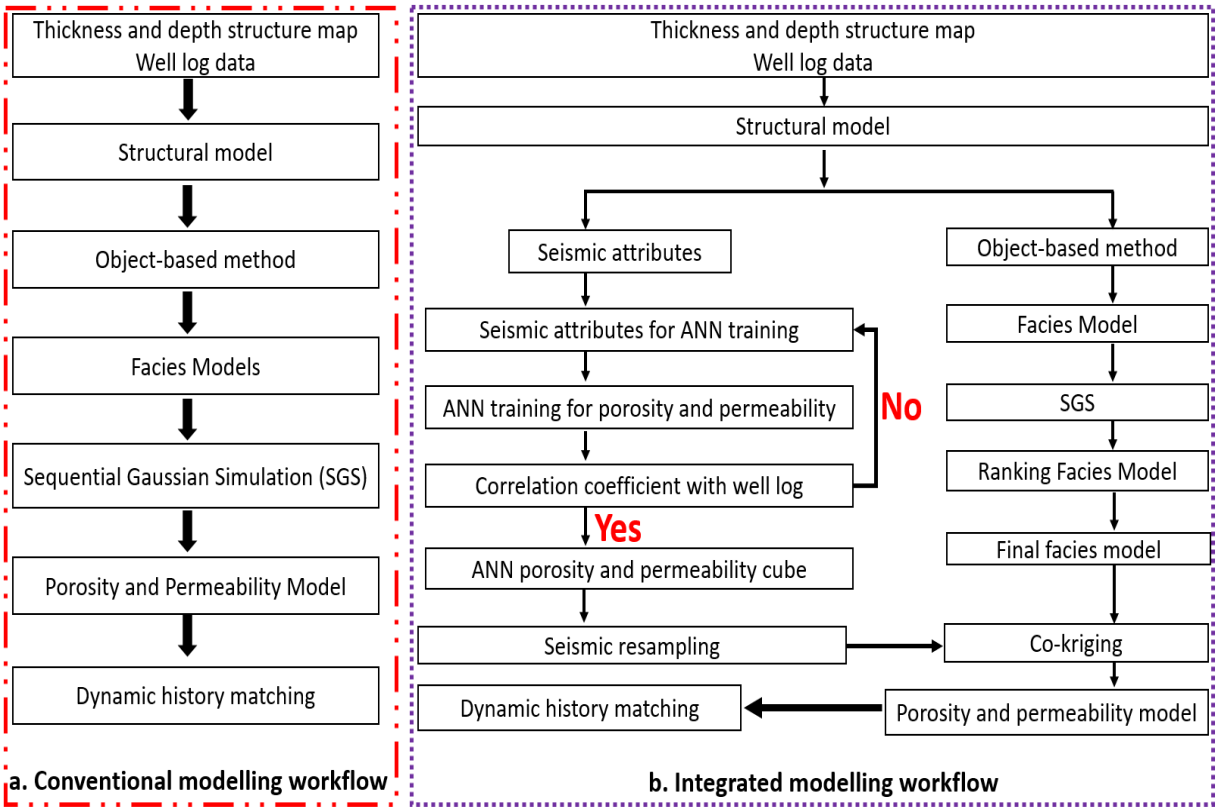

Figure 3.1 Schematic of modelling workflow for this study

3. 3. Result and Discussion

3. 3. 1. Structural modelling

The first step in constructing the 3D geological model was structural modelling. The structural model represented the setting of the geosystem for the reservoir to be used for the static and dynamic geological model. The structural model is constructed on top and base horizons of the reservoir. Subsequently, the pillar gridding was conducted based on the skeleton framework.

The skeleton is a grid consisting of a top, middle, and base skeleton grid. The selected dimensional of each grid in the corner gridding was 25 m × 25 m. The structural model of fluvial sandstone is depicted in **Figure 3.2**.

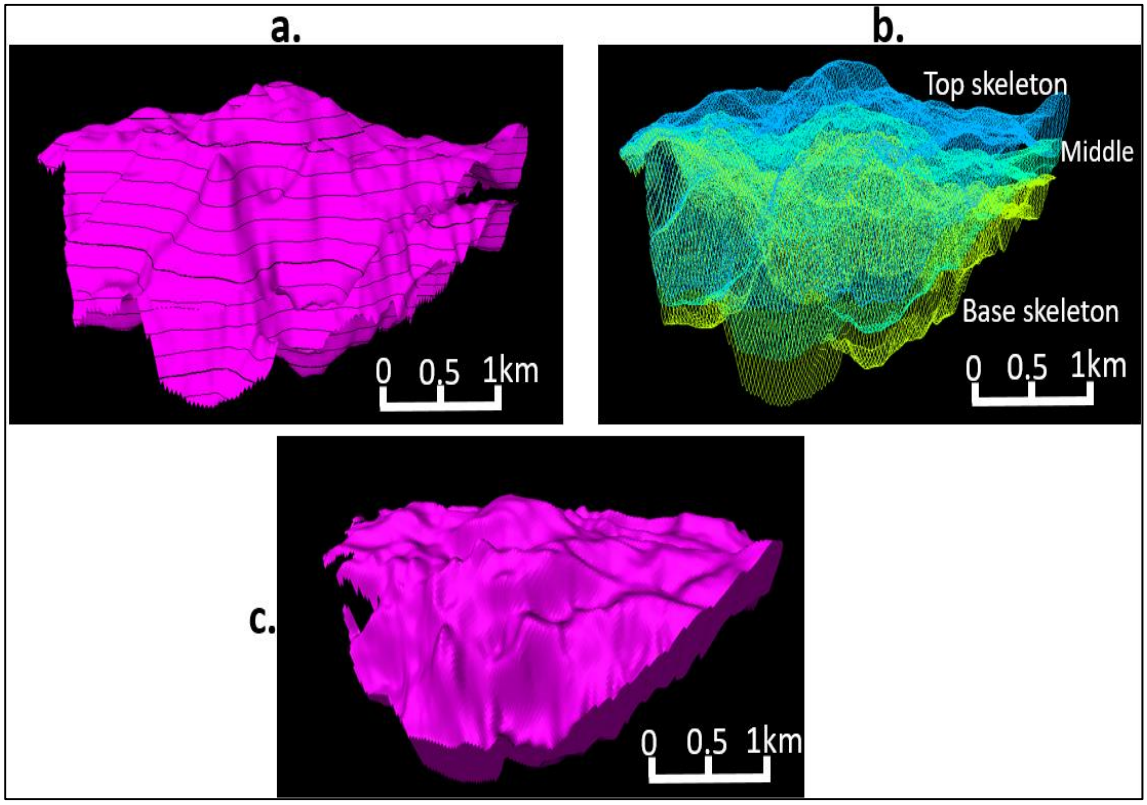

Figure 3.2 Structural modelling process of fluvial sandstone reservoir. (a) top and base horizons. (b) The skeleton grid. (c) final structural model

The number of grids cells in X direction was 148, and in Y direction was 176. To create a more realistic geological model, the reservoir was divided into 100 layers to have approximately 1 m depth for each layer. Therefore, the number of grids in the Z direction was 100 grid cells. The final structural model had 2,604, 800 grid cells—this extensive grid system allowed representing the fluvial channel sandstone reservoir with high accuracy.

3. 3. 2. Object-based modelling

The OBM was adapted to construct 3D lithofacies distribution for the Oligocene formation. Before evaluating the accuracy of the 3D lithofacies for the Oligocene structure of the Nam Vang field. The depositional environment was considered for the reservoir. The depositional environment studies indicated that Oligocene formation was a meandering fluvial system. The well log data was upscaled to apply geostatistical modelling for lithofacies and petrophysical properties (**Figure 3.3**). The well log upscale was conducted to increase the size of logs that follow the grid cell size.

Then, the object-based method was used for 3D lithofacies simulation to represent the most reliable depositional environment and geological heterogeneity. The geometry of the channel had the same characteristic of the depositional environment of studied formation used for object-based modelling. **Table 3.1** highlights the main parameters and value of lithofacies, as considered for the modelling (Vo Thanh et al., 2019c).

In this work, the lithofacies model was simplified by grouping the channels, crevasses, and leeves into one channel sand, while the background shale became the shale facies.

Figure 3.4 depicts the model with channel sand and floodplain shale facies. The facies model is the main conditional geological factor in petrophysical modelling.

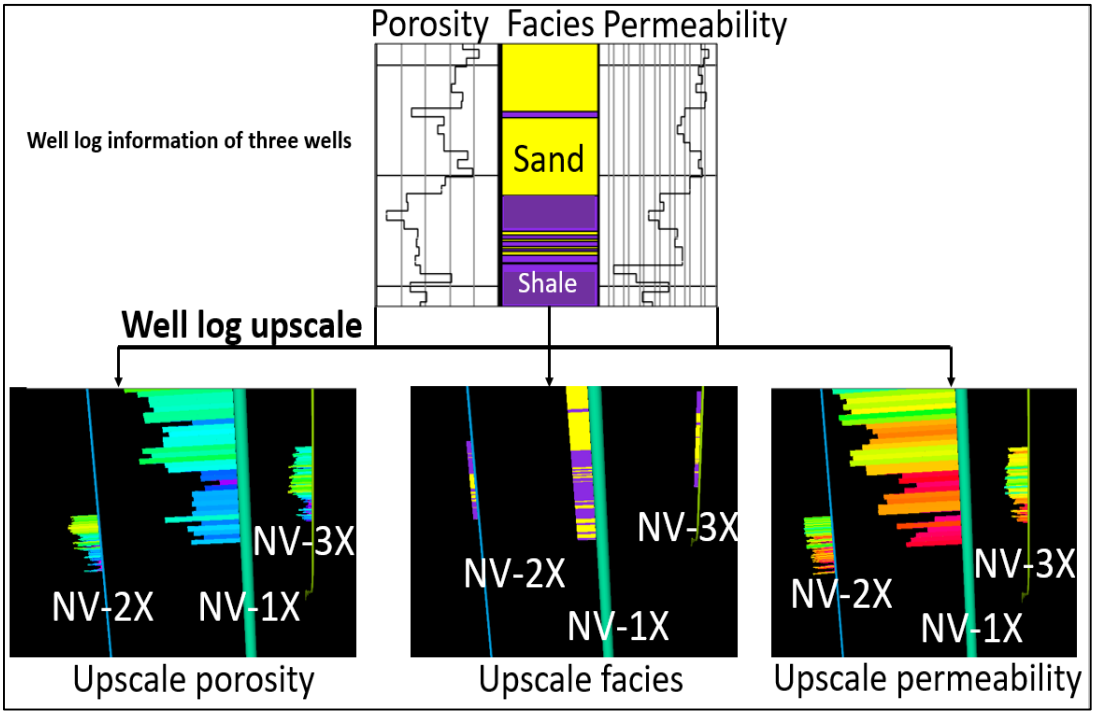

Figure 3.3 Well log upscale for facies and petrophysical modelling

Table 3.1 Input parameters used for lithofacies modelling

	Min	Mean	Max
Orientation		60	
Channel amplitude (m)	400	600	800
Channel wavelength (m)	1200	1700	2200
Channel width (m)	150	300	450
Channel thickness (m)	10	15	20

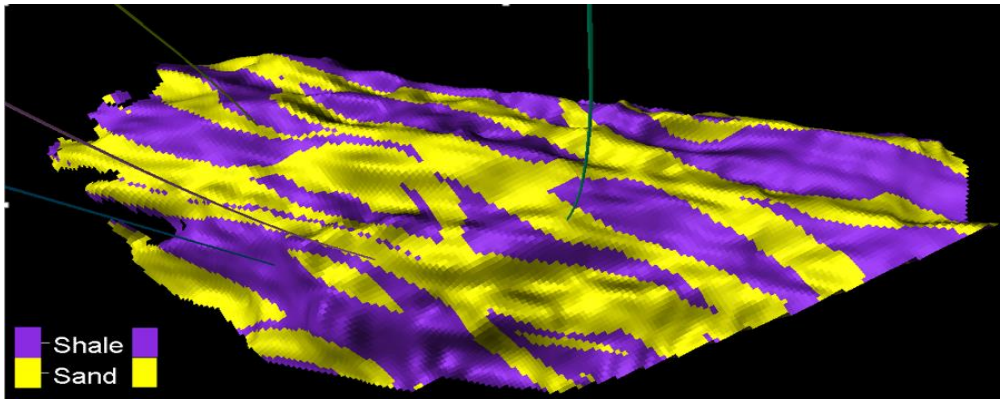

Figure 3.4 Facies model build from Object-based method (Vo Thanh et al., 2019b)

3. 3. 2. 1. Conventional Petrophysical Modelling Result

The Sequential Gaussian Simulation used for 3D porosity and permeability distribution after the object-based modelling. The object-based facies modelling was conditioned for the petrophysical model to preserve the character of fluvial reservoirs.

Figure 3.5 depicts the porosity, horizontal, and vertical permeability given object-based modelling. These models represented the channel distribution through conditioning lithofacies. This process used for ranking multiple facies model in the integrated modelling workflow.

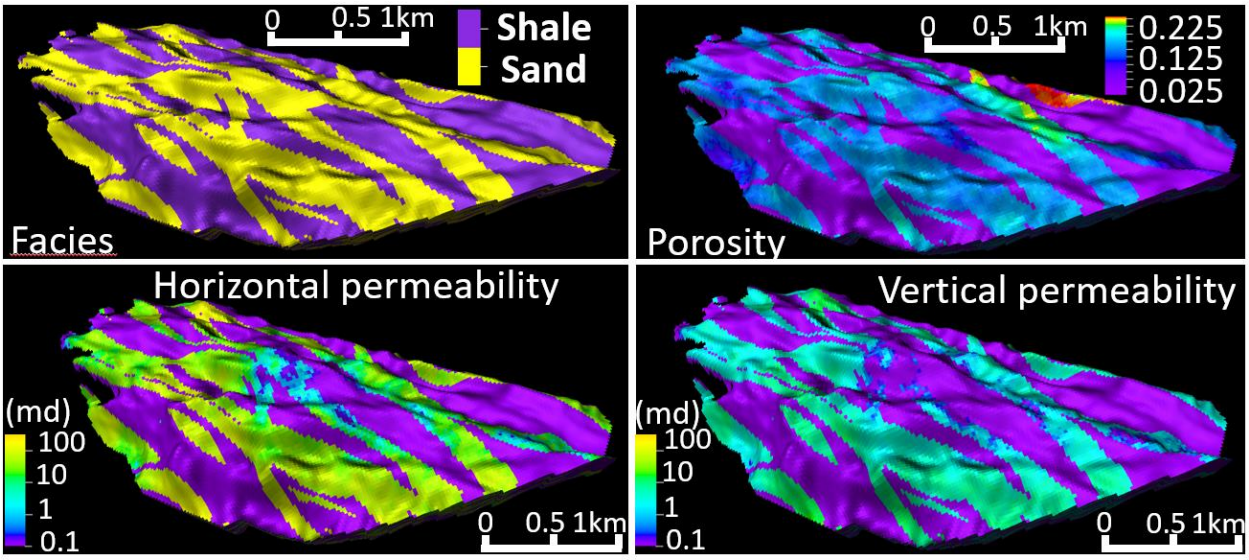

Figure 3.5 The result of porosity and permeability model using conventional modelling workflow (Vo Thanh et al., 2019b)

3. 3. 2. 2. Ranking facies

Multiple geological realizations generated to determine the true lithofacies to condition for porosity and permeability model. The seed number was changed randomly to create a large

number of realizations for cross-validation. This seed number can change the distribution of channel forms in the facies model. **Figure 3.5** highlights the example of the geological realization created to validate the object-based model.

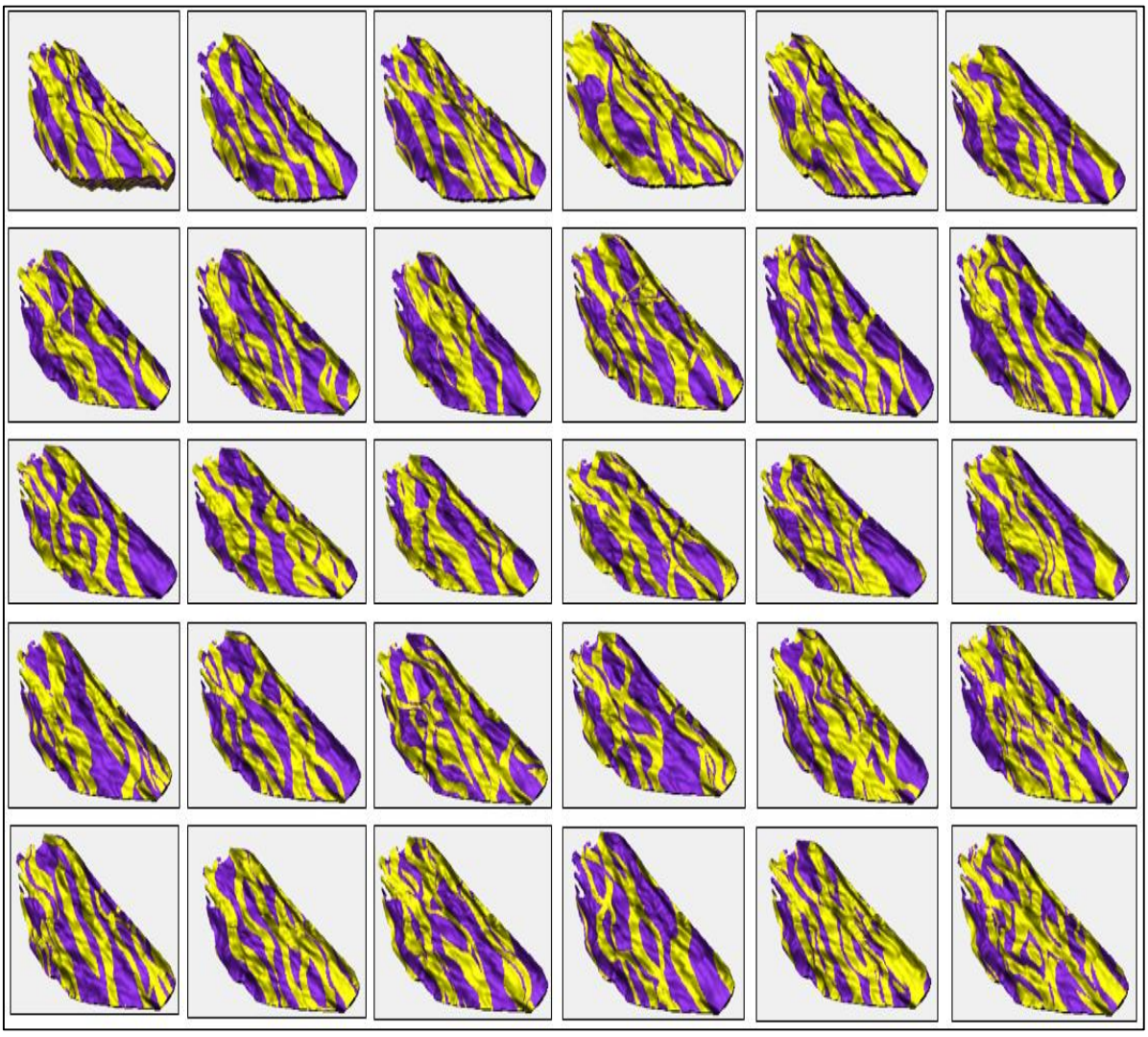

Figure 3.6 The multiple realizations created for ranking facies model (Vo Thanh et al., 2019b)

The selected rock-type models showed no mismatch between the spatially predicted and the measured values in the petrophysical model.

As shown in **Figure 3.6**, the cross plot indicated an excellent relationship between the measured and predicted porosity and permeability as given by the Sequential Gaussian Simulation of the Object-based facies model (see **Figure 3.5**).

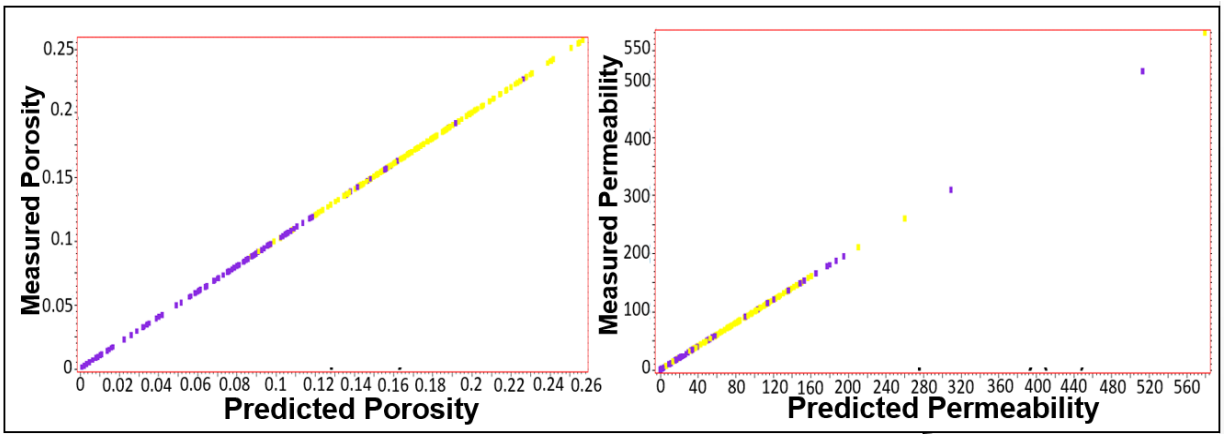

Figure 3.7 Cross plot shown the relationship between predicted and measured of porosity and permeability conditioning the true lithofacies model (Vo Thanh et al., 2019b)

The suitable lithofacies are illustrated in **Figure 3.8**. These lithofacies later are considered for ANN and co-kriging process to complete the petrophysical modelling.

The realistic petrophysical models closely mimicking the depositional environment were expected to enhance accuracy models by history matching.

The best-ranked lithofacies model sharply reduced uncertainty after the object-based modelling. Therefore, the selected facies was able to condition porosity and permeability in the fluvial channel reservoir. The lithofacies model was necessary to represent the depositional environment in the reservoir. Therefore, the cross-validation was required to check whether the object-based facies model described the accurate distribution of the fluvial system. This step was imperative to reduce history matching time by determining

the correct geological distribution through many simulation runs. It was because history matching deals with many uncertain parameters.

The most influential setting is geological uncertainty, especially facies and petrophysical parameters. Hence, controlling the geological risk in static modelling is the most critical step to provide the optimal solution for saving time and human efforts during history matching as well as the other simulation processes.

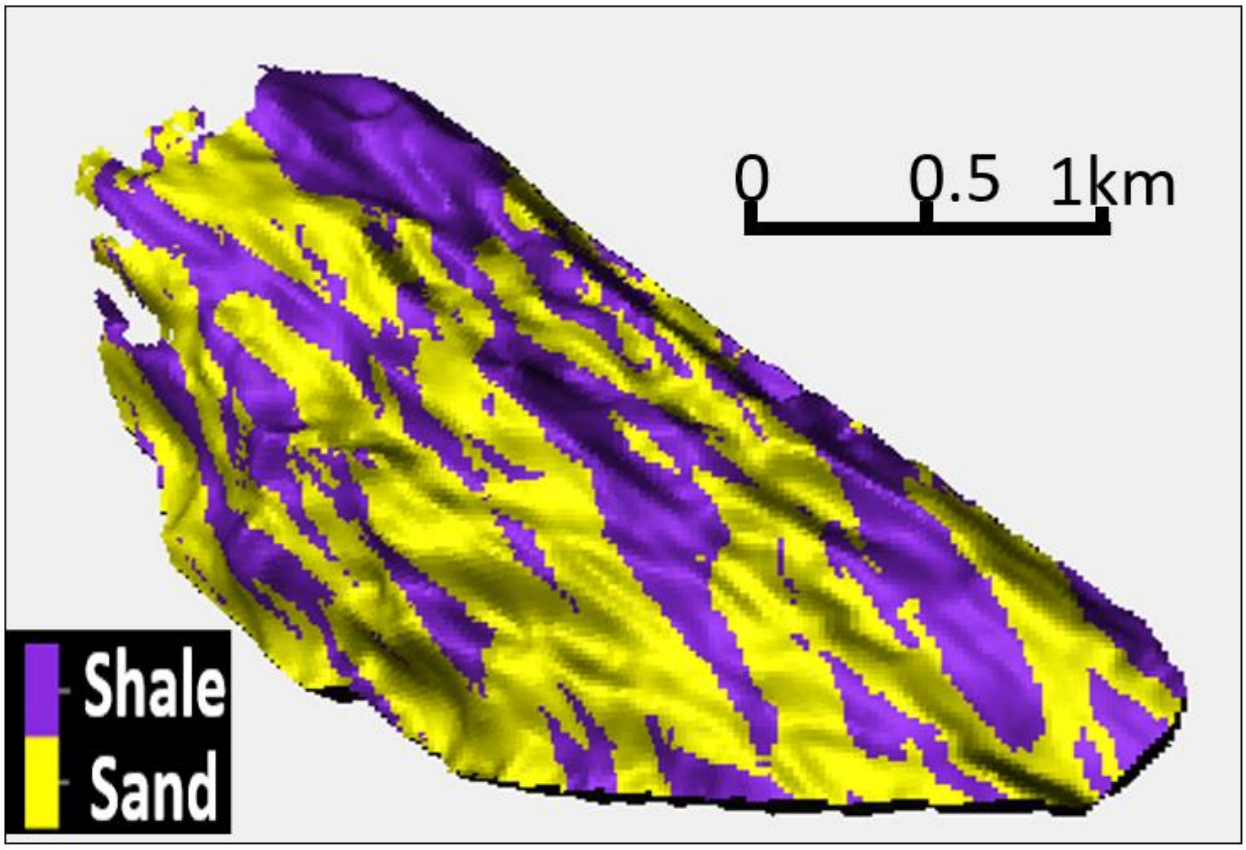

Figure 3.8 The ranking lithofacies model (Vo Thanh et al., 2019b)

3. 3. 3. Petrophysical modelling using Artificial Neural Network

The application of ANN is to improve the accuracy of the generation porosity and permeability models. **Figure 3.9** depicts the ANN structure for enhancing the petrophysical

models. Seismic attributes and well log data (input layer) were used for the ANN training to predict porosity and permeability properties (output layer).

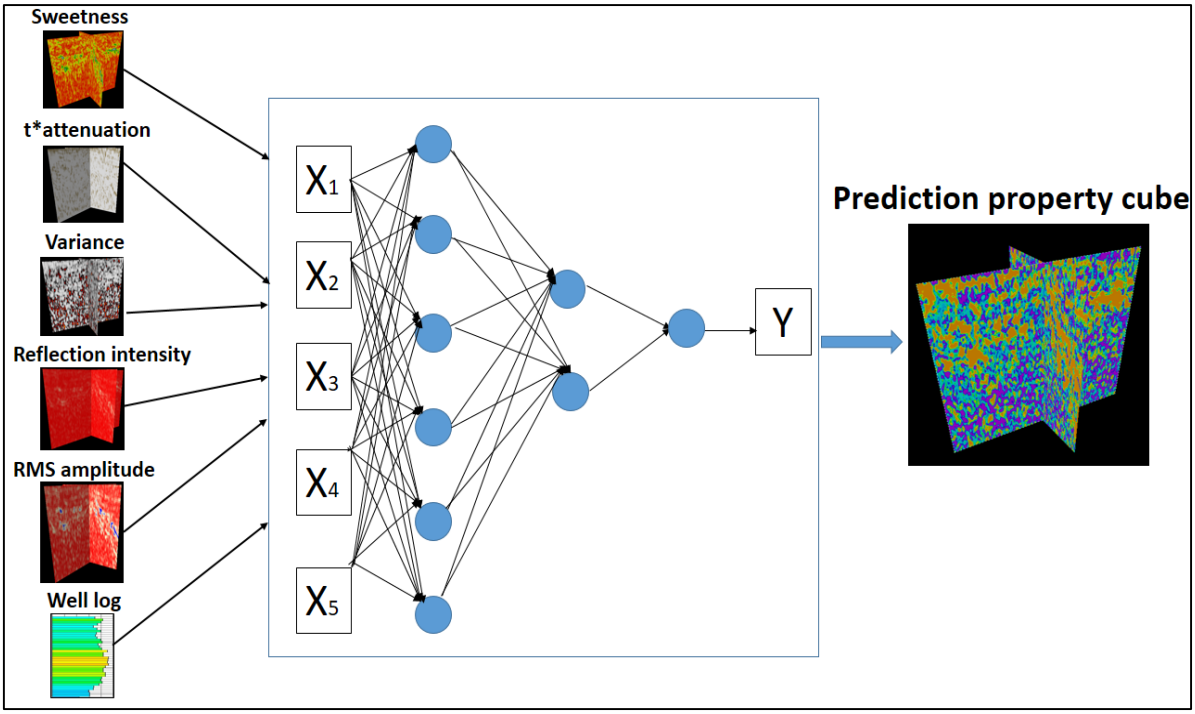

Figure 3.9 ANN architecture for prediction petrophyiscal models.

The seismic data divided into specific seismic attributes. The attributes comprise four sets: signal processing method, sophisticated trace attributes, structural attributes, and stratigraphic attributes. The collection of seismic characteristics as used for the ANN training is as follows: Variance, Sweet, t*attenuation, RMS amplitude, Intensity. **Figure 3.10** shows an example of the generated seismic attributes for the training process. From these scenarios, the correlation factor between well log and ANN predicted values calculated to determine the best scenario for predicting the porosity and permeability model. The result of the ranking scenario is highlighted in **Table 3.2.**

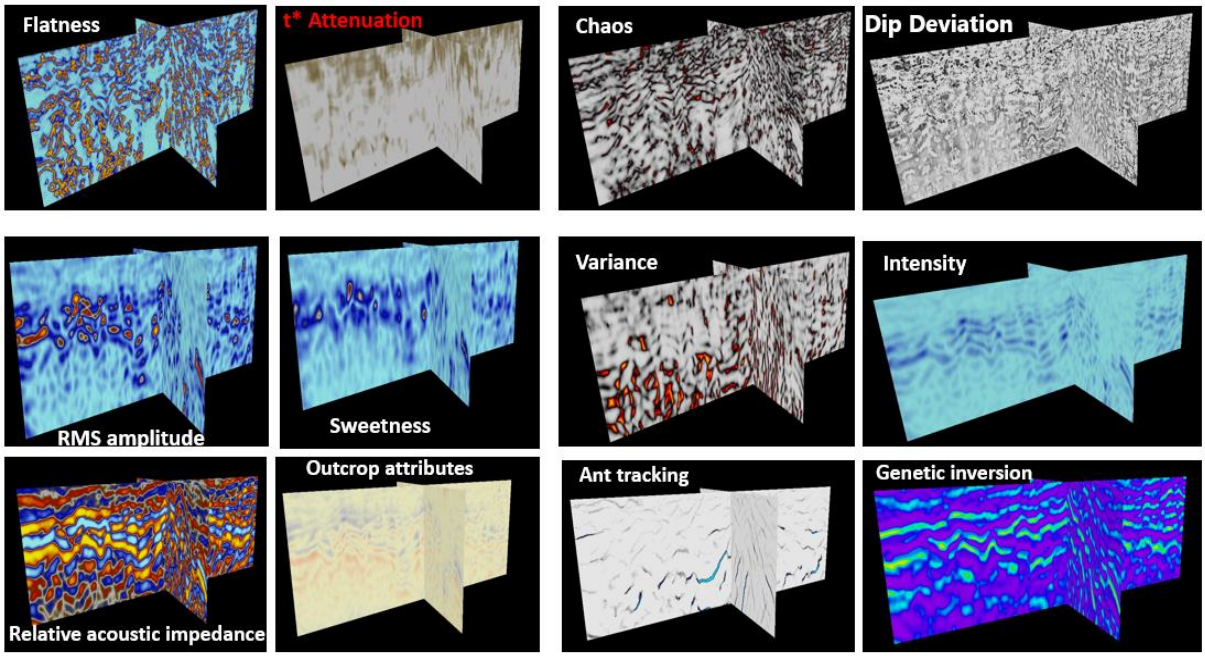

Figure 3.10 Example of seismic attributes for ANN training (Vo Thanh et al., 2019b)

Table 3.2 The result of ranking seismic attributes (Vo Thanh et al., 2019b)

Scenario	Seismic attributes	Correlation factor
1	Flatness, Chaos, Dip Deviation, Ant-Tracking, Polarity, Genetic inversion	0.59
2	RMS amplitude, Dip Deviation, Intensity, Sweet, Variance	0.68
3	Variance, t* Attenuation, Intensity, Genetic Inversion, Ant tracking, RMS amplitude, Outcrop attributes	0.74
4	Variance, Chaos, Dip Deviation, Sweet, t* Attenuation, Genetic Inversion	0.85
5	Variance, Sweet, t* Attenuation, RMS amplitude, Intensity,	0.91

Figure 3.11 depicts the result of ANN training. This result came from a selection of suitable seismic attributes and many trails to define the percentage for training and validation (**Figure 3.11.a** and **11.b**). **Figure 3.11c** indicates the correlation between ANN and well log values.

It noted that the ANN correlated positively to the well log values with a minimal error of less than 5%. **Figure 3.11.d** shows the cross plot between ANN and well log porosity values. As shown in **Figure 3.11**, the cross-validation is reliable and accurate, judging by the high R^2 equal to 0.956. The predicted cubic porosity seismic after the ANN training highlights in **Figure 3.11.e**.

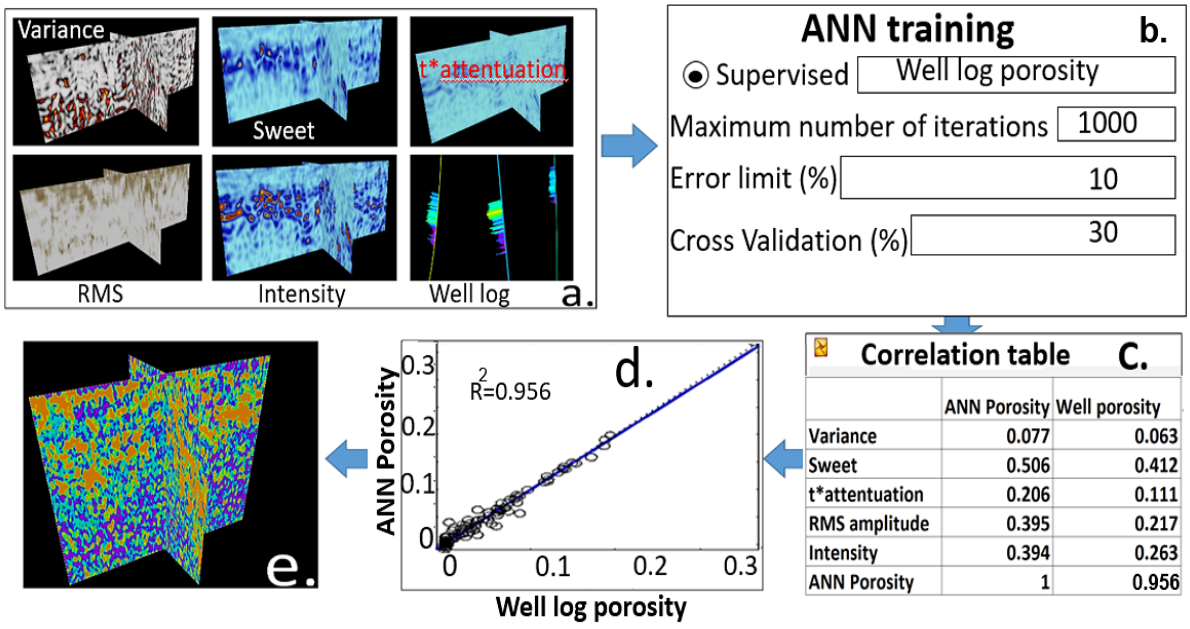

Figure 3.11 ANN training process for porosity: (a) ranked attributes; (b) ANN training set up; (c) correlation table between seismic attributes and well log porosity; (d) ANN and well porosity correlation; (e) ANN prediction porosity cube (Vo Thanh et al., 2019b)

In the same vein as conducted for porosity, the predicted permeability obtained similarly. The seismic resampling converted from seismic cube to the 3D model. **Figure 3.12** depicts the ANN predicted porosity and permeability models.

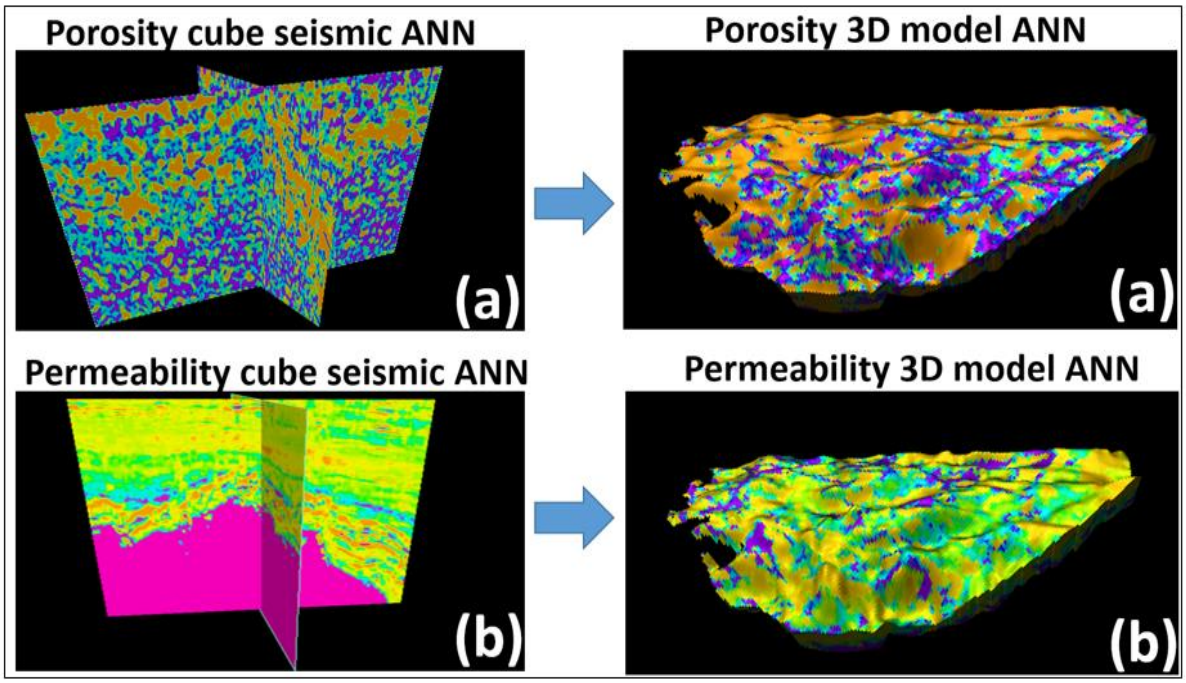

Figure 3.12 ANN model prediction resampling form seismic cube to 3D model: (a) ANN porosity model; (b) ANN permeability model (Vo Thanh et al., 2019b)

3. 3. 3. 1. The boundary of the developed ANN Model

The edge of the developed ANN model investigated using ANN-MATLAB to demonstrate the quality control of model training. The performance of the developed ANN model based on training, verification, and testing data set. The correlation factor and mean square error (MSE) used to evaluate the quality and accuracy of the developed ANN model. After repeated trial training, it was found that the neural network model with eight hidden neurons in the hidden layer obtained the best performance for the porosity and permeability with a validation MSE value of 3.9×10−5 and 2.78×10−4, respectively. The illustration of

the ANN network shows in **Figure 3.13**. For the porosity-type ANN model, the training process achieved at 35 epochs with a validation MSE of 3.9×10−5 (**Figure 3.13a**). **Figure 3.13b** depicts the best validation performance and the regression plots of ANN porosity model for training, validation and blind testing groups, respectively (Ansah and Vo Thanh, 2020)

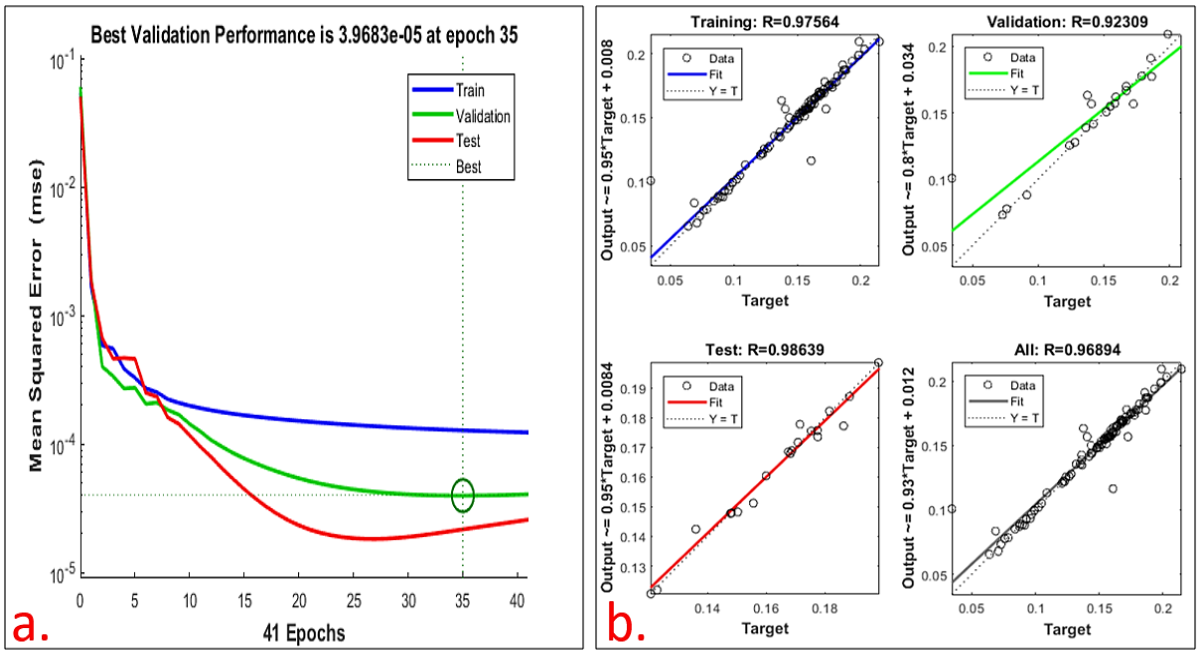

Figure 3.13 Best validation performance (a) and regression of ANN porosity (b) (Ansah , Vo Thanh, Sugai et al., 2020)

The ANN porosity model fits so well to the well-log porosity values for all training, verification, and testing groups, as can be observed in their correlation factor (R) of 0.946, 0.988 and 0.994 for training, verification, and testing, respectively. Similarly, the performance and regression plot of the ANN permeability model highlight in **Figure 3.14**. For the permeability ANN model, the training process was successfully truncated at 86 epochs with a validation MSE of 2.78×10−4. Also, the ANN permeability model matches so well to the well log permeability values for all training, verification and testing groups

as can be recognized in their correlation factor (R) of 0.989, 0.983 and 0.978 for training, verification, and testing, respectively (Ansah and Vo Thanh, 2020).

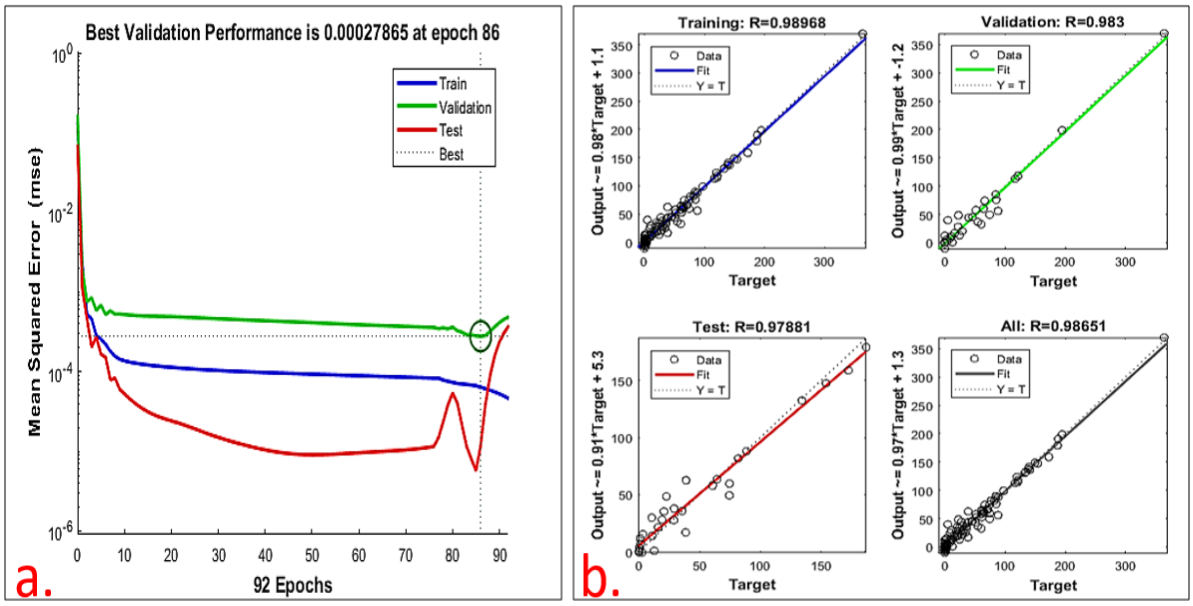

Figure 3.14 Best validation performance (a) and regression plot of permeability (b) (Ansah ,Vo Thanh, Sugai et al., 2020)

3. 3. 3. 2. Comparison of the ANN model and previous studies

Many previous studies are focusing on the prediction of porosity and permeability using artificial intelligence (AI) and machine learning (ML). **Table 3.3** lists out some of these related studies, and the comparison between those AI, ML models, and our work. As shown in **Table 3.3**, it is indicated that the prediction accuracy of this work significantly differs from several previous studies. In that, the developed ANN model of this study is outperformed other AI and ML models. The main reason is that the current ANN model uses less number of neurons in the hidden layer as compared to the previous AI and ML model. Regarding the results in terms of error and efficiency, the ANN models in this work

are more suitable for prediction of porosity and permeability due to higher R^2 and low MSE compared to previous AI and ML models (Ansah and Vo Thanh, 2020)

Table 3.3 Comparison between this work and previous studies

References	Method	R^2	MSE
(Aminian and Ameri, 2005)	ANN	0.976	Not stated
(Kumar, 2012)	ANN	0.87	0.0024
(Yeganeh et al., 2012)	ANN	0.974	0.003
(Esmaeilzadeh et al., 2013)	ANN	0.978	Not stated
(Fegh et al., 2013)	ANN	0.84	Not stated
(Iturrarán-Viveros and Parra, 2014)	ANN	0.906 3	0.1876
(Esmaeilzadeh et al., 2013)	ANN	0.978	Not stated
(Nguyen et al., 2014)	ANN	0.871	Not stated
(Konaté et al., 2015)	GRNN	0.97	0.278
(Al-Mudhafar, 2017)	MLR	0.955	Not stated
(Jamalian et al., 2018)	LSSVM	0.984	1.42
(Zolotukhin and Gayubov, 2019)	ANN	0.92	Not stated
This study	**ANN**	**0.988**	**2.78×10^{-4}**

3. 3. 4. Combination the facies model into ANN prediction models

The Co-kriging algorithm will use to include the facies models in ANN petrophysical model. The main objective of co-kriging is to combine the primary factor and secondary factor using the computed correlation factor. In this work, the primary consideration is well log data, and the second factor is the ANN prediction porosity and permeability model. Also, the object-based facies model considers as a geological factor in the co-kriging process. **Figure 3.15** shows the process of co-kriging for porosity and permeability models. The result of the final porosity and permeability models is depicted in **Figure 3.16**.

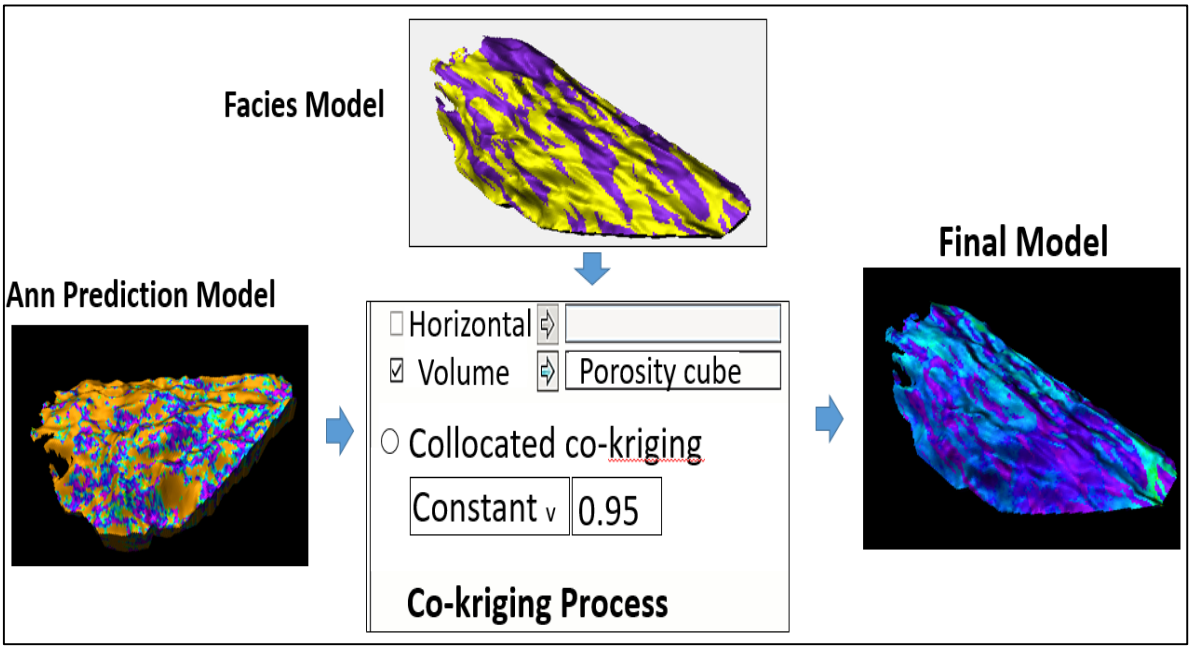

Figure 3.15 Co-kriging process for final porosity and permeability models (Vo Thanh et al., 2019b)

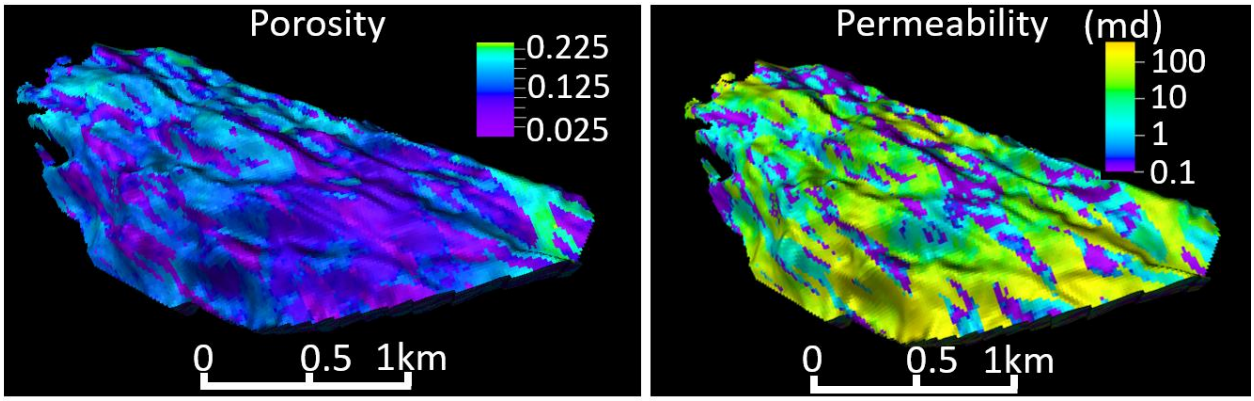

Figure 3.16 Final porosity and permeability after co-kriging process (Vo Thanh et al., 2019b)

The extremely heterogeneous nature of these models is necessary to investigate the fluid flow behavior using dynamic simulation. Then, the accuracy of co-kriging results validated

through the history matching process. The Drill Stem test (DST) data will be used for comparison of the conventional and integrated workflow to validate the efficiency of the developed framework.

3. 3. 5. Reservoir simulation for DST matching

The dynamic simulation was used the original grid cell from geological modelling without upscaling to coarse grid cell size. The main objective of this section has validated the accuracy of modelling workflow. Thus, the large grid cell used for the DST matching process. The ECLIPSE 100 black-oil simulator used for reservoir simulation. The reservoir model consists of 2,604, 800 grid cells. Also, the dynamic data such as fluid contact, PVT, and relative permeability data have included in the reservoir model. **Figure 3.17** shows the relative permeability curves used for the history matching process.

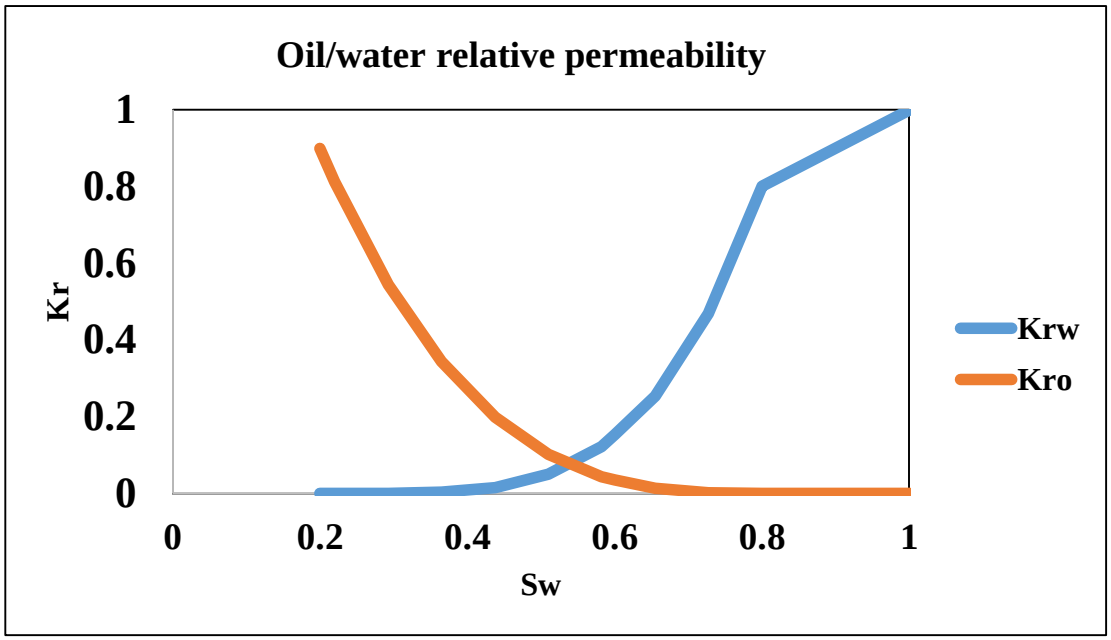

Figure 3.17 Relative permeability curves for history matching model

The DST matching was performed on the well bottom hole pressure of NV-2X well controlled by the oil flow rate. **Figure 3.18** highlights the history matching of both

conventional (**Figure 3.5**) and integrated geological models (**Figure 3.16**). The integrated model indicated better matching than a traditional model by reservoir simulation. Therefore, the accuracy modelling facies and petrophysical modelling play an essential role in improving the history matching reservoir models. Also, the root mean square error (RMSE) calculated the mismatch between simulation results and measurement data. **Table 3.4** depicts the result of the RSME of history matching models. We can observe that the error of the integrated model was less than the conventional models. Thus, the integrated model could use for further investigation because it can reflect the fluid flow behavior in a reservoir. This model will apply for CO_2 sequestration simulation and optimization in **chapter 4**.

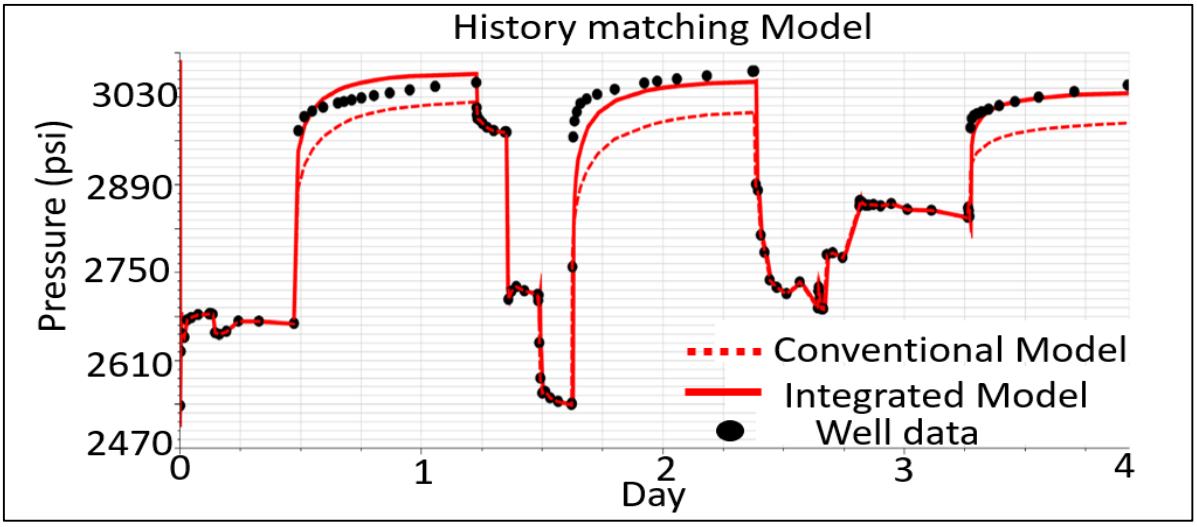

Figure 3.18 DST matching results of both modelling workflows

Table 3.4 The root mean square error of history matching results

Type of Modelling workflow	Root Mean Square Error
Conventional model	9.9
Integrated model	5.3

3. 4. Conclusions

Some key points could be drawn in this chapter.

1. An integrated modelling framework is proposed the new approach for improving the distribution of porosity and permeability models. The workflow is useful to support to select the CO_2 sequestration locations. In many geo-storage reservoirs, subsurface data, such as core, well logs, and accurate long production history, are not always available. The developed framework will contribute to enhancing the accuracy quality of the 3D model in storage formations.
2. The Object-based method is proposed as an efficient way capture the realistic facies model. This method was useful for fluvial sandstone reservoirs.
3. To verify the lithofacies model, geological realizations generated to determine the suitable facies distribution using Sequential Gaussian Simulation
4. Artificial Neural Network is used the seismic attributes and well log data to predict porosity and permeability with high correlation factor. The ANN method can estimate porosity and permeability values with reasonable accuracy.
5. The co-kriging algorithm is a useful method to combine ANN and Object-based modelling for better distribution of porosity and permeability models. The good correlation and consistent between co-kriging and well log values as, per this work, was indicated the high reliability of the porosity and permeability models.
6. Good Drill Stem Test matching demonstrated that the 3D porosity and permeability models are reliable for further investigation of dynamic reservoir simulation.

CHAPTER 4

RESERVOIR SIMULATION OF CO_2 SEQUESTRATION

4. 1. Introduction

This chapter presents the basic workflow and results of field-scale reservoir simulation of CO_2 sequestration. Reservoir simulation is combined with mathematical and numerical techniques to create a model that studies fluid flow behavior in porous media (Fanchi, 2018). During this process, the reservoir model is divided into grid cells into three dimensions. The reservoir and fluid properties are simulated by space and time in a series of discrete steps (Li, 2014).

In the petroleum reservoir, the main goal of reservoir simulation is to forecast future field performance for decision making.

The future performance is comprised many optimization plans such as infill drilling, water injection, gas injection, and well production control (Al-Mudhafar, 2016). In this work, the compositional reservoir simulator is employed to evaluate the CO_2 sequestration performance in the fluvial sandstone reservoir in the Nam Vang field offshore Vietnam.

4. 2. Reservoir simulation workflow

The basic workflow used to construct the reservoir model consists of the following steps (Aziz and Settari, 1979):

1. Define the reservoir engineering problem with a specific purpose
2. Collect all static and dynamic data required to perform the simulation scenarios
3. Include the geological, geophysical, and petrophysical data into geological modelling
4. Fluid definition to analyze the PVT behavior
5. Choose the type of simulator to be used and designed reservoir engineering problem

6. Adjust the reservoir model parameters by the actual historical performance of the reservoir
7. Predict a future reservoir performance under different conditions to achieve the goals of the study.

Even though the above steps are typical, they could vary widely from a case by case. Therefore, these steps are flexible depended on the available data and reservoir engineering problems. The necessary steps of this research elaborated below.

4. 2. 1. Defining the reservoir simulation problem

The reservoir simulation is a useful approach to evaluate the performance of CO_2 sequestration through different injection scenarios (i.e., continuous and Water Alternating Gas injection). The field-scale reservoir models were adapted from Chapter 3 to conduct the simulation scenarios in this chapter. The predicted CO_2 trapping was estimated and compared. For the continuous injection, the CO_2 was injected over 20 years. The WAG injection consisted of 10 years of CO_2 injection, followed by 10 years of water injection. Both injection scenarios were followed 40 years post-injection period.

4. 2. 2. Static and dynamic data

The static and dynamic data are necessary to build the reservoir simulation model. The data comprises well production/injection history, and well completion. Also, capillary pressure and relative permeability curves are needed to represent rock types in the reservoirs. This study selects the Brooks and Corey models for the relative permeability curves (Brooks and Corey, 1964) and the Van Genuchten function for the capillary pressure curves (Genuchten, 1980). Furthermore, the performance of residual CO_2 trapping in the present study used the hysteresis model of Land (Land, 1968).

Figure 4.1 and Figure 4.2 show Land's residual trapping model and relative permeability curves adopted in this study. In this study, CO_2 injection and subsequent movement and storage within the reservoir considered in the absence of mineral trappings

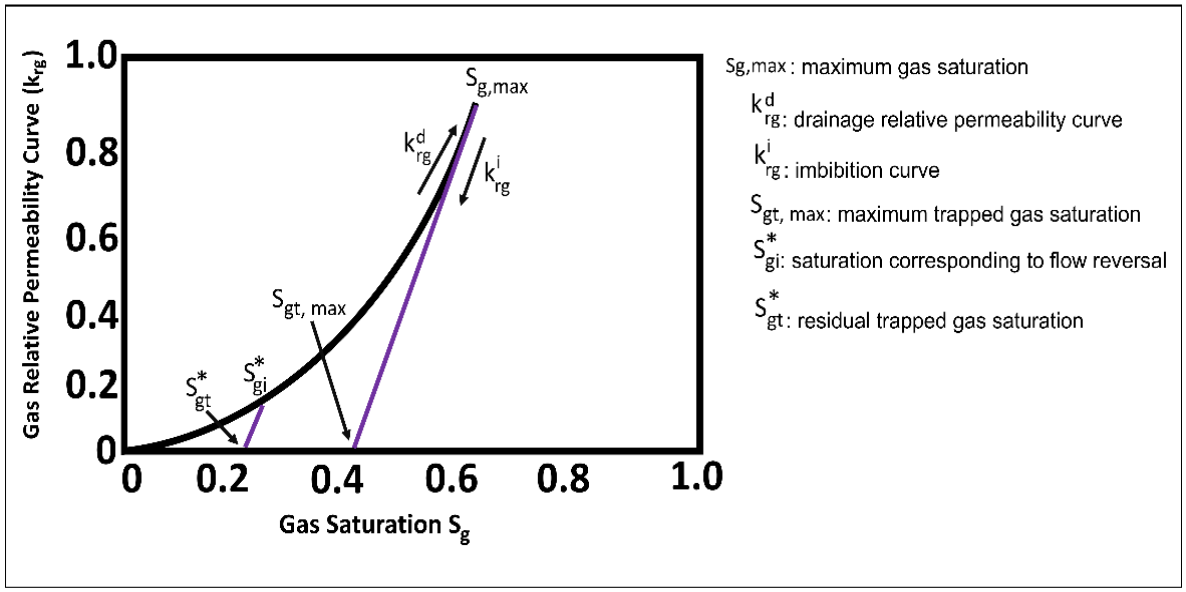

Figure 4.1 Land trapping model — gas saturation as a function of relative gas permeability (Vo Thanh et al., 2020)

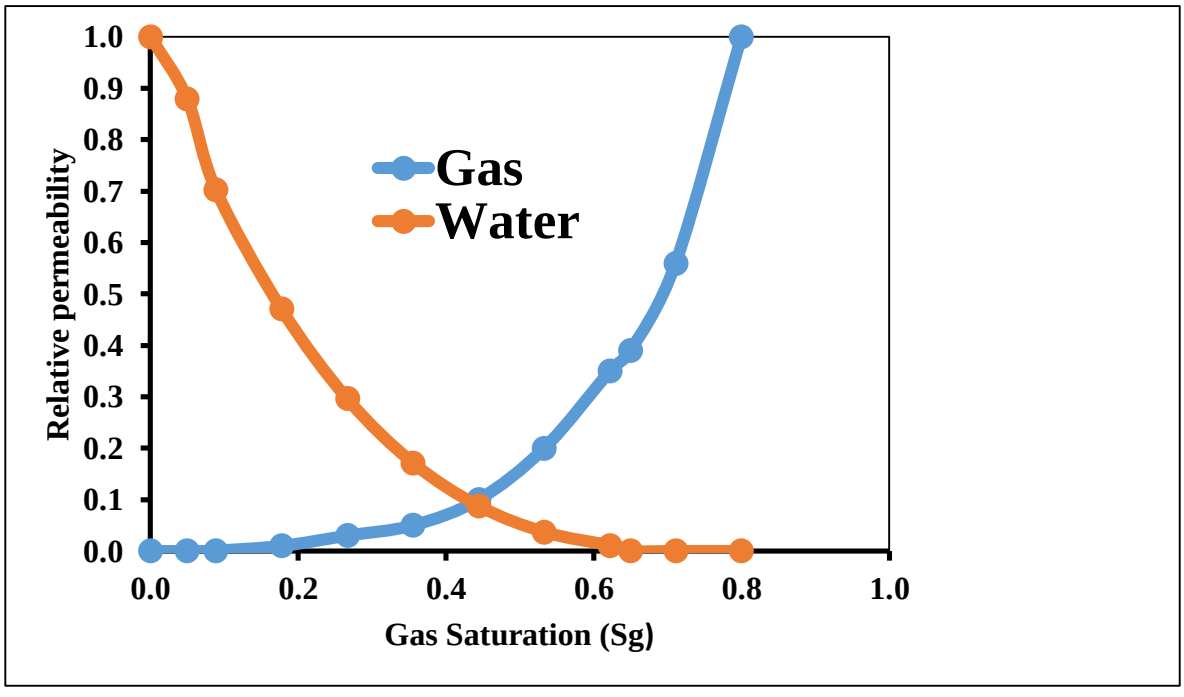

Figure 4.2 Relative permeability for CO_2 sequestration study

4. 2. 3. Geological Modelling

The integrated geological modelling was used to distribute 3D porosity, permeability, and facies model. The complete modelling workflow was described as detail in Chapter 3. These models will upscale for reservoir simulation and optimization studies.

4. 2. 4. Fluids definition

In this study, the reservoir models have used the Equation of State (EOS) for fluid definition. For generating the compositional fluid model for the dataset, we used the WinProp package within the CMG simulator. For Winprop, the fluids were defined in terms of their components to allow the interaction of the compositional fluid in porous media (CMG, 2019). The procedures of fluids definition include:

1. Select units for fluid component
2. Component selection for reservoir model
3. Define the composition fraction
4. Define the water properties

4. 2. 5. Geological models upscaling

The fine-scale geological model has 148, 176, and 100 grid cells in I, J, K directions, respectively. The size of grid blocks in the model is 25 m × 25 m, and the total number of grid cells is more than 2600000. Because such a large model needed high computation time, the fine-scale model was upscaled to obtain a coarse-scale grid size.

The grid cell numbers in the upscaled model in I, J, and K directions were 40, 48, and 25 grids (total = 48000 grids). The harmonic and arithmetic means method applied for well permeability and porosity upscaling.

These methods could preserve the data variations to meet the acceptance of the upscaling criteria. **Figure 4.3** presents the 3D coarse-scale geological model that includes porosity, horizontal, and vertical permeability (Vo Thanh et al., 2020).

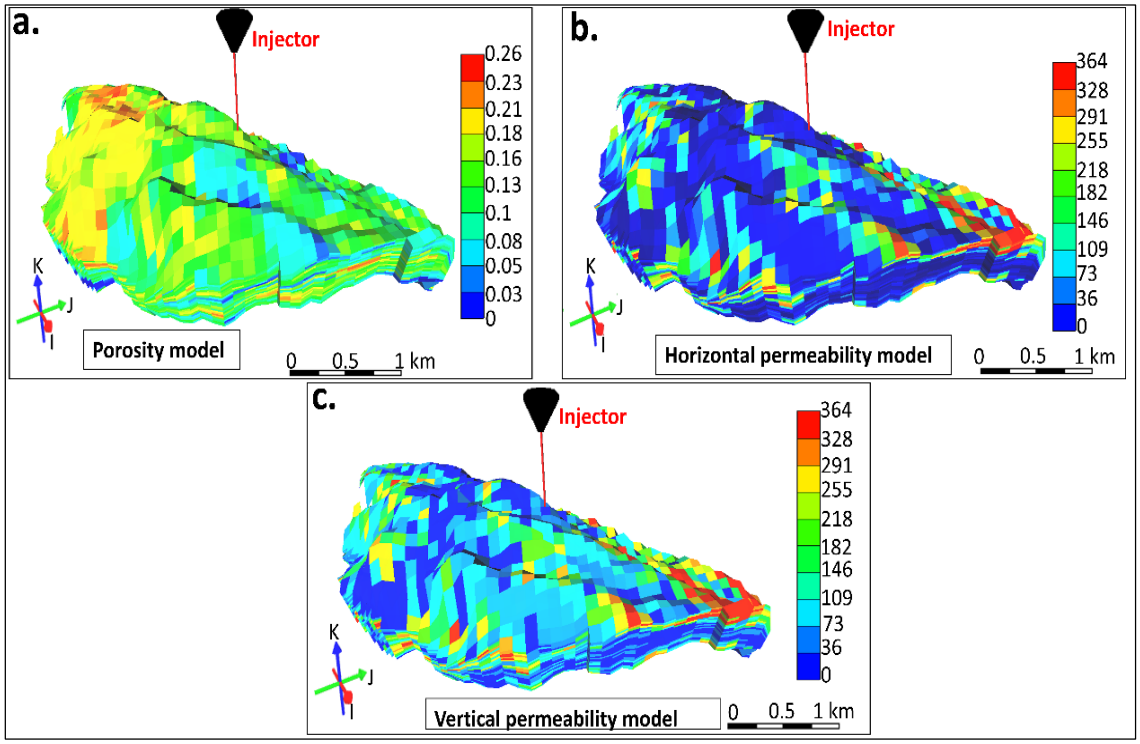

Figure 4.3 Porosity (a), horizontal permeability (b), and vertical permeability (c) models as simulated in the base case scenario (Vo Thanh et al., 2020)

To validate the accuracy of the upscaled model, and reducing simulation error, to match between the fine and coarse-scale geological models was conducted by cell angles, cell inside out factors, and grid bulk volume. The near similarity of the pore volume is required for two models. The minimum percentage difference in volume is less than 7% (Petrel, 2017), precisely a percentage volume difference of 4.34% in this work. Thus, the coarse models are acceptable for further investigation through dynamic simulation.

Moreover, the geometrical property cell angle that is demonstrated the maximum deviation was 90 degrees (not exceeding 15 degrees). The cell-inside-out is determined to ensure having zero values in all areas of the reservoir model.

The histogram properties between fine and coarse-scale models are also considered to evaluate the quality of the upscaling process, as presents in **Figures 4.4**.

In these histograms, there are a non-significant difference in percentage distribution between the fine and coarse-scale models regarding lithofacies and petrophysical properties.

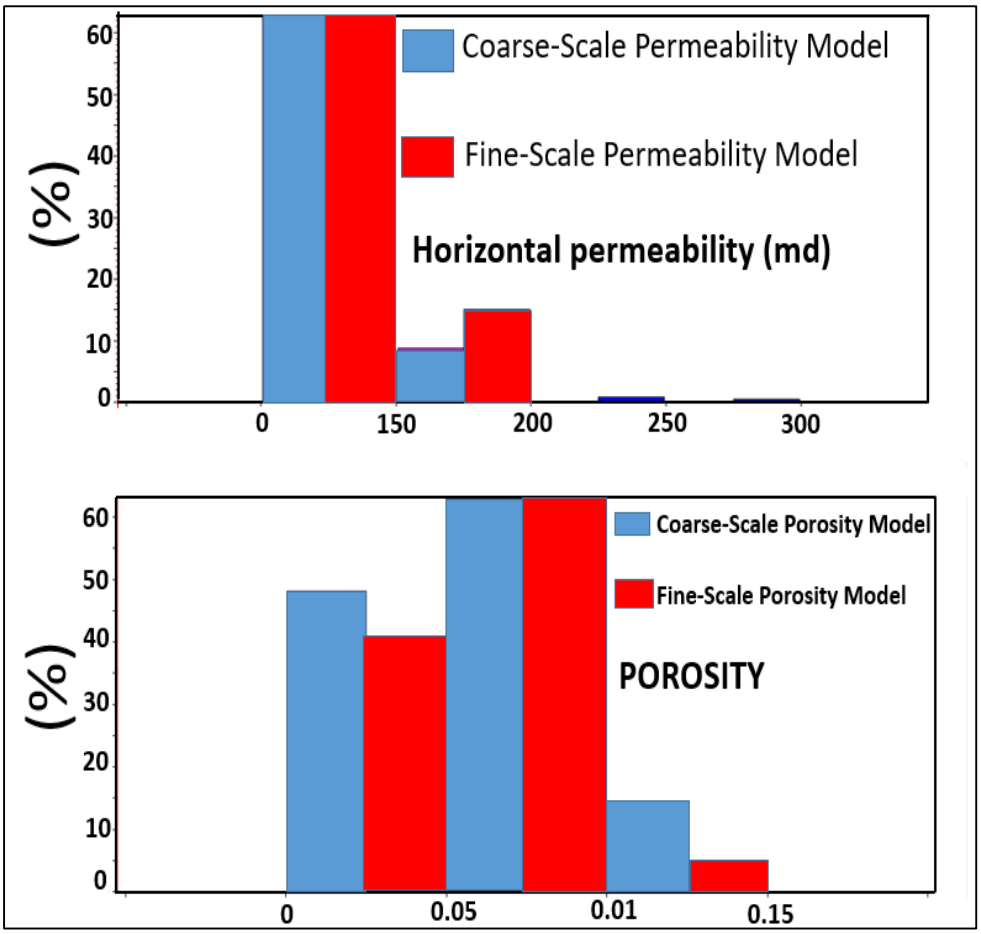

Figure 4.4 Upscaling histogram between fine and coarse model

4. 2. 6. CO_2 sequestration simulation

The fluvial sandstone reservoir in the Nam Vang field was adapted for compositional reservoir simulation to CO_2 sequestration through continuous and WAG process. The principal pay did not contain the faults or complex structures in the reservoir. It classified as two lithology types such as sand and shale. The detailed reservoir description has been described in Chapter 3.

The upscale geological models were exported to construct the compositional reservoir simulation for CO_2 sequestration study. First, the sensitivity analysis was performed for the injection rate and geological modelling aspect. Then, the comparison of continuous injection and WAG technique was conducted to demonstrate the effectiveness of injection strategies on CO_2 sequestration performance. The base case of the WAG process will be employed in Chapter 5 for optimization purposes.

4. 3. Result and Discussion

4. 3. 1. Sensitivity analysis

4. 3. 1. 1. Injection rates

The injection rates vary from 50000 tons/year to 142000 tons/year. The pressure build-up is the criterion for selecting the injection rates. The fracture pressure of this study was defined as 32MPa. This pressure prevents the cap-rock broken during the injection process. **Figure 4.5** depicts the result of the sensitivity analysis for injection rates in this study. The sensitivity analysis of the injection rate is necessary for CO_2 sequestration in terms of economic and safety projects.

The injection rate at 142000 tons/year is a suitable case for this study because the pressure build-up is below 32 MPa. This injection rate is approximate with the previous research to

perform the CO_2 injection in a meandering fluvial system (Nguyen et al., 2017a). These authors were injected 100000 ton/year in the deep saline aquifers at the Shenhua site, Ordos Basin, China.

Table 4.1 Input parameters for simulation study

Parameters	Values
Length (m)	5000
Width (m)	2000
Thickness (m)	100
Depth of top of the reservoir (m)	2076
Depth of bottom of the reservoir (m)	2176
Number of cells (I × J × K)	48000
Pressure at 2076 m depth (bar)	200
Temperature (°C)	70
Vertical to horizontal permeability ratio	0.1
Salinity (ppm)	40000
Injection depth (m)	2160
Fracture pressure (MPa)	40
Safety pressure (MPa)	32

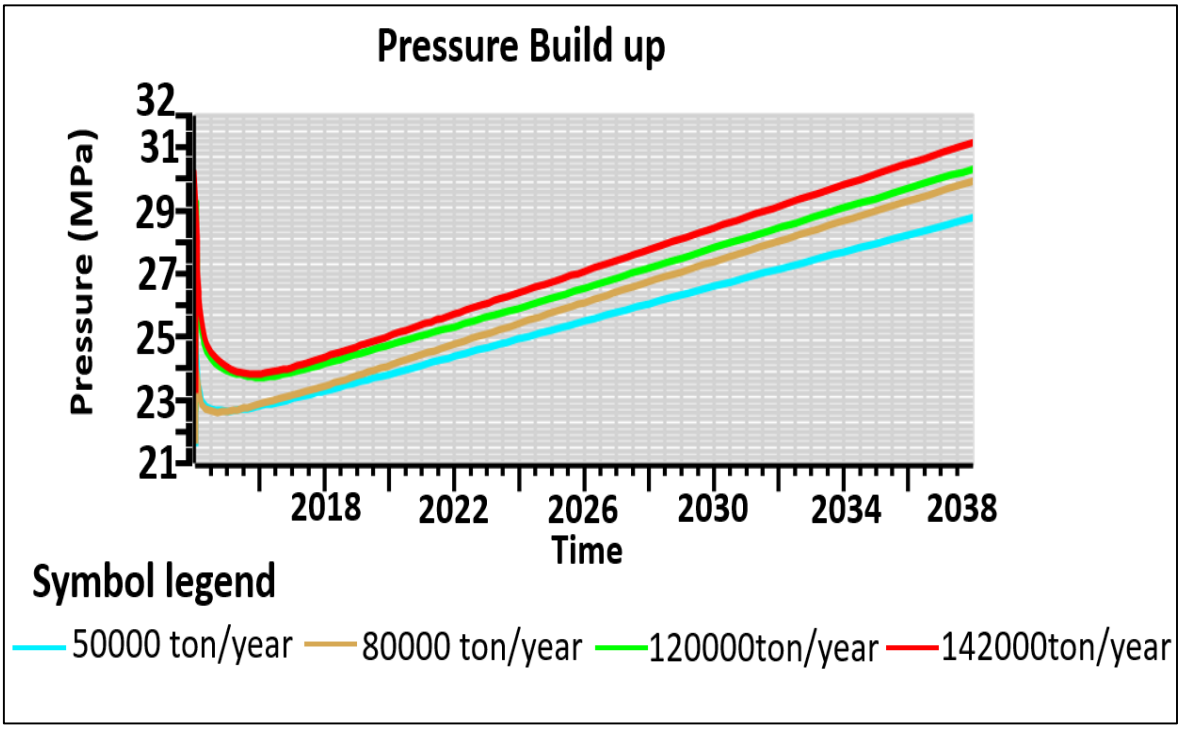

Figure 4.5 The sensitivity analysis of injection rate in this study

4. 3. 1. 2. Geological parameters

The CO_2 injection is performed in a fluvial channel sandstone reservoir. Therefore, it is necessary to consider the effect of channel geometry on the CO_2 plume dynamic. Also, the anisotropy is investigated for the CO_2 plume shape. This parameter is influenced by the vertical permeability distribution of the reservoir. **Table 4.2** summarizes the sensitivity parameters for geometry and anisotropy.

Table 4.2 The geological parameters for sensitivity analysis

Scenarios	Channel width	Anisotropy
Case 1	300-900 (m)	0.1
Case 2	900-1350 (m)	0.5
Base case	150-450 (m)	0.7

The simulation results show that the CO_2 plume shape is so sensitive to the geometry channel. As can be observed in **Figure 4.6,** the CO_2 migration changes in different forms when we compare three cases. For this reason, the geometry of a channel is one of the essential parameters for the CO_2 injection in a fluvial depositional environment. Thus, the facies modelling should be carefully considered for the fluvial channel reservoir.

Chapter 3 was mentioned how successful distribution for the facies model.

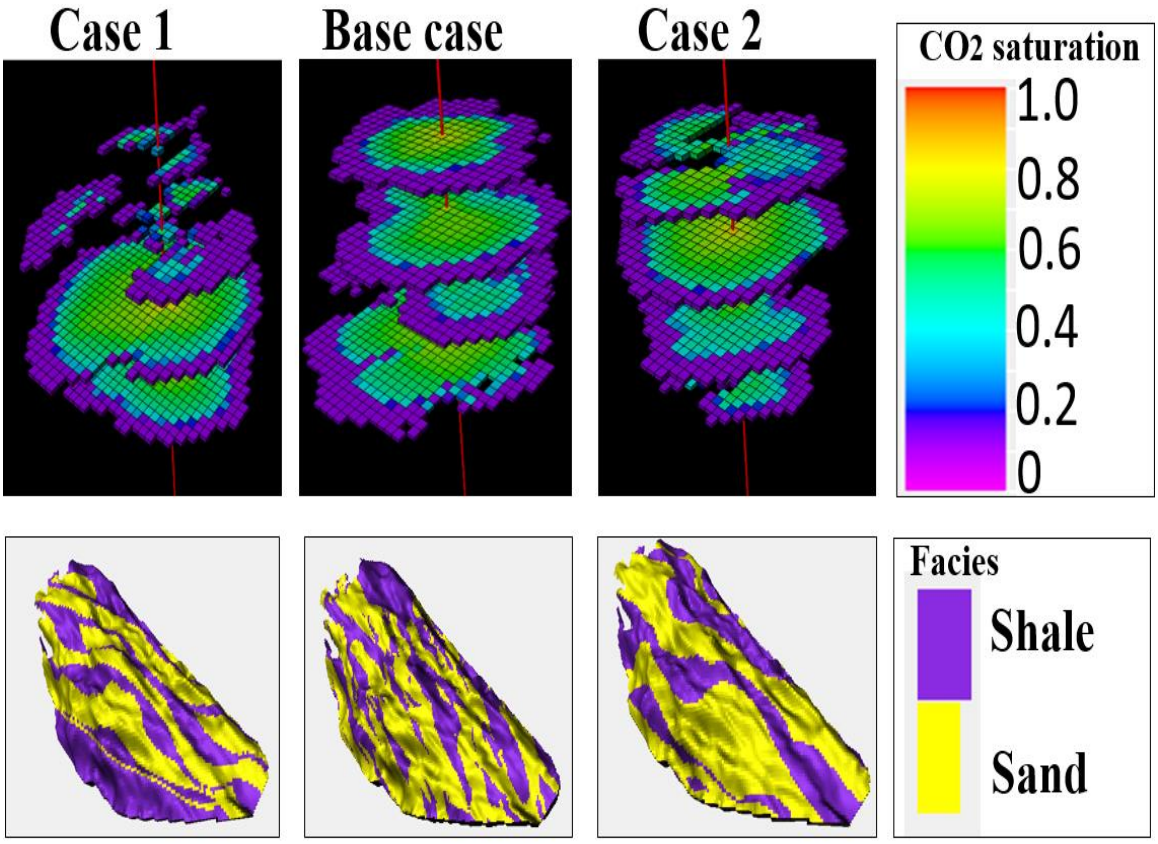

Figure 4.6 Channel geometry and CO_2 plume dynamic

Then, the anisotropy is continued the sensitivity analysis for CO_2 plume dynamic. The anisotropy (k_v/k_h) is considered as the ratio of vertical permeability (k_v) and horizontal permeability (k_h). This ratio is effect by the vertical permeability distribution for the reservoir simulation model.

Figure 4.7 depicts the CO_2 evolution in the fluvial sandstone reservoir. The CO_2 saturation in the high case is extent large than the low case. As can be seen in Figure 4.7, the CO2 plume shape of base case expanded the immense distance because of the anisotropy ratio higher than Case 1 and Case 2. It is because of the permeability effect of CO_2 flow.

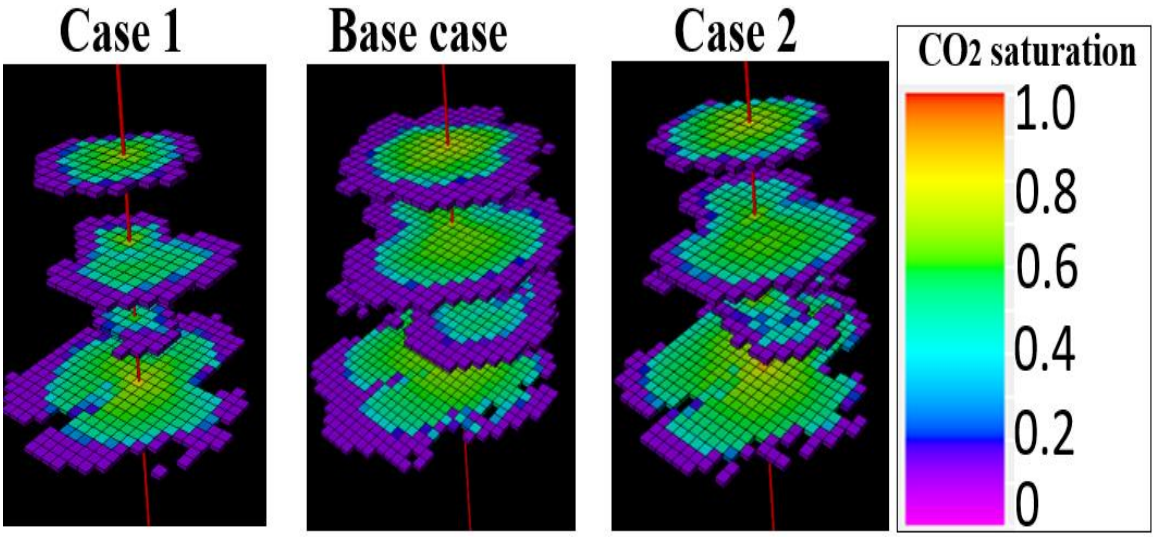

Figure 4.7 Anisotropy effect to CO_2 plume shape

The result of sensitivity analysis demonstrated the important geological factors in CO_2 storage assessment. Thus, the geological factors will be considered for optimization CO_2 storage in Chapter 5.

4. 3. 2. Impact of injection strategies on enhancing CO_2 sequestration performance

The WAG process was simulated and compared with continuous CO_2 injection to demonstrate the effectiveness of WAG injection concerning the specific reservoir.

In both injection scenarios, 1420000 tons of CO_2 were injected over 20 years. The rate of continuous CO_2 injection was set at 0.071 Mt/year. In the WAG process, the injection rate was set at 0.142 Mt/year. The WAG process consisted of 10 years of CO_2 injection, followed by 10 years of water injection with 60-day water injection and 60-day CO_2 injection phases. All injection scenarios were followed by a 40-year observation period, during which the residual and solubility trapping capacities for CO_2 were compared (Vo Thanh et al., 2020).

Figure 4.8 depicts the results of residual and solubility CO_2 trapping for the WAG technique in comparison with continuous CO_2 injection. For instance, the residual and solubility CO_2 were 398 000 and 131 000 tons, respectively, in the continuous injection case by the end of the simulation period. The total CO_2 trapping of continuous injection was 529 000 tons. However, the WAG process resulted in 579 000 and 296 000 tons for residual and solubility CO_2 trapping, respectively. The total CO_2 trapping of the WAG process is 875 000 tons. This result indicated that WAG injection considerably enhances CO_2-trapping efficiency (Vo Thanh et al., 2020).

Moreover, the WAG injection improved the residual trapping by improving macro-scale and micro-scale sweep efficiencies within the reservoir. WAG process increases CO_2 trapping by increasing residual CO_2 saturation and enhancing CO_2 imbibition (Herring et al., 2016). Also, the water injection cycle was prevented CO_2 bubble moving upward and promoted CO_2 spreading in the porous media (Nghiem et al., 2009).

In the case of enhanced solubility trapping during cyclical WAG injections, a more abundant CO_2–water contact surface has increased the lateral spreading of CO_2 (Doughty, 2010).

Moreover, water flooding not only increases the water available for dissolution of CO_2, but also pushes the CO_2 plume further away from the injection well, which improves the plume volume subject to residual immobilization (Joodaki et al., 2017)

CO_2 trapping in WAG and continuous injection scenarios increased rapidly after the 20-year injection period and the subsequent shutting down of the well. This increase was due to the migration of CO_2 after injection caused by drainage and imbibition processes.

CO_2 trapping led to the displacement of brine in the aquifer at the leading end of the flow and the subsequent trapping of CO_2 as brine displaced CO_2 (Blunt, 2018).

CO_2 trapping was demonstrated to be advantageous for long-term storage, as trapped CO_2 accumulates and may dissolve or react with the host rock but cannot flow and escape from the saline aquifer.

Also, Iglauer (Iglauer, 2017) stated that a significant fraction of the initial saturation of injected CO_2 could be trapped after injection, thereby limiting the migration of mobile CO_2 and decreasing leakage.

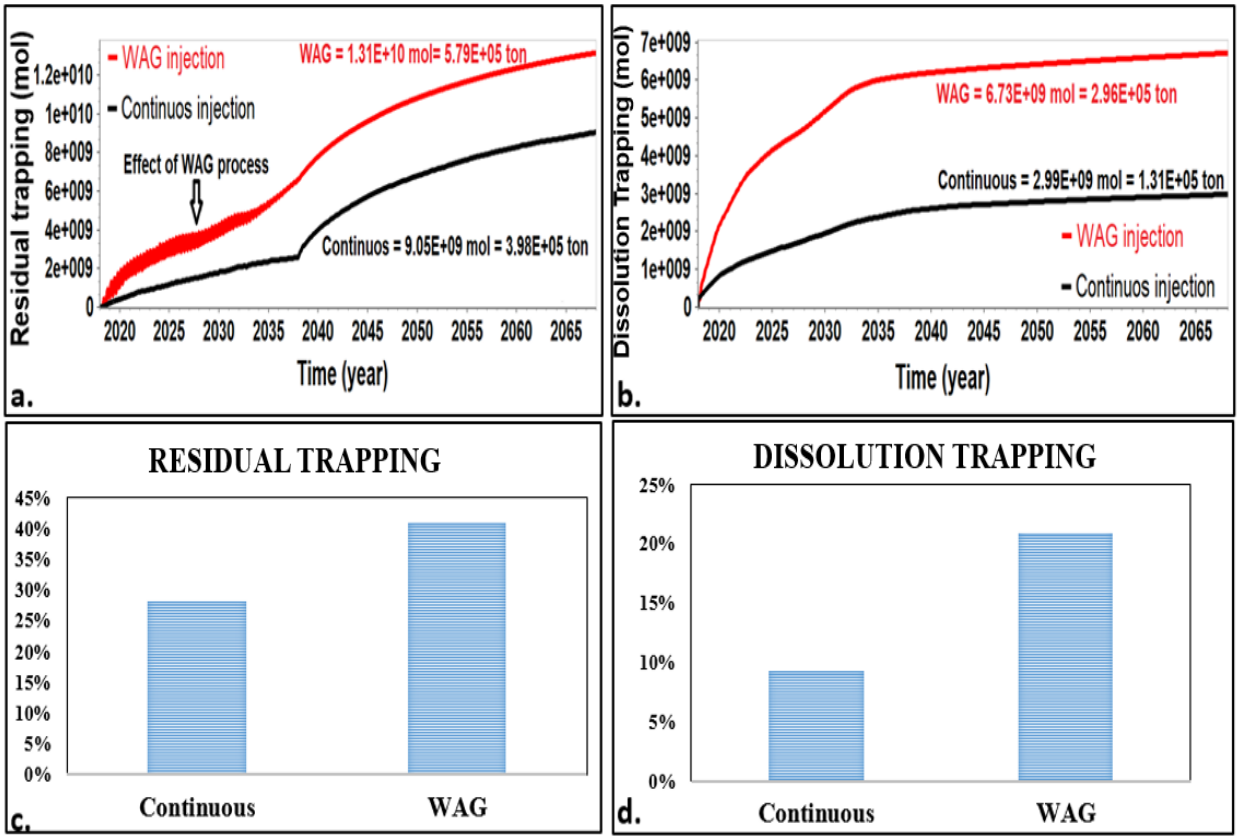

Figure 4.8 CO_2-trapping comparison between WAG and continuous CO_2 injections: (a) & (c) residual CO_2 trapping, (b) & (d) solubility CO_2 trapping (Vo Thanh et al., 2020)

The result of WAG injection is considered a base case scenario for optimization studies in Chapter 5. We can see that the amount of CO_2 trapping could enhance by optimization water and gas cycle lengths. The optimization task will be elaborated detail in Chapter 5. The critical role of cyclic water injection will be illustrated in the pore-scale of storage rocks. The water flooding was prevented the CO_2 bubble rising to the cap-rock by buoyancy effect. Therefore, the residual trapping was improved by CO_2 bubble moving back into the pore throats of porous media. In the case of dissolution trapping, the water injection was enhanced the CO_2 trapping by supplying the water for the convection mixing process of CO_2 and water in saline aquifers. Also, cyclic water injection has supported a more abundant CO_2–water contact surface that increased the lateral spreading of CO_2. Figure 4.9 illustrates the CO_2 trapping mechanism in porous media.

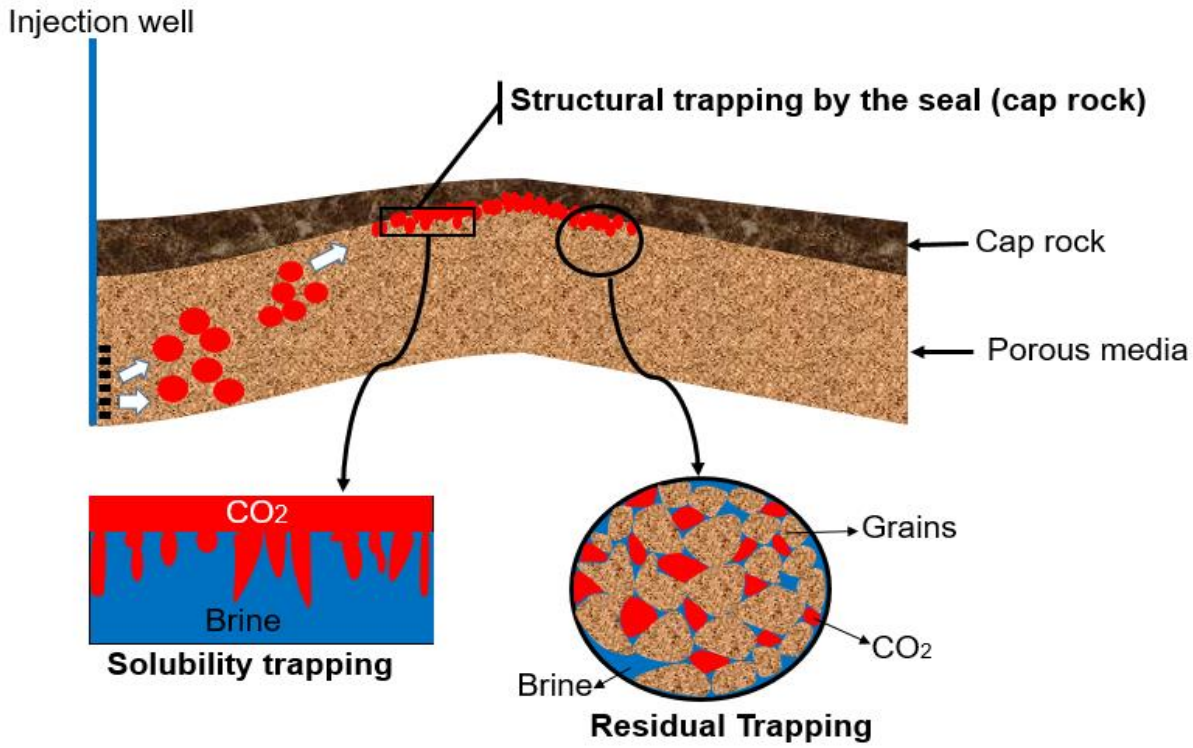

Figure 4.9 Schematic of CO_2 trapping in porous media

4. 4. Conclusions

Some key points need to highlight in this chapter.

1. The geometry of the channel was the most important in a fluvial deposit. The CO_2 plume migration is so sensitive to the parameters of fluvial channels. The higher anisotropy led to extend more CO_2 movement on the flat side. Thus, facies modelling should consider carefully in a fluvial reservoir for CO_2 storage purposes.
2. Our results were demonstrated that improved the residual and solubility trapping in heterogeneous fluvial sandstone reservoirs. The WAG injection was improved total CO_2 trapping by approximately 25% compared with the continuous CO_2 injection process.
3. Our simulation results were proposed as the way for improving the CO_2 storage efficiency in terms of residual and solubility trapping. Thus, WAG was a high recommendation for the injection scheme.

CHAPTER 5

ROBUST OPTIMIZATION OF CO_2 TRAPPING USING WATER ALTERNING GAS PROCESS UNDER GEOLOGICAL UNCERTAINTIES

5. 1. Introduction

As described in Chapter 4, the Water Alternating Gas (WAG) injection has been recommended for enhancing CO_2 trapping in the reservoir. The performance of the WAG process could improve by optimization approaches. Besides, the optimization of the WAG technique requires a solution for finding the most optimal injection rates and cycle length for CO_2 sequestration. Recently, Zhang and Agarwal (2013) used the genetic algorithm to define the CO_2 and water injection rates for the enhancement of CO_2 trapping. However, this work did not include the gas and cycle lengths under geological uncertainties on the optimization approaches. Geological uncertainties are an inherent characteristic of the petroleum exploration and exploitation process. The uncertainty can be related to subsurface data collection and interpretation of those data (CMG, 2019). Also, Geological uncertainties exhibit notable influences on the behavior of CO_2 injection (Aminu et al., 2017; Welkenhuysen et al., 2017). Thus, the effect of geological uncertainties must be before the robust optimization CO_2 sequestration solution can be confirmed.

Many studies have been integrated geological modeling and robust optimization process to determine optimal solutions while considering geological uncertainties.

This process, including low-salinity water injection process (Dang et al., 2016), hybrid alkaline-surfactant-polymer flooding (Dang et al., 2018), gas-assisted gravity drainage

process (Al-Mudhafar et al., 2018), unconventional reservoirs (Nguyen et al., 2016), well placement optimization (Jesmani et al., 2020), water flooding optimization (Pinto et al., 2019; Yasari and Pishvaie, 2015), steam-assisted gravity drainage process (Fedutenko et al., 2013; Yang et al., 2011), has been adapted in several improved oil recovery/Enhanced Oil Recovery studies. However, the robust optimization of CO_2 trapping using WAG technology has not been studied.

Therefore, this chapter presents an optimization workflow to maximize field-scale trapping of CO_2 using the WAG process while considering the effects of geological uncertainties on the simulation results.

5. 2. Methodology

5. 2. 1. Optimization techniques

In this study, the optimization approaches of the WAG process included experimental design techniques, such as design exploration and controlled evolution (DECE) and Latin Hypercube Design (LHD). The DECE algorithm was applied through the following steps: Design exploration and controlled evolution. In the design exploration step, simulation jobs were created by randomly selecting levels for each parameter through a Tabu search and experimental design (CMG, 2019; Yang et al., 2007). In the controlled evolution step, the statistical analysis was observed for the simulation results received from the design exploration stage (Yang et al., 2007). A gene and allele represented each parameter and level, respectively. Analyzing which gene had notable effects on the objective function was completed by observing which allele diminished the undesirable results.

This process aims to reach the maximum amount of information with a minimized number of simulation experiments. The main advantages of the DECE approach are its capability

to obtain an optimal solution rapidly compared with other designs of experimental tools and deviate from being trapped in the local optima while inspecting deactivated alleles. The duplicated validation of the deactivated alleles guaranteed that these alleles would not be returned into the approach (CMG, 2019; Yang et al., 2007). The DECE was adopted in this work for the nominal optimization of the WAG process under geological uncertainties. The LHD was a statistical sampling tool used to generate samples from the input parameters to develop numerous computer experiments from a multi-dimensional distribution (Mckay et al., 2000). The minimum experiments could capture several levels of variation for each parameter through sampling techniques to provide limited data points via the design domain in uniform dissemination through a space-filling design (Bhat, 2001). The LHD was also an enhancement procedure for creating a new group of experiments in a random manner if the initial dataset did not represent the problem. According to Stein (1987) (Stein, 1987), no accuracy workflow is available to help determine the number of experiments that could be generated.

In this work, the LHD was used for the robust optimization of the WAG process under geological uncertainties that were defined by generating several realizations. This tool generated the training dataset of simulation jobs that were assessed by the CMG reservoir simulation software to calculate the amount of CO_2 storage. This procedure allowed users to accomplish an optimization study easily.

5. 2. 2. Optimization under geological uncertainties

Geological uncertainties were important concerns in reservoir simulation, which aims to capture a highly realistic geological environment. Because of the evaluated effects of reservoir properties on the WAG process for CO_2 sequestration, the optimization workflow

should consider the geological uncertainties and not depend on a single realization. For this reason, a large number of realizations were generated by combining object-based modelling and sequential Gaussian simulation. Then, these realizations were evaluated in CMG-CMOST optimizer integration with Petrel software to rank them and determine the three quantiles (P10, P50, and P90). These realizations were represented the overall geological uncertainty. Subsequently, the selected geological realizations and experimental design were incorporated into the optimization process. This type of optimization under geological uncertainty was named as robust optimization (CMG, 2019; Yang et al., 2011). The nominal and robust optimization approaches were used for the WAG process.

5. 2. 3. Robust optimization workflow

The nominal optimization was based on a single realization of each reservoir parameter. The core sample and well logs were combined with various geological properties, such as porosity and permeability, due to inherent uncertainties from seismic data. Including these uncertainties in the optimization process is crucial (Yang et al., 2011).

Multiple realizations of reservoir properties were created by the geostatistical stochastic method to quantify uncertainties in a geological model (Fedutenko et al., 2013). The following equation described the unknown space (Θ) from the three ranked geological realizations for each reservoir property (θ_d).

$$\theta_d = \left\{\theta_1, \theta_2, ..., \theta_{N_r}\right\} \subset \Theta , \quad (1)$$

where N_r is the total number of ranked geostatistical realizations.

The objective function in this optimization problem was CO_2 residual and dissolution trapping calculated by the end of 20-year injection and 40-year post-injection prediction periods.

Suppose that the CO_2 trapping (objective function) in the WAG process optimization is *J*, the optimization parameter is *L*, and the geostatistical realization is θ_d. The objective function under geological uncertainties is defined as follows (Yang et al., 2011):

$$J = H\left(L, \theta_d\right), \tag{2}$$

where *H* is a transfer function. To consider the uncertainty expressed by multiple geological realizations, the objective function in robust optimization J_{RO} can be formulated as follows (Van Essen et al., 2009):

$$J_{RO} = E_{\theta_d}\left[H\left(L, \theta_d\right)\right] - r.\sqrt{\sigma_{\theta_d}\left[H\left(L, \theta_d\right)\right]}, \tag{3}$$

where E_{θ_d} denotes the expected value over the geostatistical uncertainty space of all realizations θ_d, σ_{θ_d} represents the variance, and r indicates the risk aversion factor (Van Essen et al., 2009).

Assuming that all realizations are equiprobable models, the expected value becomes the average of all geological realizations:

$$E_{\theta_d}\left[H\left(L, \theta_d\right)\right] = \frac{1}{N_r}\sum_{i=1}^{N_r} H\left(L, \theta_d\right) = \overline{J}\ . \tag{4}$$

By taking Equation (4) into Equation (3), the final equation of a robust optimization objective function could be rewritten as follows (Yang et al., 2011):

$$J_{RO} = \overline{J} - r.\sqrt{\frac{1}{N_R - 1}\sum_{i=1}^{N_r}\left(H\left(L, \theta_d\right) - \overline{J}\right)^2}\ . \tag{5}$$

Figure 5.1 illustrates the flowchart of robust optimization. The workflow of the robust optimization process was summarized as follows (Vo Thanh et al., 2020):

1. Create the geological realizations. A big-loop modeling workflow was adapted to create N_T geological realizations (N_T = 200 realizations).
2. Rank N_T geological realizations using a reliable method. For this study, the direct numerical simulations of the ranking process using a coarse grid adapted from chapter 4 to complete for the 200 generated geological realizations, and the results were ranked based on calculated performance (e.g., cumulative CO_2 injection). The baseline WAG parameter was the same as the datasets in Chapter 4.
3. Choose a number of representative realizations (N_R) for robust and nominal optimizations. Cumulative CO_2 injection from the 200 previously generated realizations was reviewed after plotting the results on the same chart. After the probability of CO_2 cumulative injection distribution was reviewed, three realizations (P10, P50, and P90) were ranked and selected for robust optimization.
4. Conduct optimization. The P50 CO_2 cumulative injection from point (3) was used for the nominal optimization, whereas the selected N_R representative realizations (P10, P50, and P90 in this study) were used to compute the objective function for robust optimization (Equation (5)).
5. In this study, the global objective function was formulated through average CO_2 trapping. This objective function was adapted from another optimization study (Nguyen et al., 2016). These average parameters were the sum of each geological realization with the same combination divided by the number of realizations (CMG, 2019):

$$Average CO_2TRAP = \frac{CO_2TRAP_1 + CO_2TRAP_2 + CO_2TRAP_3}{3} \quad (6)$$

Where the variables CO_2TRAP_1, CO_2TRAP_2, and CO_2TRAP_3 are CO_2 trappings for the P10, P50, and P90 geological realizations, respectively.

6. Quality control and comparative analysis. The results of the robust and nominal optimization workflows were reviewed and compared for conclusive analysis.

Figure 5.2 depicts the comparison of two workflows.

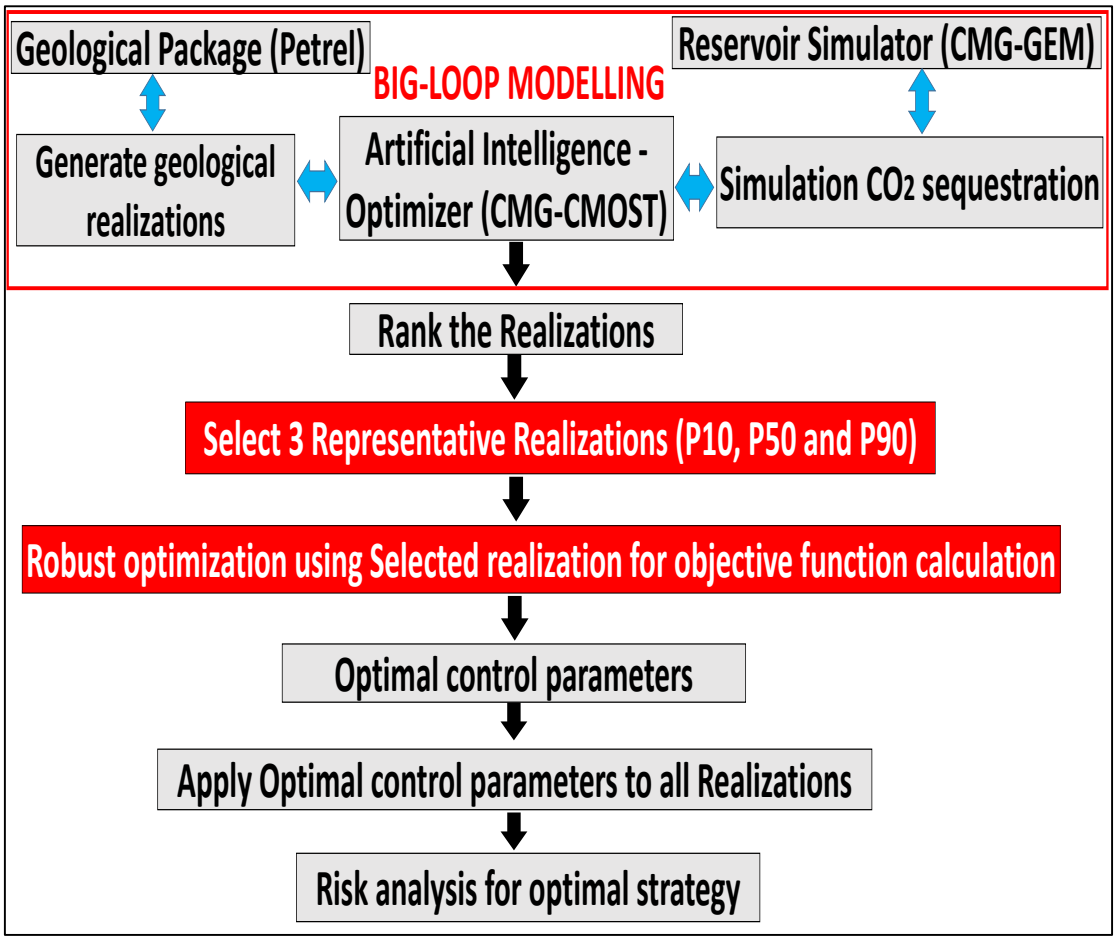

Figure 5.1 Optimization flowchart used for this study (Vo Thanh et al., 2020)

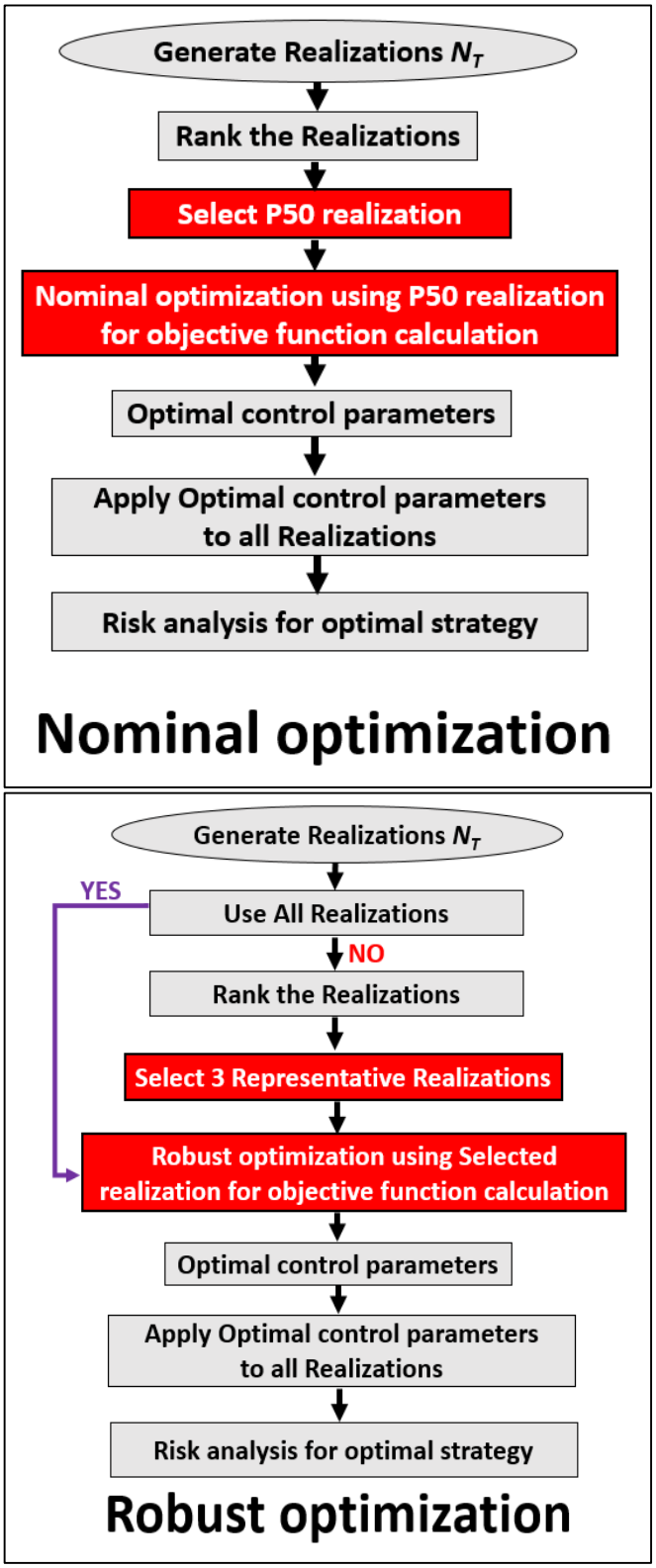

Figure 5.2 Comparison workflow of Nominal optimization and robust optimization

5. 3. Result and Discussion

5. 3. 1. Optimization of CO_2 trapping

The length of cycles in the WAG process is discrete known parameters, while the porosity and permeability are treated as uncertainty parameters to optimize the objective function (cumulative CO_2 trapping). **Table 5.1** describes the design parameters for the WAG optimization process (Vo Thanh et al., 2020).

Table 5.1 Variable constraints used in optimizing study (Vo Thanh et al., 2020)

Parameter	Lower bound	Base case	Upper bound	Step
Gas cycle length (days)	30	60	120	10
Water cycle length (days)	30	60	120	10

Variable constraints represented for the minimum and maximum pore volume (PV) injected. We can compute the PV injected for the range of injected CO_2 (30–120 days) by using the CO_2 injection rate and the reservoir PV.

For instance, the PV of the reservoir is 115 518 000 m^3. The cumulative CO_2 injection as the base case injected within 60 days is 2 251 308 m^3. The total slug size is 1.95 PV when the cumulative CO_2 is divided by the PV. This procedure will act as the base to calculate the lower and upper limits for the optimization process. In this case, the lower bound is 0.97 PV, and the upper bound is 3.9 PV (Vo Thanh et al., 2020).

Furthermore, the ranking process in this work was achieved by integrating a geological modeling package (Petrel), a reservoir simulator (CMG-GEM), and an Intelligence optimizer (CMG-CMOST) into a single workflow (**Figure 5.1**). 200 realizations of the geological model were created from the base-case model (Vo Thanh et al., 2020).

A range of geological variables, including the global seed number, variogram (horizontal and vertical ranges), and azimuth values, was created using the Petrel geological package (**Table 5.2**). Consequently, Petrel was used to create the new realization considering the varied global seed number, variogram, and azimuth values while CMOST-AI was running. These values are uncertainty variables in modelling process. Thus, determining the minimum and maximum amounts to change the distribution of facies, porosity, and permeability in the reservoir was necessary (Vo Thanh et al., 2020).

Table 5.2 Parameters for a creation of geological realizations (Vo Thanh et al., 2020)

Parameter	Lower Limit	Base case	Upper Limit	Step
Horizontal range	1000	1800	3600	200
Vertical range	10	20	30	2
Azimuth	15	25	35	5
Global seed number	1000	8000	16000	500

Then, these geological realizations were automatically transferred to the reservoir simulator to perform the WAG simulation and compute the cumulative trapped CO_2 within a 20 year injection period. After that, the reservoir simulation results were input into the AI-optimizer, which subsequently created the new geological model realization and initiated the next simulation. The rate and pressure of WAG injection were the same as those for the base case model.

Figure 5.3 highlights the cumulative CO_2 injection results for the 200 randomly generated geological realizations. Also, **Figure 5.4** depicts the probability distribution function of the cumulative CO_2 injection and highlights the P10, P50, and P90 realizations.

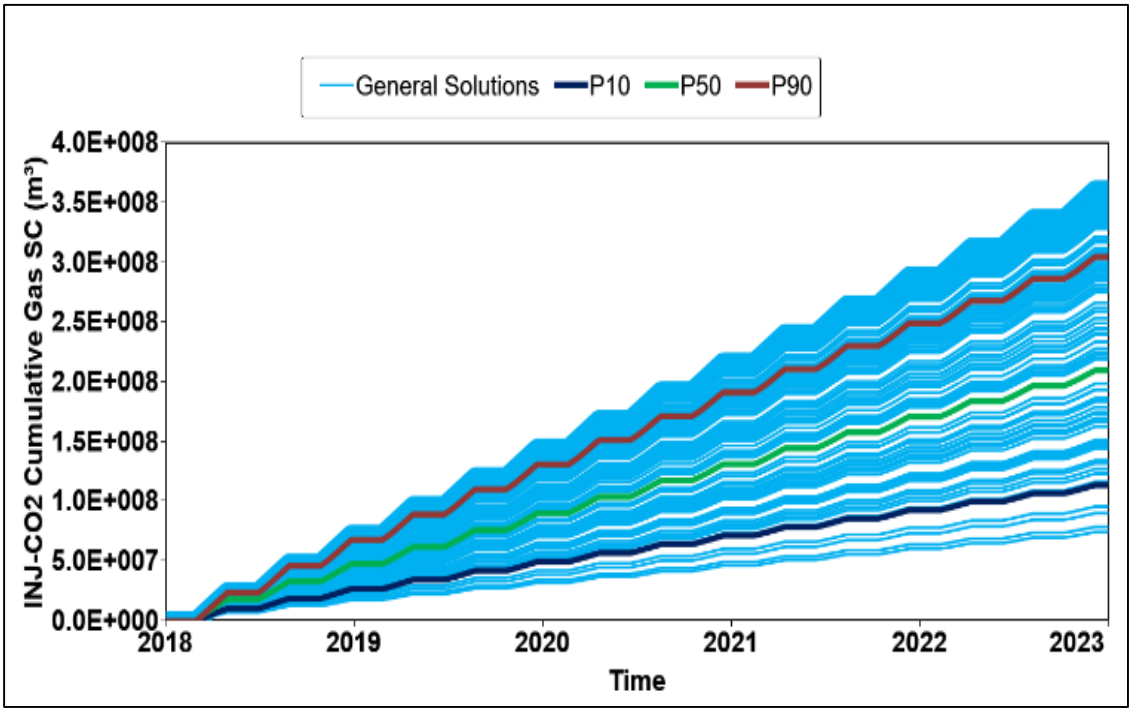

Figure 5.3 The plausible scenarios for the cumulative CO_2 injection, later used for the ranking process (Vo Thanh et al., 2020)

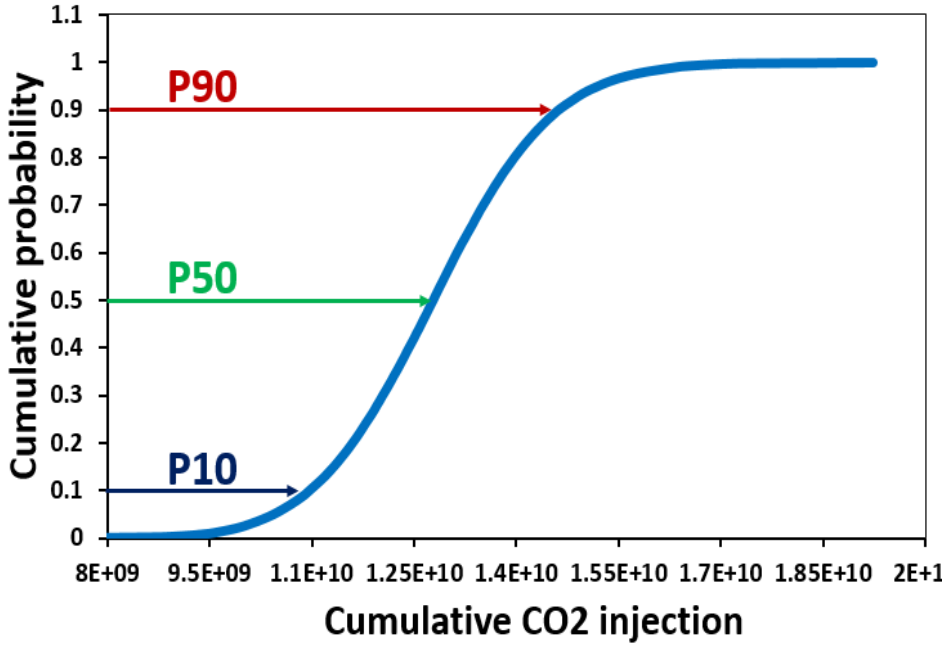

Figure 5.4 The probability density function of the cumulative CO_2 injection (Vo Thanh et al., 2020)

Moreover, **Figures 5.5** depicts the three-dimensional images of the selected porosity and horizontal and vertical permeability for each of the P10, P50, and P50 realizations, respectively

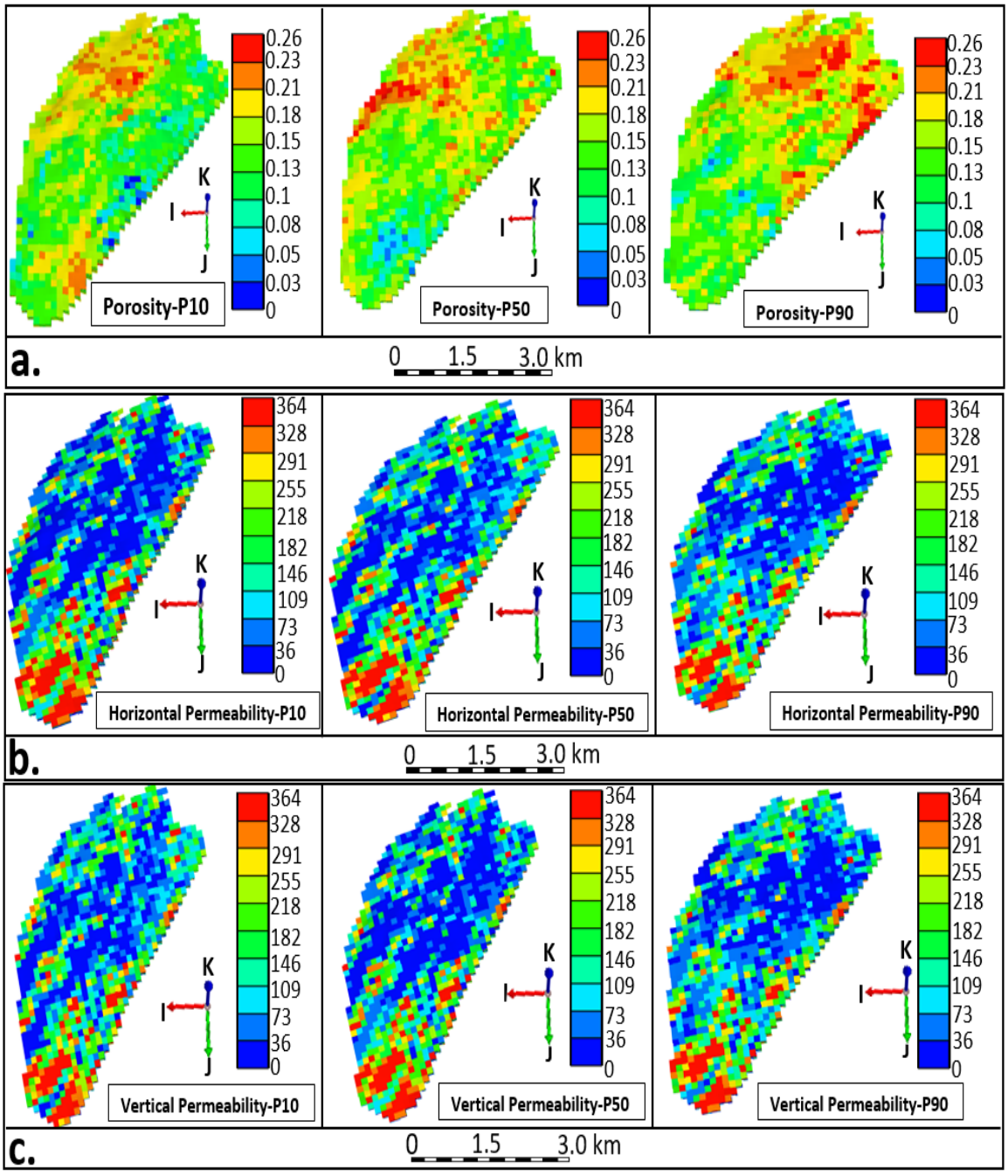

Figure 5.5 The ranked of 3D porosity, horizontal permeability, and vertical permeability models (Vo Thanh et al., 2020)

As shown in these figures, the notable differences observed among the three selected realizations are indicative of the overall uncertainty of the reservoir.

We presented the results of the ranked P10, P50, and P90 realizations for the robust optimization framework following the method of Al-Mudhafar et al. (2018).

These authors proposed a successful framework for the robust optimization of a GAGD process by considering the three realizations to reduce risks through a precise analysis of the model uncertainties. Besides, the P50 cumulative CO_2 injection scenario adapted for the nominal optimization approach. This scenario later used for comparison with the robust optimization framework (Vo Thanh et al, 2020).

5. 3. 2. Result of robust optimization

The P10, P50, and P90 realizations of porosity and permeability distribution were used to constrain the geological models adapted in the robust optimization workflow.

The parameterization used to conduct the robust optimization framework is highlighted in **Table 5.1**. The robust optimization approach investigated 250 optimal samples from a total of 750 simulation jobs across the three ranked geological realizations. This large number of simulation runs enabled enhancement of the robustness of the optimal solution identified by the robust optimization framework relative to the result of the nominal optimization framework. The dual-core computer (3.6 GHz, 16 GB) was used for the optimization approaches.

The CPU time of each simulation job was 1 hour and 30 minutes to finish one simulation run. Thus, the main issue of the robust optimization framework is computation cost. To address this issue, the CPU resources should be upgraded to reduce the simulation time.

Figure 5.6 shows the amount of dissolved and residually trapped CO_2 computed for all the simulations tested as a part of the robust optimization framework. As observed, the most optimal solution (**Figure 5.6**, a highlight in red) reveals the highest amount of trapped CO_2, as estimated at the end of the injection and post-injection phases.

Figure 5.7 displays numerous general solutions and the optimal solution created by the robust optimization framework in comparison with the base case. The optimal solution, recommended by the dashed purple line, defines the highest residual and solubility trapping CO_2 at the end of the injection and post-injection phases.

Figure 5.8 indicates the cross plot between trapped CO_2 and the input WAG parameters as defined for the robust optimization, demonstrating the optimal level of each parameter corresponding to the robust optimal solution.

Hereto, the optimal strategy (30/120 cycle lengths) was 30 days of CO_2 injection followed by 120 days of water injection.

In the next sections, results from the nominal optimization and further comparison with the robust optimization are investigated, respectively (Vo Thanh et al., 2020)

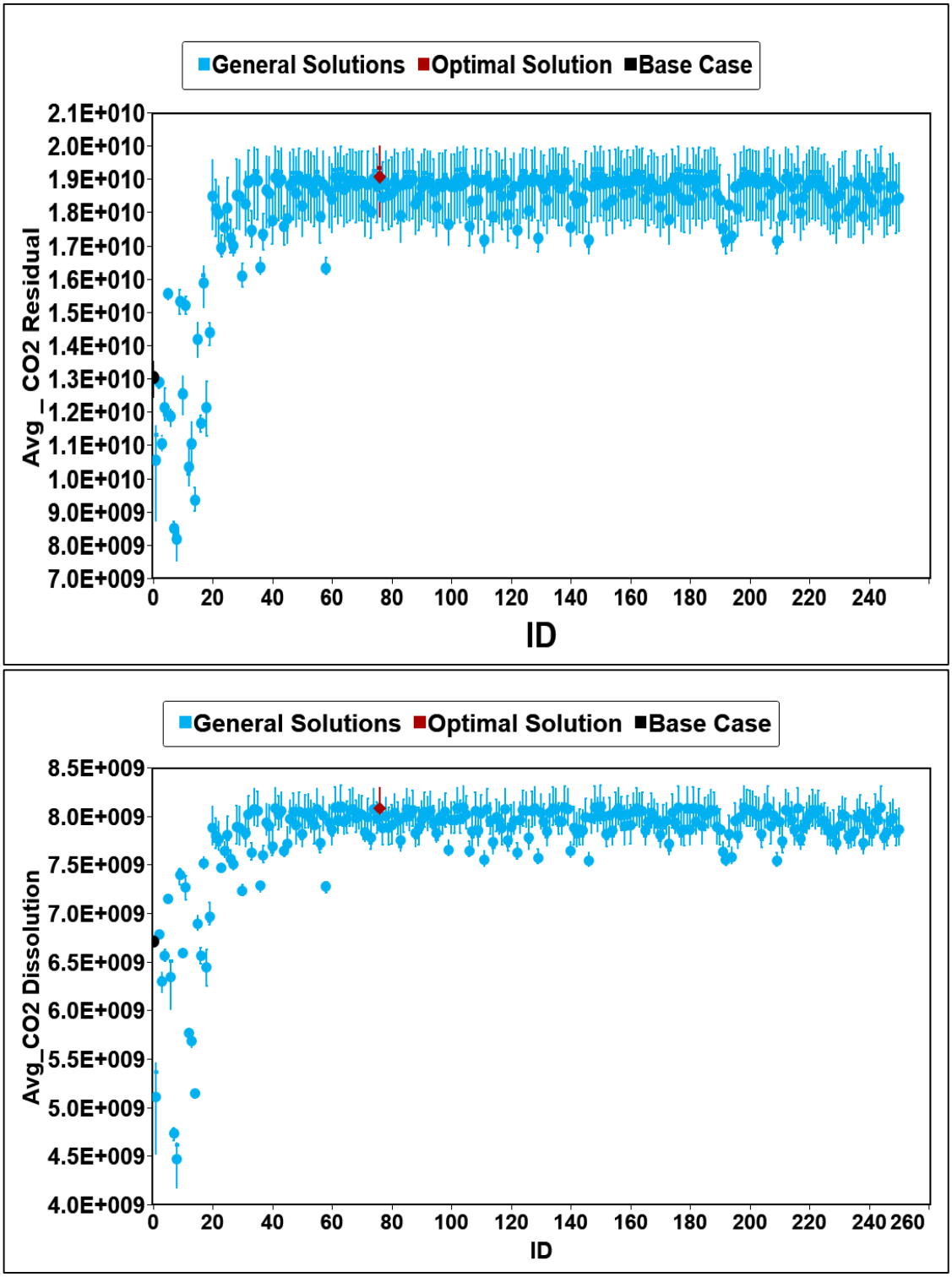

Figure 5.6 The robust optimization process from Latin Hypercube Design for residual (top) and dissolution trapping (bottom) (Vo Thanh, et al., 2020)

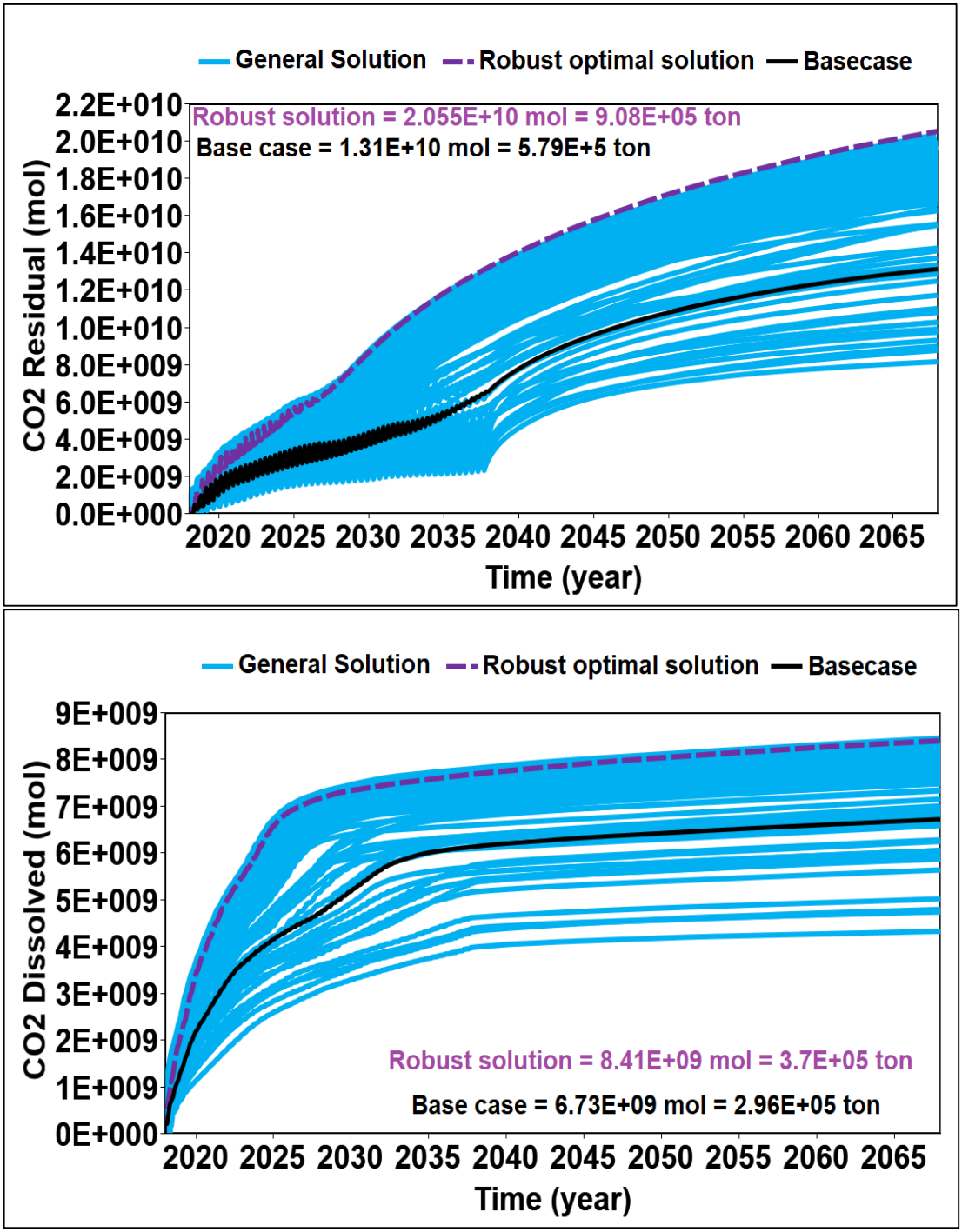

Figure 5.7 The time series of residual (top) and dissolution trapping (bottom) for robust optimization workflow (Vo Thanh et al., 2020)

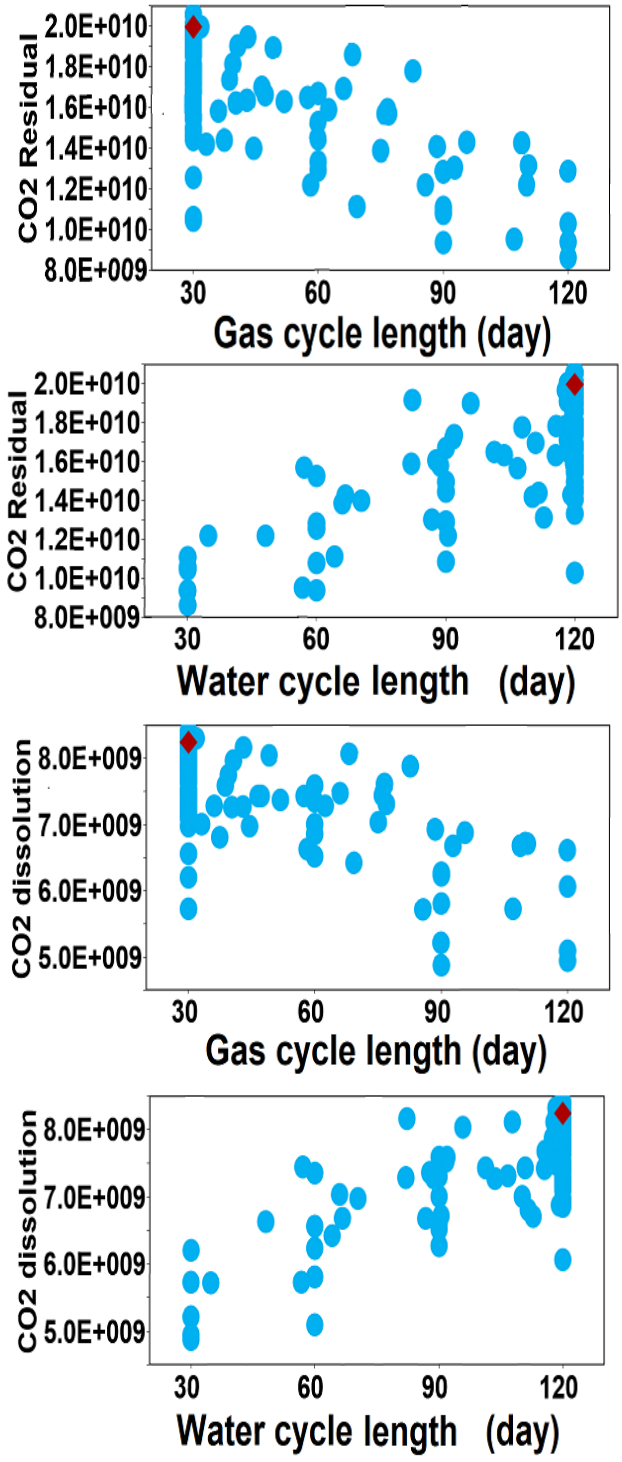

Figure 5.8 Cross plot depicting the relationship between the objective function (trapped CO_2) and WAG cycle length (Vo Thanh et al., 2020).

5. 3. 3. Result of nominal optimization

Similar in the previous section, this section explains the results from the nominal optimization workflow based on the P50 geological realization to enhance the performance of the WAG process relative to that calculated for the initial base case. The DECE approach applied to the nominal optimization of the WAG process. This approach determines the optimal solution with few simulation jobs compared with other experimental design methods.

Figure 5.9 depicts the objective function based on simulation experiments from the nominal optimization workflow as computed for the 20-year injection and 40-year post-injection periods. In these figures, the optimal solution obtained in a small number of simulation experiments without being trapped by local optimal. To verify the efficacy of the optimization workflow, the results of the base case scenario before optimization illustrate in black filled circles (**Figure 5.9**). Relative to this base-case scenario, the effects for the optimal experiments (red-filled diamonds) enhance through a series of iterative experiments (blue circles, **Figure 5.9**). The amounts of residual and solubility trapping CO_2 computed for the WAG injection base case and the nominal optimal solution display in **Figure 5.10.**

The optimal solution is the highest value of residual and solubility trapping. Comparison between the base case and the optimal solution based on the P50 realization of the geological model indicates that a significant increase in CO_2 trapping can be obtained through WAG process optimization. The nominal optimization values of residual and solubility trapping CO_2 were 747,000 and 327,000 tons, which were 168,000 and 310,000 tons more than those computed for the base case.

Also, **Figure 5.11** shows the optimal WAG parameter for nominal optimization. The optimal strategy (50/100 cycle lengths) was 50 days of CO_2 injection, followed by 100 days of water injection.

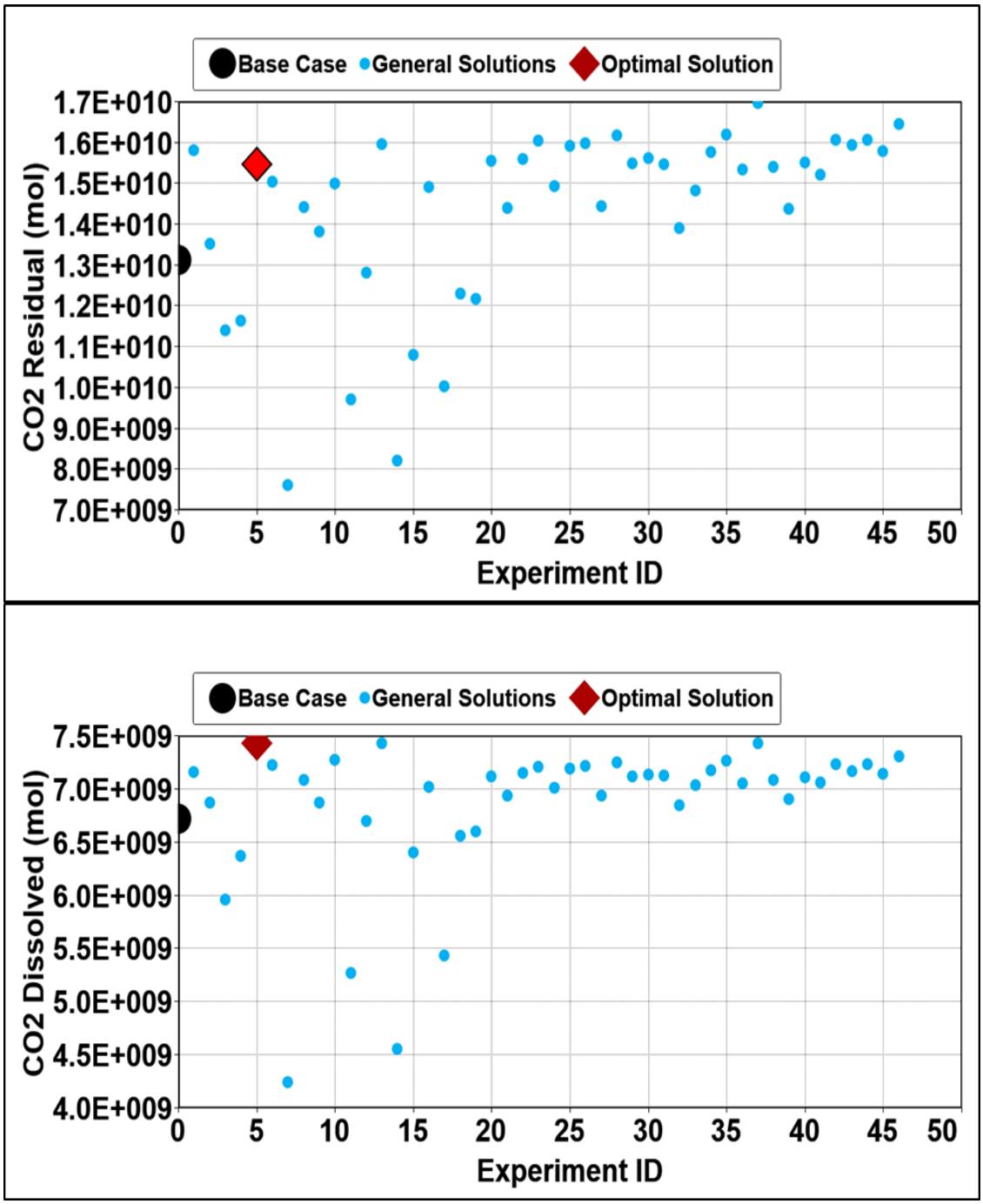

Figure 5.9 The nominal optimization process from DECE for residual (top) and dissolution trapping (bottom) (Vo Thanh, et al., 2020)

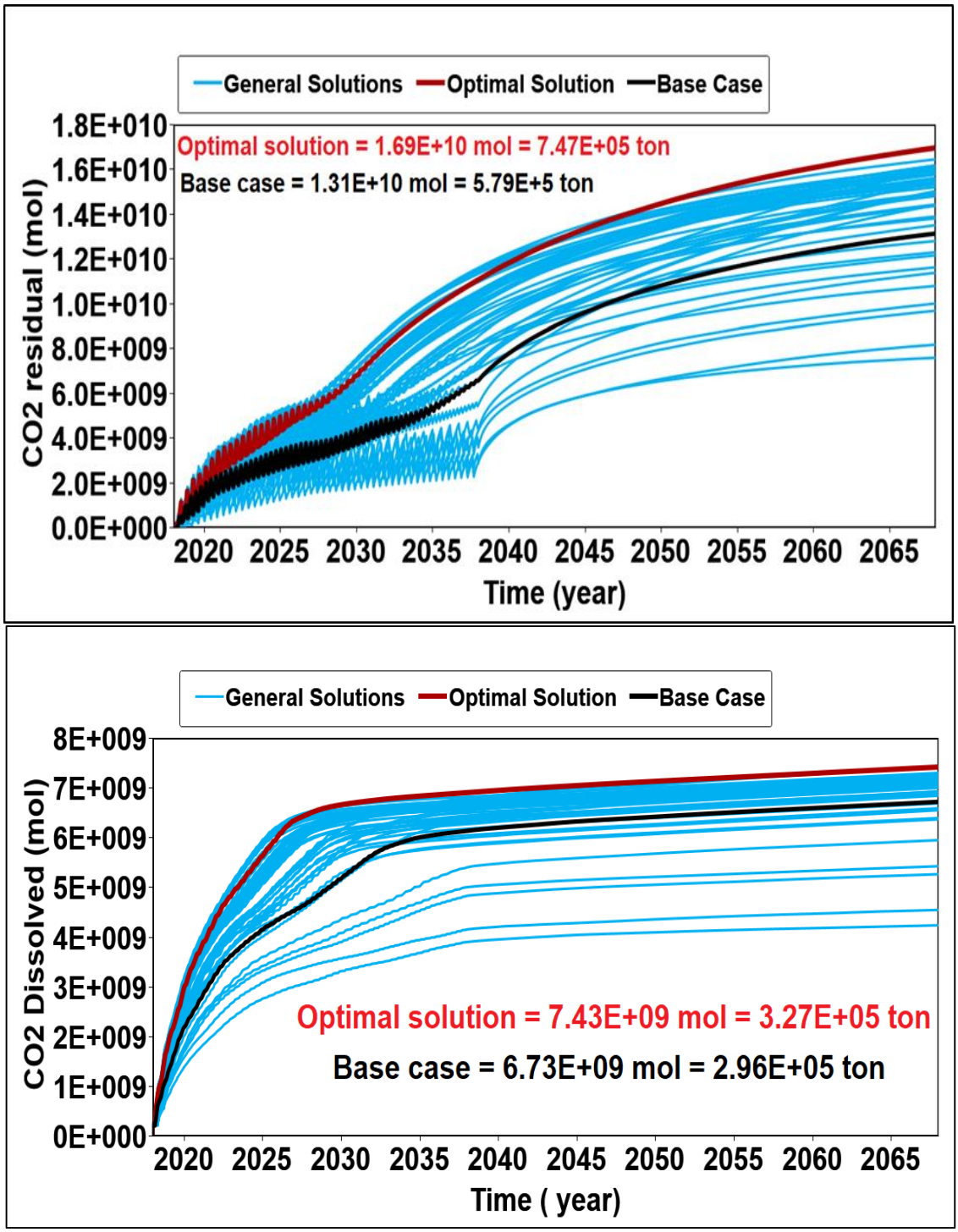

Figure 5.10 The time series of residual (top) and dissolution trapping (bottom) for nominal optimization workflow (Vo Thanh et al., 2020)

5. 3. 4. Robust optimization versus P50 nominal optimization for CO_2 trapping

The robust optimization result is now compared with nominal optimization to demonstrate effectiveness in handle geological uncertainties. **Figure 5.11** highlights the comparison of dissolution and residual CO_2 trapping between nominal and robust optimizations from WAG optimization.

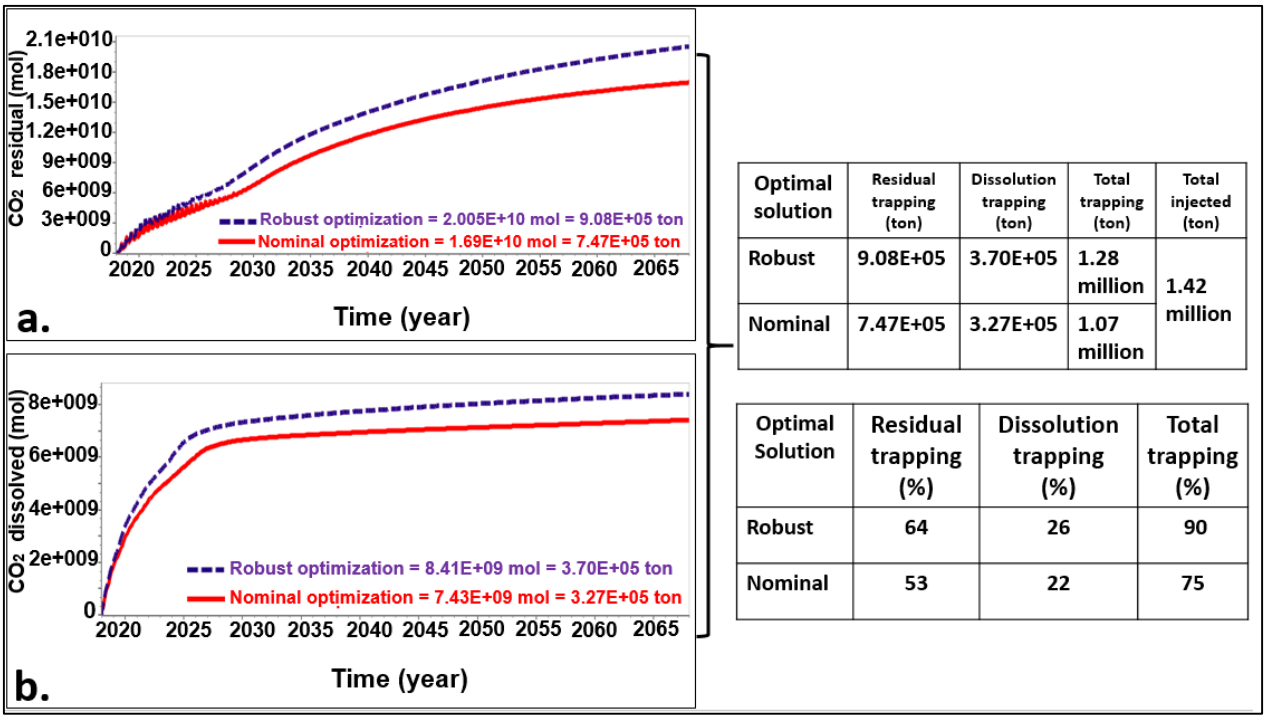

Optimal solution	Residual trapping (ton)	Dissolution trapping (ton)	Total trapping (ton)	Total injected (ton)
Robust	9.08E+05	3.70E+05	1.28 million	1.42 million
Nominal	7.47E+05	3.27E+05	1.07 million	

Optimal Solution	Residual trapping (%)	Dissolution trapping (%)	Total trapping (%)
Robust	64	26	90
Nominal	53	22	75

Figure 5.11 Comparison of CO_2 trapping between robust and nominal optimization (Vo Thanh et al., 2020)

The robust optimization procedure for improving total CO_2 trapping (residual and dissolution) led to the output of 1.278 million tons, resulting in approximately 204,000 tons of total CO_2 trapped, which is higher than that of the nominal optimization. For instance, after a 40-year storage period, 90% of CO_2 was residual and dissolution trapped in the case of robust optimization, whereas only 75% of CO_2 was trapped in nominal optimization. In

the statistical aspect, the mobile CO_2 was only 10% for robust optimization, whereas it was 25% for nominal optimization.

Moreover, this section uses individual analysis results for both robust and nominal optimization, and we now address the question: how is robust optimization better than nominal optimization? To answer this, we sought a comparative analysis between robust and nominal optimization and explored questions to bring clarity to which optimization procedure accounts for most geological uncertainty during CO_2 sequestration.

The ultimate goal is to determine which of these two workflows fully capture all uncertainties associated with CO_2 sequestration, clarifying all operational ambiguity.

Therefore, two-cycle lengths: 30/120 and 50/100, were used to simulate three realizations-P10, P50, and P90 in the case of robust optimization for valid comparison to one realization (P50) in the case of nominal optimization. **Figure 5.12a** and **5.12c** depict the quantitative comparison of trapped CO_2 (soluble and residual) for both the nominal and robust optimal solutions, respectively (Vo Thanh et al.,2020).

In all cases, the P10 of the robust optimization lies below the P50 result for nominal optimization, and the P90 of robust optimization provides the highest value for trapped CO_2. A similar analysis illustrates in **Figure 5.12b** and **5.12d**, for the case of 50/100 cycle lengths. Therefore, in all likelihood, the comparative results for the two optimal scenarios demonstrate that the robust strategy is better than the nominal plan.

This is because the robust optimization gives three different scenarios, compared with only one for nominal optimization; this, it provides a flexible possibility of having more trapped CO_2 (i.e., P90) by tuning the geological and reservoir parameters in this direction. Furthermore, to demonstrate the robust nature of randomly generating geological

realizations and applying our proposed workflow, five random realizations were sampled from the overall set of 200 created realizations to contrast CO_2 trapping in both optimal strategies effectively.

Figure 5.13 depicts a comparison of residual and dissolved CO_2 using five random realizations. As can be seen in this figure, the 30/120 cycle lengths led to an on-average higher amount of CO_2 trapping than 50/100 cycle lengths in all five realizations. Besides, on average, during robust optimization, 30/120 cycle lengths are recommended over 50/100 cycle lengths.

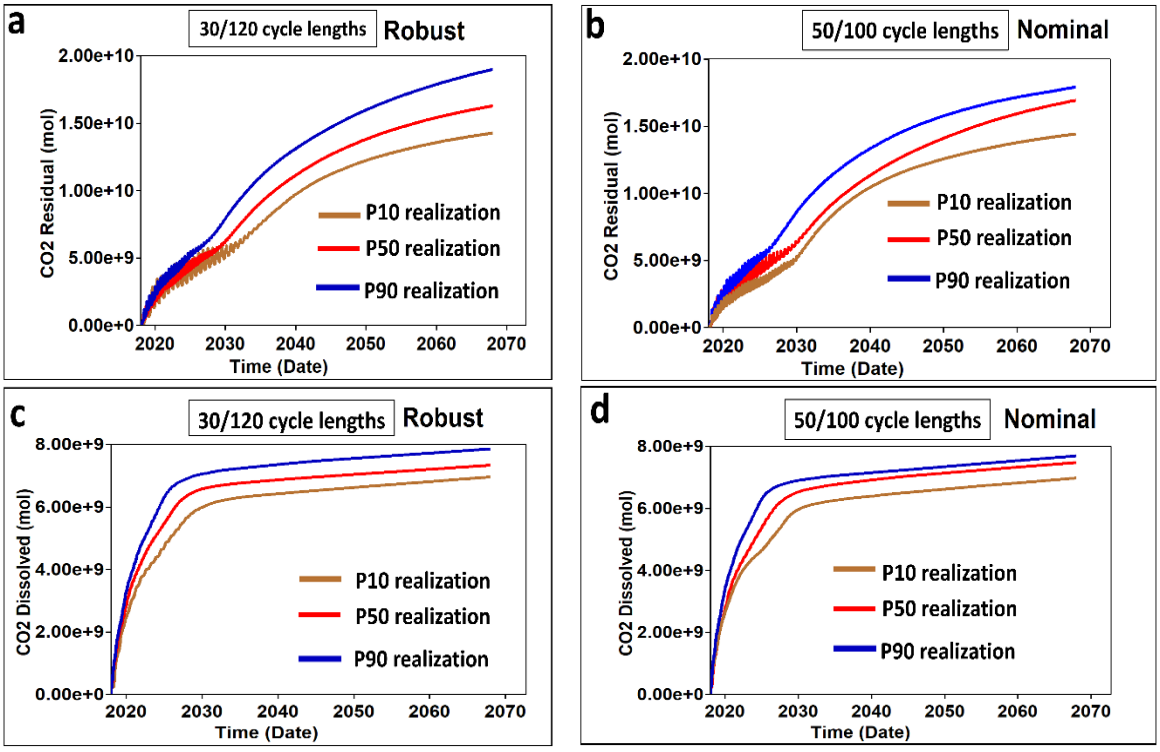

Figure 5.12 Nominal and robust strategy applied for three realizations (P10, P50, and P90): (a) comparative residual CO_2 trapping against time; (b) comparative solubility CO_2 trapping against time; (c) CO_2 residual trapping for the two optimal strategies; (d) CO_2 solubility trapping for the two optimal strategies (Vo Thanh, et al., 2020)

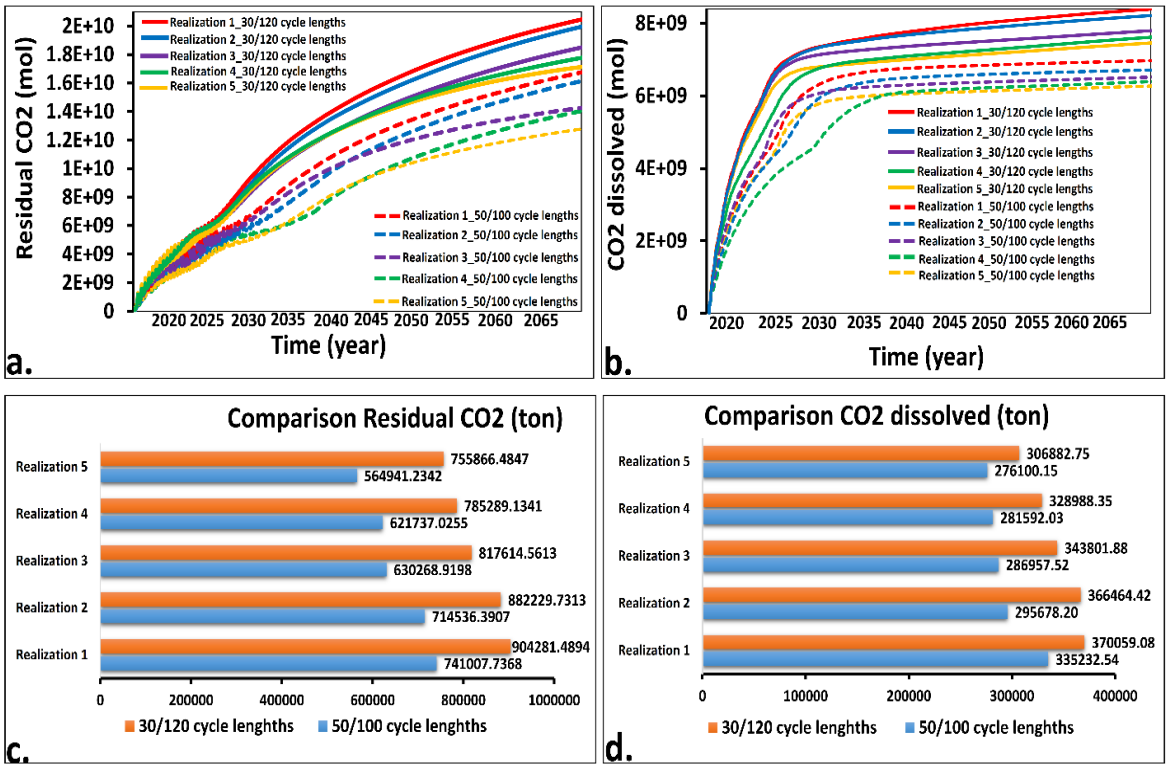

Figure 5.13 Robust optimization for five randomly generated geological realizations: (a) comparative residual CO_2 trapping against time; (b) comparative soluble CO_2 trapping against time; (c) amount of CO_2 residual trapping for each assessed cycle length; (d) amount of soluble trapped CO_2 for each cycle length (Vo Thanh et al., 2020)

After obtaining the optimal solutions based on the robust optimization, the uncertainty quantification was conducted using statistical theory (such as probability density function and cumulative distribution function. The strengths of the robust optimization was showed by providing the ranges of distribution of input parameters. **Figure 5.14** depicts the histogram and cumulative probability distribution function of the quantified uncertainty effect on CO_2 trapping. The figure also highlights the P10, P50, and P90 results of the residual and solubility trapping. The wide range of calculated trapped CO_2 demonstrates

the crucial role of quantifying the geological uncertainty in the WAG process for CO_2 storage. Moreover, robust Optimization takes geological uncertainty into account, by considering 200 realizations in combination with other optimization parameters in an attempt to find a risk-weighted solution that will work for all scenarios (CMG, 2019). This rigorous optimization workflow significantly reduces risk and increases the probability of success.

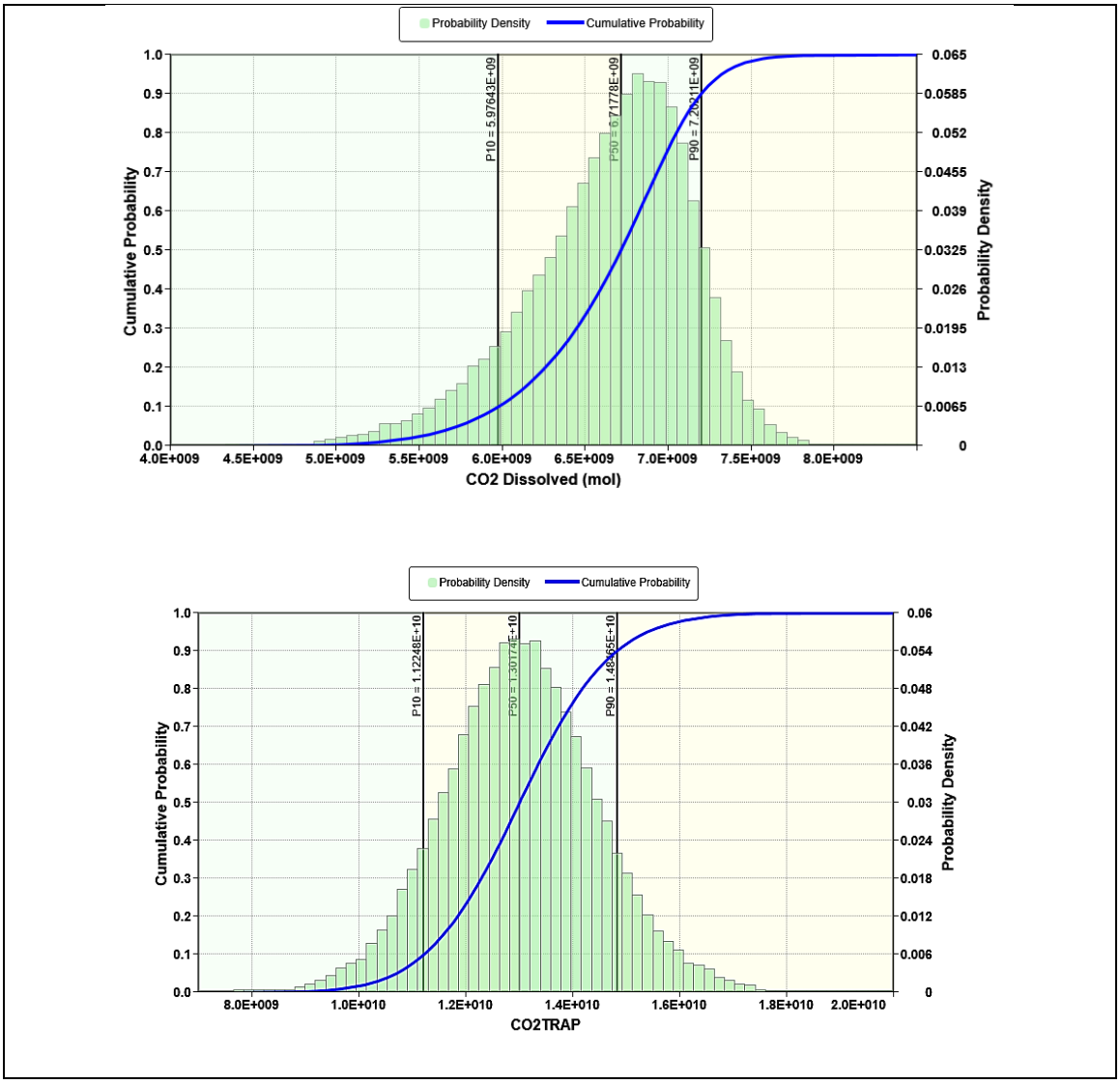

Figure 5.14 Uncertainty assessment for robust optimization: (a) residual CO_2 trapping; (b) dissolved CO_2 trapping (Vo Thanh et al., 2020)

Moreover, **Figure 5.15** illustrates the CO_2 saturation for the base case and the nominal and robust optimizations. As can be observed in this figure, the less free gas remained at the top of the formation after maximizing CO_2 trapping under geological uncertainties. This result demonstrates how robust optimization improves safety storage through either maximizing the residual trapping and dissolution of CO_2 or minimizing free CO_2.

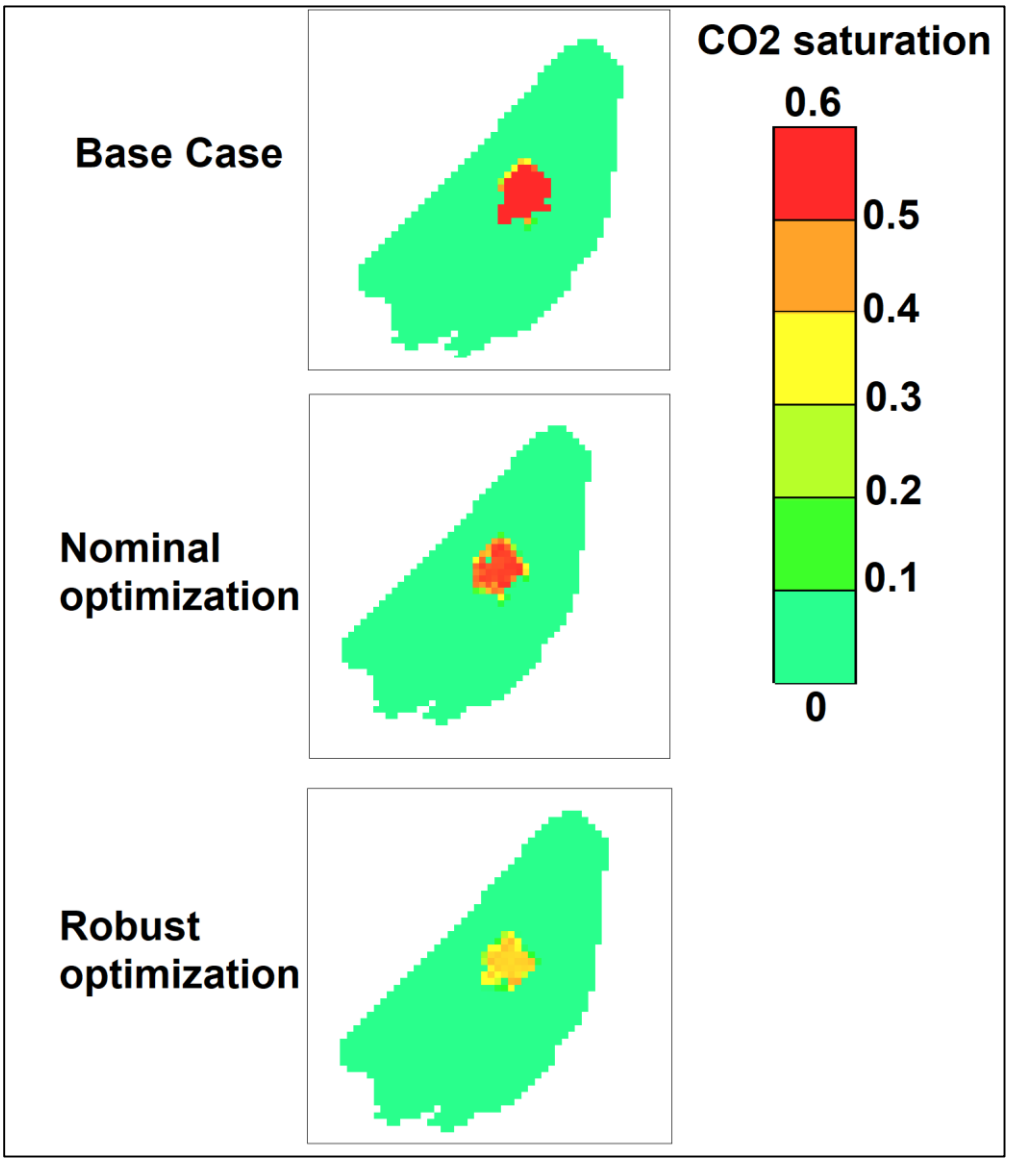

Figure 5.15 Free CO_2 saturation for the base case and the nominal and robust optimizations for the WAG process (Vo Thanh et al.,2020)

The efficiency of robust optimization workflow is clear confirmation through it shifts the whole CO_2 trapping to a higher value. However, it has a limitation in the high computational cost; one of the important problems is the determination of the number ranked geological realizations. The long run time for large geological models may lead to robust optimization impractical. For that reason, there are two main points for this problem: (1) capturing the effect of geological uncertainty parameters; (2) optimized the computation costs and ran time-based on available computer sources.

The more geological realizations selected, the better the uncertainty analysis accomplished, and the reducing risk for prediction and development. Besides, the number of ranked geological realizations for robust optimization depends on some factors, such as the structure of reservoir geology, the number of grid cells in the reservoir model, and the capacity of computer sources. Thus, there are no limited minimum or maximum realizations selected for robust optimization workflow, and these must be determined for a specific study. This study introduces an investigation of robust optimization with three ranked geological realizations for the WAG process in this particular. Based on the result of comparison with nominal optimization, robust optimization using three representative geological realizations supports the better way to consider geological uncertainties for the WAG process to enhance CO_2 trapping, for this specific case study. It is important to mention that this may not be true for all reservoir models to conduct a WAG process in CO_2 sequestration. The number of selected ranked should be carefully considered for each study to evaluated the effect of a geological model as well as to optimal available computer sources. In summary, this study proposed the integrated modeling and robust optimization workflow to enhance CO_2 storage efficiency under geological uncertainties in a

heterogeneous fluvial sandstone reservoir. The presented workflow can be employed to improve CO_2-trapping capacity within other real-scale field projects. This methodology can also be adapted in different aspects of CO_2 storage, EOR, and other engineering/science.

5. 4. Conclusions

This chapter presented a robust optimization workflow to determine the optimal strategy of the WAG process for CO_2 sequestration in a real fluvial sandstone reservoir. The following key points can be drawn from our results:

- Ranking of plausible geological models as presented in this study is a highly accurate method of integrating geology and reservoir parameters in developing field-scale models of CO_2 sequestration
- A robust optimization workflow that explicitly considers geological uncertainty can be successfully used to optimize CO_2 trapping in a real heterogeneous reservoir. This robust optimization method could not only improve CO_2 trapping efficiency but also reduce project risks in light of geological uncertainties.
- Although the nominal optimization workflow can also be used to enhance CO_2 sequestration by WAG injection, the optimal solution based on a single realization of the geologic model does not capture the effects of the significant uncertainties inherent in a large number of plausible geological models.
- If multiple realizations of the geological models are investigated for the effectiveness of CO_2 sequestration, the techniques demonstrated by this study could be further applied to similar projects to provide rapid technical or economic analyses. Because the robust optimization process is relatively easy to perform, the method used in this study can readily contribute to future studies of CO_2 sequestration by WAG injection.

CHAPTER 6

CONCLUSIONS AND RECOMMENDATIONS

6. 1. Conclusions

The geological uncertainties are very decisive factors to accomplish reliable predictions for future reservoir performance in CCS projects. Thus, integrated geological modelling for lithofacies (rock-type) and petrophysical properties was employed to generate the most reasonable geo-system. Then, the integrated geological models are acquired to construct accurate reservoir simulation models to enhancement the CO_2 trapping through the Water Alternating Gas (WAG) process. Ultimately, the robust optimization framework was developed to determine the optimal injection strategies under geological uncertainties.

The key findings were obtained from the entire research in this dissertation that is outlined below:

6. 1. 1. Integrated geological modelling

A new geological modelling workflow has been successfully developed to predict the distribution of 3D lithofacies, porosity, and permeability models. It was compared with the conventional modelling workflow to prove the accuracy models by the history matching process. In particular, the object-based modelling (OBM) was adapted for 3D lithofacies modelling of fluvial sandstone main pay in the Nam Vang field, southern offshore Vietnam. Moreover, multiple lithofacies realizations were generated for ranking purposes.

The Sequential Gaussian Simulation (SGS) was used to conditioning the lithofacies distribution to porosity and permeability models. Then, the correlation between SGS values and measurement values was plotted to select the most suitable lithofacies model using OBM. Also, the ANN plays an essential role in improving the reasonable 3D porosity and

permeability models. The Artificial Neural Networks could support for petrophysical modelling with limitation subsurface data. Furthermore, the co-kriging techniques are instrumental in combining the lithofacies and ANN values into a single model. Last but not least, Drill Stem Test (DST) data is vital to evaluate the accuracy models from static modelling to dynamic simulation.

6. 1. 2. Reservoir simulation of CO_2 sequestration

The reservoir simulation was found that the reservoir heterogeneity and injection techniques affect CO_2 storage performances. The channel shapes are so sensitive to CO_2 plume migration. Therefore, the lithofacies model must be carefully constructed in fluvial deposits to improve CO_2 sequestration assessment.

Moreover, this study was proven that the Water Alternating Gas process was strongly enhancement of CO_2 trapping. The WAG technology improved residual and solubility trapping greater than 25% compared with the continuous CO_2 injection process. Thus, we proposed that the WAG technique improve CO_2 storage efficiency, and the WAG process is the preferred injection strategy in CCS project.

6. 1. 3. Robust optimization of CO_2 trapping using Water Alternating Gas process under geological uncertainties

We found that the nominal optimization no long suits full-field simulation for CO_2 sequestration, considering for geological uncertainties. The nominal optimization approaches only evaluate a single distribution of petrophysical properties; thence, the optimization results cannot be validated in light of known uncertainties in reservoir simulation models. However, our proposed robust optimization framework consists of

geological uncertainties, by that removing any vagueness associated with CO_2 sequestration project.

Moreover, the nominal optimization used 50 days of gas injection and 100 days of water injection. But the robust optimization used 30 days of gas injection and 120 days of water injection. We demonstrated that the strategy recommended by the "robust" optimization (i.e., 30/120 cycle lengths) is better than the plan supported by the "nominal" optimization (i.e., 50/100 cycle lengths) based on a variety of metrics.

Thus, the robust optimization method (using three realizations) is superior to the nominal optimization method (using only one realization). Therefore, the proposed robust optimization framework can improve the CO_2 trapping efficiency as well as reduce the project risks in light of geological uncertainties

Besides, the nominal optimization led to 13% enhance in total CO_2 trapping over the WAG base case. However, the robust optimal solution increased the full CO_2 trapping by 15% over the nominal optimization case (28% larger than the WAG base case).

More specifically, the base case, nominal, and robust optimization of the WAG process led to total trapping of 0.875, 1.074, and 1.278 million tons of CO_2, respectively. All these results reflect the necessity of considering geological uncertainties in the optimization approach of the WAG injection application in real reservoir evaluations.

6. 2. Recommendations

Although an extensive study was conducted to continue this study. The future works are suggested to perform, as outlined below:

1. More geological realizations could be incorporated into the robust optimization workflow to improve the optimal solution in the CO_2 storage project.
2. The Artificial Neural Networks could be applied to generate the data-driven models to predict the CO_2 storage performance in other storage sites.
3. A machine learning-based optimization framework could apply to build the smart proxy model for predictive purposes.
4. The robust optimization workflow could be adapted to assess the CO_2 storage performance in fractured reservoirs and unconventional formations.
5. The WAG simulation in this research was conducted based on the object-based modelling. It is recommended to implement the WAG simulation based on the multi-point statistic to compare between two approaches in terms of history matching, optimization, and uncertainty analysis.
6. Optimization of injection CO_2/production brine well locations could conduct to maximize the CO_2 trapping in future projects.
7. For fast and robust prediction tools, the comprehensive machine learning methods could apply for the WAG process in the real reservoir.

References

Adibifard, M., Tabatabaei-Nejad, S.A.R., Khodapanah, E., 2014. Artificial Neural Network (ANN) to estimate reservoir parameters in Naturally Fractured Reservoirs using well test data. J. Pet. Sci. Eng. 122, 585–594. https://doi.org/10.1016/j.petrol.2014.08.007

Ahmadi, M.A., 2015. Developing a Robust Surrogate Model of Chemical Flooding Based on the Artificial Neural Network for Enhanced Oil Recovery Implications. Math. Probl. Eng. 2015, 1–9. https://doi.org/10.1155/2015/706897

Ajayi, T., Gomes, J.S., Bera, A., 2019. A review of CO2 storage in geological formations emphasizing modeling, monitoring and capacity estimation approaches. Pet. Sci. 16, 1028–1063. https://doi.org/10.1007/s12182-019-0340-8

Al-Khdheeawi, E.A., Vialle, S., Barifcani, A., Sarmadivaleh, M., Iglauer, S., 2018a. Enhancement of CO2 trapping efficiency in heterogeneous reservoirs by water-alternating gas injection. Greenh. Gases Sci. Technol. 12, 1–12. https://doi.org/10.1002/ghg.1805

Al-Khdheeawi, E.A., Vialle, S., Barifcani, A., Sarmadivaleh, M., Zhang, Y., Iglauer, S., 2018b. Impact of salinity on CO2containment security in highly heterogeneous reservoirs. Greenh. Gases Sci. Technol. 8, 93–105. https://doi.org/10.1002/ghg.1723

Al-Mudhafar, W., 2016. STATISTICAL RESERVOIR CHARACTERIZATION, SIMULATION, AND OPTIMIZATION OF FIELD SCALE-GAS ASSISTED GRAVITY DRAINAGE (GAGD) PROCESS WITH UNCERTAINTY ASSESSMENTS.

Al-mudhafar, W.J., 2018. How is Multiple-Point Geostatistics of Lithofacies Modeling Assisting for Fast History Matching ? A Case Study from a Sand-Rich Fluvial Depositional

Environment of Zubair Formation in South Rumaila Oil Field, in: Offshore Technology Conference. Houston, Texas, USA, 30 April–3 May 2018. This. https://doi.org/https://doi.org/10.4043/28662-MS

Al-Mudhafar, W.J., 2017. Integrating well log interpretations for lithofacies classification and permeability modeling through advanced machine learning algorithms. J. Pet. Explor. Prod. Technol. 7, 1023–1033. https://doi.org/10.1007/s13202-017-0360-0

Al-Mudhafar, W.J., Rao, D.N., Srinivasan, S., 2018. Robust Optimization of Cyclic CO2 flooding through the Gas-Assisted Gravity Drainage process under geological uncertainties. J. Pet. Sci. Eng. 166, 490–509. https://doi.org/10.1016/j.petrol.2018.03.044

Alcalde, J., Marzán, I., Saura, E., Martí, D., Ayarza, P., Juhlin, C., Pérez-Estaún, A., Carbonell, R., 2014. 3D geological characterization of the Hontomín CO2 storage site, Spain: Multidisciplinary approach from seismic, well-log and regional data. Tectonophysics 627, 6–25. https://doi.org/10.1016/j.tecto.2014.04.025

Alpak, F.O., Jennings, J.W., Gelderblom, P., Chen, C., Gao, G., Du, K., 2017. A Direct Overparameterize and Optimize Method for Stratigraphically Consistent Assisted History Matching of Object-Based Geomodels: Algorithm and Field Application. SPE J. 22, 1280–1295. https://doi.org/10.2118/181269-pa

Ambrose, W.A., Lakshminarasimhan, S., Holtz, M.H., Núñez-López, V., Hovorka, S.D., Duncan, I., 2008. Geologic factors controlling CO2storage capacity and permanence: Case studies based on experience with heterogeneity in oil and gas reservoirs applied to CO2storage. Environ. Geol. 54, 1619–1633. https://doi.org/10.1007/s00254-007-0940-2

Amini, S., Mohaghegh, S., 2019. Application of Machine Learning and Artificial Intelligence in

Proxy Modeling for Fluid Flow in Porous Media. Fluids 4, 126. https://doi.org/10.3390/fluids4030126

Aminian, K., Ameri, S., 2005. Application of artificial neural networks for reservoir characterization with limited data. J. Pet. Sci. Eng. 49, 212–222. https://doi.org/10.1016/j.petrol.2005.05.007

Aminu, M.D., Nabavi, S.A., Rochelle, C.A., Manovic, V., 2017. A review of developments in carbon dioxide storage. Appl. Energy 208, 1389–1419. https://doi.org/10.1016/j.apenergy.2017.09.015

Ampomah, W., Balch, R., Will, R., Cather, M., Gunda, D., Dai, Z., 2017. Co-optimization of CO2-EOR and Storage Processes under Geological Uncertainty. Energy Procedia 114, 6928–6941. https://doi.org/10.1016/j.egypro.2017.03.1835

Ampomah, W., Balch, R.S., Cather, M., Will, R., Gunda, D., Dai, Z., Soltanian, M.R., 2017. Optimum design of CO2 storage and oil recovery under geological uncertainty. Appl. Energy 195, 80–92. https://doi.org/10.1016/j.apenergy.2017.03.017

Anderson, D., McNeill, G., 1992. Artificial neural networks technology for neutron spectrometry and dosimetry, A DACS state-of-the-art report. https://doi.org/10.1093/rpd/ncm084

Ansah, E.O., Vo Thanh, H., 2020. Microbe induced fluid viscosity variation : field scale simulation , sensitivity and geological uncertainty. J. Pet. Explor. Prod. Technol. 1–24. https://doi.org/10.1007/s13202-020-00852-1

Aziz, K., Settari, A., 1979. Petroleum Reservoir Simulation, Applied Science Publ. Ltd., London, UK.

Bachu, S., 2002. Sequestration of CO2 in geological media in response to climate change: Road map for site selection using the transform of the geological space into the CO2 phase space. Energy Convers. Manag. 43, 87–102. https://doi.org/10.1016/S0196-8904(01)00009-7

Bachu, S., Gunter, W.D., Perkins, E.H., 1994. Aquifer disposal of CO2: Hydrodynamic and mineral trapping. Energy Convers. Manag. 35, 269–279. https://doi.org/10.1016/0196-8904(94)90060-4

Balch, R., McPherson, B., 2016. Integrating enhanced oil recovery and carbon capture and storage projects: A case study at Farnsworth field, Texas, in: Society of Petroleum Engineers - SPE Western Regional Meeting. Anchorage, Alaska, USA, 23–26 May. https://doi.org/10.2118/180408-ms

Bhat, C.R., 2001. Quasi-random maximum simulated likelihood estimation of the mixed multinomial logit model. Transp. Res. Part B 35, 677–693.

Blunt, M.J., 2018. Multiphase Flow in Permeable Media. A Pore-Scale Perspective, Groundwater. Cambridge University Press. https://doi.org/10.1111/gwat.12812

Bojesen-Koefoed, J.A., Nytoft, H.P., Dau, N.T., 2009. Petroleum composition in the Cuu Long Basin (Mekong Basin) offshore southern Vietnam. Mar. Pet. Geol. 26, 899–908. https://doi.org/10.1016/j.marpetgeo.2008.04.011

Brooks, R.H., Corey, A.T., 1964. HYDRAULIC PROPERTIES OF POROUS MEDIA. Hydrol. Pap. 3, Color. State Univ. Fort Collins 27. https://doi.org/citeulike-article-id:711012

Bruant, R.G., Jr., J., Celia, M.A., Guswa, A.J., Peters, C.A., 2002. Peer Reviewed: Safe Storage of CO2 in Deep Saline Aquifiers. Environ. Sci. Technol. 36, 240A–245A.

https://doi.org/10.1021/es0223325

Chen, B., Harp, D.R., Lu, Z., Pawar, R.J., 2020. Reducing uncertainty in geologic CO2 sequestration risk assessment by assimilating monitoring data. Int. J. Greenh. Gas Control 94, 102926. https://doi.org/10.1016/j.ijggc.2019.102926

Christensen, J.R., Stenby, E.H., Skauge, A., 2001. Review of WAG Field Experience. SPE Reserv. Eval. Eng. 4, 97–106. https://doi.org/10.2118/71203-PA

CMG, 2019. Manual of Computer Modelling Group's Software. Calgary, Cananda.

Cuong, T.X., Warren, J.K., 2009. Bach ho field, a fractured granitic basement reservoir, Cuu Long Basin, offshore SE Vietnam: A "buried-hill" play. J. Pet. Geol. 32, 129–156. https://doi.org/10.1111/j.1747-5457.2009.00440.x

Dai, Z., Middleton, R., Viswanathan, H., Fessenden-Rahn, J., Bauman, J., Pawar, R., Lee, S.-Y., McPherson, B., 2014a. An Integrated Framework for Optimizing CO_2 Sequestration and Enhanced Oil Recovery. Environ. Sci. Technol. Lett. 1, 49–54. https://doi.org/10.1021/ez4001033

Dai, Z., Stauffer, P.H., Carey, J.W., Middleton, R.S., Lu, Z., Jacobs, J.F., Hnottavange-Telleen, K., Spangler, L.H., 2014b. Pre-site characterization risk analysis for commercial-scale carbon sequestration. Environ. Sci. Technol. 48, 3908–3915. https://doi.org/10.1021/es405468p

Dai, Z., Zhang, Y., Bielicki, J., Amooie, M.A., Zhang, M., Yang, C., Zou, Y., Ampomah, W., Xiao, T., Jia, W., Middleton, R., Zhang, W., Sun, Y., Moortgat, J., Soltanian, M.R., Stauffer, P., 2018. Heterogeneity-assisted carbon dioxide storage in marine sediments. Appl. Energy 225, 876–883. https://doi.org/10.1016/j.apenergy.2018.05.038

Dang, C., Nghiem, L., Fedutenko, E., Gorocu, S.E., Yang, C., Mirzabozorg, A., Nguyen, N., Chen, Z., 2020. AI based mechanistic modeling and probabilistic forecasting of hybrid low salinity chemical flooding. Fuel 261, 116445. https://doi.org/10.1016/j.fuel.2019.116445

Dang, C., Nghiem, L., Nguyen, N., Chen, Z., Nguyen, Q., 2016. Evaluation of CO2Low Salinity Water-Alternating-Gas for enhanced oil recovery. J. Nat. Gas Sci. Eng. 35, 237–258. https://doi.org/10.1016/j.jngse.2016.08.018

Dang, C., Nghiem, L., Nguyen, N., Chen, Z., Yang, C., Nguyen, Q., 2017. A framework for assisted history matching and robust optimization of low salinity water fl ooding under geological uncertainties. J. Pet. Sci. Eng. 152, 330–352. https://doi.org/10.1016/j.petrol.2017.03.009

Dang, C., Nghiem, L., Nguyen, N., Yang, C., Chen, Z., Bae, W., 2018. Modeling and optimization of alkaline-surfactant-polymer flooding and hybrid enhanced oil recovery processes. J. Pet. Sci. Eng. 169, 578–601. https://doi.org/10.1016/j.petrol.2018.06.017

Dempsey, D., O'Malley, D., Pawar, R., 2015. Reducing uncertainty associated with CO2injection and brine production in heterogeneous formations. Int. J. Greenh. Gas Control 37, 24–37. https://doi.org/10.1016/j.ijggc.2015.03.004

Deutsch, C.V., Tran, T.T., 2002. ALLUVSIM: A program for event-based stochastic modeling of fluvial depositional systems. Comput. Geosci. 28, 525–535. https://doi.org/10.1016/j.cageo.2008.09.012

Deutsch, C. V., 2006. A sequential indicator simulation program for categorical variables with point and block data: BlockSIS. Comput. Geosci. 32, 1669–1681. https://doi.org/10.1016/j.cageo.2006.03.005

Doughty, C., 2010. Investigation of CO2 plume behavior for a large-scale pilot test of geologic carbon storage in a saline formation. Transp. Porous Media 82, 49–76. https://doi.org/10.1007/s11242-009-9396-z

Eigestad, G.T., Dahle, H.K., Hellevang, B., Riis, F., Johansen, W.T., Øian, E., 2009. Geological modeling and simulation of CO2 injection in the Johansen formation. Comput. Geosci. 13, 435–450. https://doi.org/10.1007/s10596-009-9153-y

Ertekin, T., Sun, Q., 2019. Artificial Intelligence Applications in Reservoir Engineering: A Status Check. Energies 12, 2897. https://doi.org/10.3390/en12152897

Esmaeilzadeh, S., Afshari, A., Motafakkerfard, R., 2013. Integrating artificial neural networks technique and geostatistical approaches for 3D geological reservoir porosity modeling with an example from one of Iran's oil fields. Pet. Sci. Technol. 31, 1175–1187. https://doi.org/10.1080/10916466.2010.540617

Ettehadtavakkol, A., Lake, L.W., Bryant, S.L., 2014. CO2-EOR and storage design optimization. Int. J. Greenh. Gas Control 25, 79–82. https://doi.org/10.1016/j.ijggc.2014.04.006

Fanchi, J., 2018. Principles of Applied Reservoir Simulation. Gulf Professional Publishing. https://doi.org/10.1016/B978-0-12-815563-9/00015-X

Fedutenko, E., Yang, C., Card, C., Nghiem, L., 2013. Optimization of SAGD Process Accounting for Geological Uncertainties Using proxy Models, in: CPSG/CESG/CWLS Geoconvention. Calgary, AB, Cananda.

Fegh, A., Riahi, M.A., Norouzi, G.H., 2013. Permeability prediction and construction of 3D geological model: Application of neural networks and stochastic approaches in an Iranian gas

reservoir. Neural Comput. Appl. 23, 1763–1770. https://doi.org/10.1007/s00521-012-1142-8

Flett, M., Gurton, R., Weir, G., 2007. Heterogeneous saline formations for carbon dioxide disposal: Impact of varying heterogeneity on containment and trapping. J. Pet. Sci. Eng. 57, 106–118. https://doi.org/10.1016/j.petrol.2006.08.016

Forooghi, A., Hamouda, A.A., Eilertsen, T., Energy, D., 2009. Co-optimization of CO 2 EOR and Sequestration Process in a North Sea Chalk Reservoir, in: SPE/EAGE Reservoir Characterization and Simulation Conference. Abu Dhabi, UAE, 19–21 October 2009. https://doi.org/10.2118/125550-MS

Francu, J., Pereszlényi, M., Riis, F., Prokop, O., Jurenka, L., Hladík, V., Krejčí, O., 2017. 3D Geological Model of Potential CO2 Storage: Abandoned Oil and Gas Field LBr-1in the Vienna Basin. Energy Procedia 114, 2772–2780. https://doi.org/10.1016/j.egypro.2017.03.1393

Genuchten, V.A.N., 1980. A Closed-form Equation for Predicting the Hydraulic Conductivity of Unsaturated Soils 1. Soil Sci. Soc. Am. J. 44, 892–898.

Georgsen, F., Syversveen, A.R., Hauge, R., Tollefsrud, J.I., Fismen, M., 2009. Local Update of Object-Based Geomodels. SPE Reserv. Eval. Eng. 12, 446–454. https://doi.org/10.2118/113532-pa

Ghaderi, S.M., Clarkson, C.R., Chen, S., 2012. Optimization of WAG process for coupled CO2 EOR-storage in tight oil formations: An experimental design approach, in: SPE Canadian Unconventional Resources Conference. Calgary, Alberta, Canada,30 October–1 November. https://doi.org/10.2118/161884-MS

Gringarten, E., Deutsch, C. V, 1999. Methodology for Improved Variogram Interpretation and Modeling for Petroleum Reservoir, in: Annual Technical Conference and Exhibition. Houston, Texas, 3–6 October, pp. 1–13.

Guardiano, F., Srivastava, R., 1993. Quantitative Geology and Geostatistics Series Editor :

Heath, J.E., Kobos, P.H., Roach, J.D., Dewers, T., McKenna, S.A., 2012. Geologic Heterogeneity and Economic Uncertainty of Subsurface Carbon Dioxide Storage. SPE Econ. Manag. 4, 32–41. https://doi.org/10.2118/158241-PA

Hellman, A.-L., T. Hultgreen, A., 2017. Decision models - Geological modelling to guide decisions. SPE Norw. Mag. 4, 22–24.

Herring, A.L., Andersson, L., Wildenschild, D., 2016. Enhancing residual trapping of supercritical CO2 via cyclic injections. Geophys. Res. Lett. 43, 9677–9685. https://doi.org/10.1002/2016GL070304.Received

Hesse, M.A., Woods, A.W., 2010. Buoyant dispersal of CO2 during geological storage. Geophys. Res. Lett. 37, 1–5. https://doi.org/10.1029/2009GL041128

Holden, L., Hauge, R., Skare, O., Skorstad, A., 1998. Modeling of fluvial reservoirs with object models. Math. Geol. 30, 473–496. https://doi.org/10.1023/A:1021769526425

Hsieh, P.S., Tien, N.C., Lin, C.K., Lin, W., Lu, H.Y., 2017. A multi-sequestration concept of CO2geological storage: Shale-Sandstone-Basalt system in Northwestern Taiwan. Int. J. Greenh. Gas Control 64, 137–151. https://doi.org/10.1016/j.ijggc.2017.07.008

Hu, L.Y., Jenni, S., 2006. History Matching of Object-Based Stochastic Reservoir Models. SPE J. 10, 312–323. https://doi.org/10.2118/81503-pa

Hung, N. Du, Le, H. Van, 2004. Petroleum Geology of Cuu Long Basin - Offshore Vietnam, in: Proceedings of AAPG International Conference. Barcelona, Spain, September 21-24.

Iglauer, S., 2017. CO2-Water-Rock Wettability: Variability, Influencing Factors, and Implications for CO2Geostorage. Acc. Chem. Res. 50, 1134–1142. https://doi.org/10.1021/acs.accounts.6b00602

IPCC, 2005. IPCC special report on carbon dioxide capture and storage. Cambridge University Press.

Issautier, B.Î., Fillacier, S., Le Gallo, Y., Audigane, P., Chiaberge, C., Viseur, S., 2013. Modelling of CO2 injection in fluvial sedimentary heterogeneous reservoirs to assess the impact of geological heterogeneities on CO2 storage capacity and performance. Energy Procedia 37, 5181–5190. https://doi.org/10.1016/j.egypro.2013.06.434

Iturrarán-Viveros, U., Parra, J.O., 2014. Artificial Neural Networks applied to estimate permeability, porosity and intrinsic attenuation using seismic attributes and well-log data. J. Appl. Geophys. 107, 45–54. https://doi.org/10.1016/j.jappgeo.2014.05.010

Jamalian, M., Safari, H., Goodarzi, M., Jamalian, M., 2018. Permeability prediction using artificial neural network and least square support vector machine methods, in: 80th EAGE Conference and Exhibition 2018. Copenhagen, Denmark,11-14 June. https://doi.org/10.3997/2214-4609.201801506

Jeong, H., Srinivasan, S., 2016. Fast assessment of CO2 plume characteristics using a connectivity based proxy. Int. J. Greenh. Gas Control 49, 387–412. https://doi.org/10.1016/j.ijggc.2016.03.001

Jesmani, M., Jafarpour, B., Bellout, M.C., Foss, B., 2020. A reduced random sampling strategy for fast robust well placement optimization. J. Pet. Sci. Eng. 184, 106414. https://doi.org/10.1016/j.petrol.2019.106414

Jia, W., McPherson, B., Pan, F., Dai, Z., Xiao, T., 2018. Uncertainty quantification of CO2storage using Bayesian model averaging and polynomial chaos expansion. Int. J. Greenh. Gas Control 71, 104–115. https://doi.org/10.1016/j.ijggc.2018.02.015

Jin, J., Kang, M., Choe, J., 2015. Optimal Well Positioning under Geological Uncertainty by Equalizing the Arrival Time. Energy Explor. Exploit. 33, 677–688. https://doi.org/10.1260/0144-5987.33.5.677

Jin, L., Hawthorne, S., Sorensen, J., Pekot, L., Kurz, B., Smith, S., Heebink, L., Herdegen, V., Bosshart, N., Torres, J., Dalkhaa, C., Peterson, K., Gorecki, C., Steadman, E., Harju, J., 2017. Advancing CO2 enhanced oil recovery and storage in unconventional oil play—Experimental studies on Bakken shales. Appl. Energy 208, 171–183. https://doi.org/10.1016/j.apenergy.2017.10.054

Johnson, J.W., 2009. Integrated modeling, monitoring, and site characterization to assess the isolation performance of geologic CO2 storage: Requirements, challenges, and methodology. Energy Procedia 1, 1855–1861. https://doi.org/10.1016/j.egypro.2009.01.242

Juanes, R., Spiteri, E.J., Orr, F.M., Blunt, M.J., 2006. Impact of relative permeability hysteresis on geological CO2storage. Water Resour. Res. 42, 1–13. https://doi.org/10.1029/2005WR004806

Kaufmann, O., Martin, T., 2008. 3D geological modelling from boreholes, cross-sections and geological maps, application over former natural gas storages in coal mines. Comput. Geosci.

34, 278–290. https://doi.org/10.1016/j.cageo.2007.09.005

Kim, Y., Jang, H., Kim, J., Lee, J., 2017. Prediction of storage efficiency on CO2 sequestration in deep saline aquifers using artificial neural network. Appl. Energy 185, 916–928. https://doi.org/10.1016/j.apenergy.2016.10.012

Konaté, A.A., Pan, H., Khan, N., Yang, J.H., 2015. Generalized regression and feed-forward back propagation neural networks in modelling porosity from geophysical well logs. J. Pet. Explor. Prod. Technol. 5, 157–166. https://doi.org/10.1007/s13202-014-0137-7

Kumar, A., 2012. Artificial Neural N etwork as s a Tool for Reservoir Characteriza ation and Its Application on in the Petroleum Engineering, in: Offshore Technology Conference. Texas, USA, 30 April–3 May, p. 12. https://doi.org/10.4043/22967-MS

Lackner, K.S., 2003. A guide to CO2 sequestration. Science (80-.). 300, 1677–1678. https://doi.org/10.1126/science.1079033

Land, C.S., 1968. Calculation of Imbibition Relative Permeability for Two- and Three-Phase Flow From Rock Properties. Soc. Pet. Eng. J. 8, 149–156. https://doi.org/10.2118/1942-pa

Lawton, D.C., Dongas, J., Osadetz, K., Saeedfar, A., Macquet, M., 2019. Development and Analysis of a Geostatic Model for Shallow CO2 Injection at the Field Research Station, Southern Alberta, Canada. Geophys. Geosequestration 280–296. https://doi.org/10.1017/9781316480724.017

Le Van, S., Chon, B.H., 2017. Evaluating the critical performances of a CO2–Enhanced oil recovery process using artificial neural network models. J. Pet. Sci. Eng. 157, 207–222. https://doi.org/10.1016/j.petrol.2017.07.034

Li, S., Zhang, Y., 2014. Model complexity in carbon sequestration: A design of experiment and response surface uncertainty analysis. Int. J. Greenh. Gas Control 22, 123–138. https://doi.org/10.1016/j.ijggc.2013.12.007

Li, Y., 2014. An Uncertainty Analysis of Modeling Geologic Carbon Sequestration in a Naturally Fractured Reservoir At Teapot Dome, Wyoming. University of Wyoming.

Ma, W., Jafarpour, B., Qin, J., 2019. Dynamic characterization of geologic CO2 storage aquifers from monitoring data with ensemble Kalman filter. Int. J. Greenh. Gas Control 81, 199–215. https://doi.org/10.1016/j.ijggc.2018.10.009

Manchuk, J.G., Deutsch, C. V., 2012. A flexible sequential Gaussian simulation program: USGSIM. Comput. Geosci. 41, 208–216. https://doi.org/10.1016/j.cageo.2011.08.013

March, R., Doster, F., Geiger, S., 2018. Assessment of CO 2 Storage Potential in Naturally Fractured Reservoirs With Dual-Porosity Models. Water Resour. Res. 54, 1650–1668. https://doi.org/10.1002/2017WR022159

Mckay, M.D., Beckman, R.J., Conover, W.J., 2000. A comparison of three methods for selecting values of input variables in the analysis of output from a computer code. Technometrics (JSTOR Abstr. 42, 55–61.

Mehnert, E., Damico, J., Frailey, S., Leetaru, H., Okwen, R., Storsved, B., Valocchi, A., 2014. Basin-scale modeling for CO2 sequestration in the basal sandstone reservoir of the Illinois Basin-improving the geologic model. Energy Procedia 63, 2949–2960. https://doi.org/10.1016/j.egypro.2014.11.317

Miocic, J.M., Gilfillan, S.M.V., Frank, N., Schroeder-Ritzrau, A., Burnside, N.M., Haszeldine,

R.S., 2019. 420,000 Year Assessment of Fault Leakage Rates Shows Geological Carbon Storage Is Secure. Sci. Rep. 9, 1–9. https://doi.org/10.1038/s41598-018-36974-0

Morley, C.K., 2002. A tectonic model for the Tertiary evolution of strike-slip faults and rift basins in SE Asia. Tectonophysics 347, 189–215. https://doi.org/10.1016/S0040-1951(02)00061-6

Nguyen, M.C., Zhang, X., Wei, N., Li, J., Li, X., Zhang, Y., Stauffer, P.H., 2017a. An object-based modeling and sensitivity analysis study in support of CO2 storage in deep saline aquifers at the Shenhua site, Ordos Basin. Geomech. Geophys. Geo-Energy Geo-Resources 3, 293–314. https://doi.org/10.1007/s40948-017-0063-5

Nguyen, M.C., Zhang, Y., Li, J., Li, X., Bai, B., Wu, H., Wei, N., Stauffer, P.H., 2017b. A Geostatistical Study in Support of CO2Storage in Deep Saline Aquifers of the Shenhua CCS Project, Ordos Basin, China. Energy Procedia 114, 5826–5835. https://doi.org/10.1016/j.egypro.2017.03.1720

Nguyen, N.T.B., Dang, C.T.Q., Nghiem, L.X., Chen, Z., Li, H., 2016. Robust Optimization of Unconventional Reservoirs under Uncertainties. SPE Eur. Featur. 78th EAGE Conf. Exhib. https://doi.org/10.2118/180108-MS

Nguyen, T.B.N., Bae, W., Nguyen, L.A., Dang, T.Q.C., 2014. A new method for building porosity and permeability models of a fractured granite basement reservoir. Pet. Sci. Technol. 32, 1886–1897. https://doi.org/10.1080/10916466.2010.551241

Obi, E.O.I., Blunt, M.J., 2006. Streamline-based simulation of carbon dioxide storage in a North Sea aquifer. Water Resour. Res. 42. https://doi.org/10.1029/2004WR003347

Pan, I., Babaei, M., Korre, A., Durucan, S., 2014. Artificial neural network based surrogate

modelling for multiobjective optimisation of geological CO2 storage operations. Energy Procedia 63, 3483–3491. https://doi.org/10.1016/j.egypro.2014.11.377

Petrel, 2017. Petrel.

Petvipusit, K.R., Elsheikh, A.H., Laforce, T.C., King, P.R., Blunt, M.J., 2014. Robust optimisation of CO2 sequestration strategies under geological uncertainty using adaptive sparse grid surrogates. Comput. Geosci. 18, 763–778. https://doi.org/10.1007/s10596-014-9425-z

Pinto, J.W.O., Afonso, S.M.B., Willmersdorf, R.B., 2019. Robust optimization formulations for waterflooding management under geological uncertainties. J. Brazilian Soc. Mech. Sci. Eng. 41. https://doi.org/10.1007/s40430-019-1970-x

Pyrcz, M.J., Deutsch, C. V., 2014. Geostastistical Reservoir Modeling. Oxford University Press, Oxford.

Rasmusson, K., Rasmusson, M., Tsang, Y., Niemi, A., 2016. A simulation study of the effect of trapping model, geological heterogeneity and injection strategies on CO2trapping. Int. J. Greenh. Gas Control 52, 52–72. https://doi.org/10.1016/j.ijggc.2016.06.020

Rogers, J.D., Grigg, R.B., 2001. A Literature Analysis of the WAG Injectivity Abnormalities in the CO2 Process. SPE Reserv. Eval. Eng. 4, 375–386. https://doi.org/10.2118/73830-PA

Ruiz- Serna, M.A., Alzate- Espinosa, G.A., Obando- Montoya, A.F., Álvarez- Zapata, H.D., 2019. Combined artificial intelligence modeling for production forecast in a petroleum production field. CT&F - Ciencia, Tecnol. y Futur. 9, 27–35. https://doi.org/10.29047/01225383.149

Sarkarfarshi, M., Malekzadeh, F.A., Gracie, R., Dusseault, M.B., 2014. Parametric sensitivity analysis for CO2 geosequestration. Int. J. Greenh. Gas Control 23, 61–71.

https://doi.org/10.1016/j.ijggc.2014.02.003

Schmidt, W.J., Hoang, B.H., Handschy, J.W., Hai, V.T., Cuong, T.X., Tung, N.T., 2019. Tectonic evolution and regional setting of the Cuu Long Basin, Vietnam. Tectonophysics 757, 36–57. https://doi.org/10.1016/j.tecto.2019.03.001

Seifert, D., Jensen, J.L., 2000. Object and pixel-based reservoir modeling of a braided fluvial reservoir. Math. Geol. 32, 581–603. https://doi.org/10.1023/A:1007562221431

Shamshiri, H., Jafarpour, B., 2012. Controlled CO 2 injection into heterogeneous geologic formations for improved solubility and residual trapping. Water Resour. Res. 48, 1–15. https://doi.org/10.1029/2011WR010455

Shishmanidi, I., Martynov, M., Kozlov, A., 2014. Advantages of Fluvial Reservoir Object Modeling (Russian), in: SPE Russian Oil and Gas Exploration and Production Technical Conference and Exhibition. https://doi.org/10.2118/171197-ru

Shmaryan, L.E., Deutsch, C. V., 1999. Object-Based Modeling of Fluvial / Deepwater Reservoirs with Fast Data Conditioning: Methodology and Case Studies, in: SPE Annual Technical Conference and Exhibition. Houston, Texas, 3-6 October 1999, pp. 1–10. https://doi.org/10.2523/56821-MS

Shogenov, K., Forlin, E., Shogenova, A., 2017. 3D Geological and Petrophysical Numerical Models of E6 Structure for CO2 Storage in the Baltic Sea. Energy Procedia 114, 3564–3571. https://doi.org/10.1016/j.egypro.2017.03.1486

Sina Hosseini Boosari, S., 2019. Predicting the Dynamic Parameters of Multiphase Flow in CFD (dam-break simulation) using artificial intelligence-(cascading deployment). Fluids 4.

https://doi.org/10.3390/fluids4010044

Siraj, M.M., Van den Hof, P.M.J., Jansen, J.D., 2016. Robust optimization of water-flooding in oil reservoirs using risk management tools. IFAC-PapersOnLine 49, 133–138. https://doi.org/10.1016/j.ifacol.2016.07.229

Song, Z., Li, Z., Wei, M., Lai, F., Bai, B., 2014. Sensitivity analysis of water-alternating-CO2flooding for enhanced oil recovery in high water cut oil reservoirs. Comput. Fluids 99, 93–103. https://doi.org/10.1016/j.compfluid.2014.03.022

Spycher, N., Pruess, K., 2005. CO2-H2O mixtures in the geological sequestration of CO2. II. Partitioning in chloride brines at 12-100°C and up to 600 bar. Geochim. Cosmochim. Acta 69, 3309–3320. https://doi.org/10.1016/j.gca.2005.01.015

Stein, M., 1987. Large Sample Properties of Simulations Using Latin Hypercube Sampling. Technometrics 29, 143–151.

Strebelle, S.B., 2006. Sequential simulation for modeling geological structures from training images. Stoch. Model. geostatistics Princ. methods, case Stud. Vol. II AAPG Comput. Appl. Geol. 5 139–149. https://doi.org/10.1306/1063812CA53231

Strebelle, S.B., Journel, A.G., 2001. Reservoir Modeling Using Multiple-Point Statistics. SPE Annu. Tech. Conf. Exhib. https://doi.org/10.2118/71324-MS

Suzuki, S., Caers, J., 2006. History Matching With an Uncertain Geological Scenario, in: SPE Annual Technical Conference and Exhibition. San Antonio, Texas, U.S.A 24–27 September.

Temitope, A., Sulemana, N., Gomes, J.S., Oppong, R., Russian, G., 2016. Statistical Uncertainty Analysis and Design Optimization of CO2 Trapping Mechanisms in Saline Aquifers, in:

International Petroleum Technology Conference.

Van't Veld, K., Mason, C.F., Leach, A., 2013. The economics of CO2sequestration through enhanced oil recovery. Energy Procedia 37, 6909–6919. https://doi.org/10.1016/j.egypro.2013.06.623

Van Essen, G., Zandvliet, M., Van den Hof, P., Bosgra, O., Jansen, J.-D., 2009. Robust Waterflooding Optimization of Multiple Geological Scenarios. SPE J. 14, 24–27. https://doi.org/10.2118/102913-PA

Vialle, S., Druhan, J.L., Maher, K., 2016. Multi-phase flow simulation of CO2 leakage through a fractured caprock in response to mitigation strategies. Int. J. Greenh. Gas Control 44, 11–25. https://doi.org/10.1016/j.ijggc.2015.10.007

Vo Thanh, H., Sugai, Y., Nguele, R., Sasaki, K., 2020. Robust optimization of CO2 sequestration through a water alternating gas process under geological uncertainties in Cuu Long Basin, Vietnam. J. Nat. Gas Sci. Eng. 76, 103208. https://doi.org/10.1016/j.jngse.2020.103208

Vo Thanh, H., Sugai, Y., Nguele, R., Sasaki, K., 2019a. Integrated workflow in 3D geological model construction for evaluation of CO2 storage capacity of a fractured basement reservoir in Cuu Long Basin, Vietnam. Int. J. Greenh. Gas Control 90, 102826. https://doi.org/10.1016/j.ijggc.2019.102826

Vo Thanh, H., Sugai, Y., Nguele, R., Sasaki, K., 2019b. Integrated Artificial Neural Network and Object-based Modelling for Enhancement History Matching in a Fluvial Channel Sandstone Reservoir Field Description, in: SPE/IATMI Asia Pacific Oil & Gas Conference and Exhibition. Society of Petroleum Engineers, Bali, Indonesia, 29-31 October 2019.

Vo Thanh, H., Sugai, Y., Nguele, R., Sasaki, K., 2019c. Integrated workflow in 3D geological model construction for evaluation of CO2 storage capacity of a fractured basement reservoir in Cuu Long Basin, Vietnam. Int. J. Greenh. Gas Control 90, 102826. https://doi.org/10.1016/j.ijggc.2019.102826

Vo Thanh, H., Sugai, Y., Sasaki, K., 2019d. Impact of a new geological modelling method on the enhancement of the CO2 storage assessment of E sequence of Nam Vang field, offshore Vietnam. Energy Sources, Part A Recover. Util. Environ. Eff. https://doi.org/10.1080/15567036.2019.1604865

Vo Thanh, H., Sugai, Y., Sasaki, K., 2018. AN OBJECT-BASE MODELING AND SIMULATION OF CO 2 PLUME DYNAMIC IN SALINE FORMATION IN NAM VANG FIELD , CUU LONG, in: 24th Formation Evaluation Symposium of Japan. Chiba, Japan.

Wang, X., van ’t Veld, K., Marcy, P., Huzurbazar, S., Alvarado, V., 2018a. Economic co-optimization of oil recovery and CO2 sequestration. Appl. Energy 222, 132–147. https://doi.org/10.1016/j.apenergy.2018.03.166

Wang, X., van ’t Veld, K., Marcy, P., Huzurbazar, S., Alvarado, V., 2018b. Economic co-optimization of oil recovery and CO2 sequestration. Appl. Energy 222, 132–147. https://doi.org/10.1016/j.apenergy.2018.03.166

Welkenhuysen, K., Rupert, J., Compernolle, T., Ramirez, A., Swennen, R., Piessens, K., 2017. Considering economic and geological uncertainty in the simulation of realistic investment decisions for CO2-EOR projects in the North Sea. Appl. Energy 185, 745–761. https://doi.org/10.1016/j.apenergy.2016.10.105

Wu, Q., Xu, H., Zou, X., 2005. An effective method for 3D geological modeling with multi-source

data integration. Comput. Geosci. 31, 35–43. https://doi.org/10.1016/j.cageo.2004.09.005

Yang, C., Card, C., Nghiem, L., Fedutenko, E., 2011. Robust Optimization of SAGD Operations under Geological Uncertainties. Proc. SPE Reserv. Simul. Symp. 21–23. https://doi.org/10.2118/141676-MS

Yang, C., Nghiem, L., Card, C., Bremeier, M., 2007. Reservoir Model Uncertainty Quantification T hrough Computer-Assisted History Matching.

Yasari, E., Pishvaie, M.R., 2015. Pareto-based robust optimization of water-flooding using multiple realizations. J. Pet. Sci. Eng. 132, 18–27. https://doi.org/10.1016/j.petrol.2015.04.038

Yeganeh, M., Masihi, M., Fatholahi, S., 2012. The estimation of formation permeability in a carbonate reservoir using an artificial neural network. Pet. Sci. Technol. 30, 1021–1030. https://doi.org/10.1080/10916466.2010.490805

Zargari, H., Poordad, S., Kharrat, R., 2013. Porosity and permeability prediction based on computational intelligences as artificial neural networks (ANNs) and adaptive neuro-fuzzy inference systems (ANFIS) in southern carbonate reservoir of Iran. Pet. Sci. Technol. 31, 1066–1077. https://doi.org/10.1080/10916466.2010.536805

Zhang, Z., Agarwal, R., 2013. Numerical simulation and optimization of CO2 sequestration in saline aquifers. Comput. Fluids 80, 79–87. https://doi.org/10.1016/j.compfluid.2012.04.027

Zhong, Z., Carr, T.R., 2019. Geostatistical 3D geological model construction to estimate the capacity of commercial scale injection and storage of CO2 in Jacksonburg-Stringtown oil field, West Virginia, USA. nternational J. Greenh. Gas Control 80, 61–75.

https://doi.org/10.1016/j.ijggc.2018.10.011

Zhong, Z., Liu, S., Carr, T.R., Takbiri-Borujeni, A., Kazemi, M., Fu, Q., 2019. Numerical simulation of Water-alternating-gas Process for Optimizing EOR and Carbon Storage. Energy Procedia 158, 6079–6086. https://doi.org/10.1016/j.egypro.2019.01.507

Zolotukhin, A.B., Gayubov, A.T., 2019. Machine learning in reservoir permeability prediction and modelling of fluid flow in porous media. IOP Conf. Ser. Mater. Sci. Eng. 700, 012023. https://doi.org/10.1088/1757-899X/700/1/012023